MAGNETOM Flash

The Magazine of MR

Issue Number 3/2010
RSNA Edition

SIEMENS

Clinical

How I do it

45

Matthias Lichy, M.D.

Dear MAGNETOM user,

Each new technology, evolution or revolution to existing ones, changes the way how we deliver healthcare to our patients. Good examples how MRI in combination with latest advantages in coil technology and image sequences can deliver all required clinical information at highest quality and replace and / or complement existing imaging in a meaningful way can be found in this issue of MAGNETOM Flash.
The impact of higher field-strength and open-bore technology can be seen in the articles by Weber et al. (Heidelberg University) dealing with complex pathologies of the spine and with young patients, exemplary cases show how the latest 3T MR technology adds important clinical information and how this also increases the confidence in treatment decision of the referring physicians.
Another good example can be found in the case report by Schneider et al. (Homburg University): whole-body imaging for tumor staging in pediatrics with diffusion-weighted imaging is now reality in clinical routine.
A few years ago this was simply not possible because of limitations in coil and MR sequence technology.
Taking into account the life cycle of a typical MR scanner and the fast progress of MR technology and its clinical applications, Siemens MR is committed to offering access to the latest developments e.g. by system upgrades. You will therefore find in this issue information on liver imaging with software version *syngo* MR B17 or an article on how to use the Tim Planning Suite for performing whole-spine examinations on your system.

MAGNETOM Flash and additional, clinically relevant information is available online at **www.siemens.com/magnetom-world.**

Enjoy reading this issue of MAGNETOM Flash!

Matthias Lichy, M.D.

The Editorial Team

We appreciate your comments.
Please contact us at magnetomworld.med@siemens.com

Antje Hellwich
Associate Editor

Okan Ekinci, M.D.
Center of Clinical Competence – Cardiology, Erlangen, Germany

Peter Kreisler, Ph.D.
Collaborations & Applications, Erlangen, Germany

Heike Weh,
Clinical Data Manager, Erlangen, Germany

Bernhard Baden,
Clinical Data Manager, Erlangen, Germany

Ignacio Vallines, Ph.D.,
Applications Manager, Erlangen, Germany

Wellesley Were
MR Business Development Manager
Australia and New Zealand

Milind Dhamankar, M.D.
Sr. Director, MR Product Marketing, Malvern, USA

Michelle Kessler, US
Installed Base Manager, Malvern, PA, USA

Gary R. McNeal, MS (BME)
Advanced Application Specialist, Cardiovascular MR Imaging
Hoffman Estates, USA

Dr. Sunil Kumar S.L.
Senior Manager Applications, Canada

Content

Content

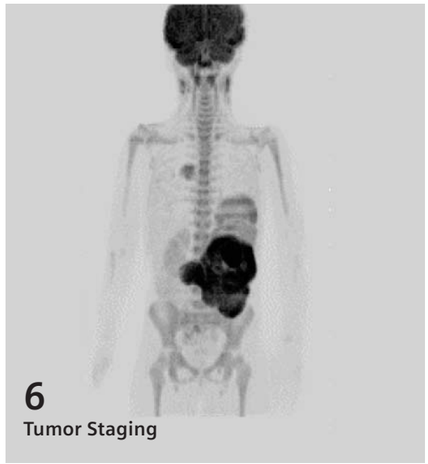

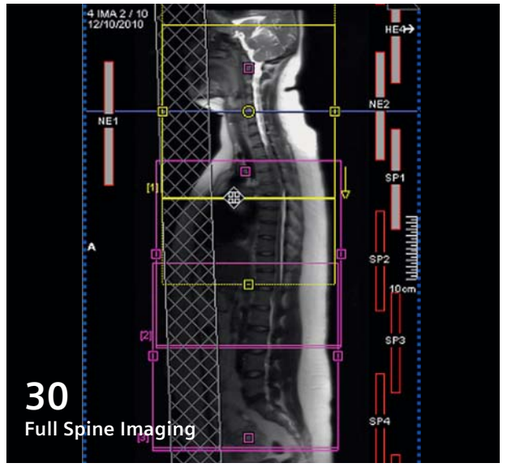

Further clinical information

Visit the MAGNETOM World Internet pages at **www.siemens.com/magnetom-world** for further clinical information and talks by international experts.

MR Tumor Staging for Treatment Decision in Case of Wilms Tumor

G. Schneider, M.D., Ph.D.; P. Fries, M.D.

Dept. of Diagnostic and Interventional Radiology, Saarland University Hospital, Homburg/Saar, Germany

Introduction

Nephroblastoma – also known as Wilms tumor – is the most frequent renal malignancy in childhood with the highest incidence of this tumor within the fourth year of life. 80% of patients are less than 5 years old, however it is a rare condition in neonates (<1%).
In general, there are no known risk factors for the development of nephroblastoma, but it may be associated with rare conditions like Denys-Drash (triad of congenital nephropathy, Wilms tumor and intersex disorders), WAGR (also called Wilms tumor-aniridia syndrome) and Beckwidth-Wiedeman (giantism associated with tumors and malformations) syndrome. The incidence is approx. 1: 100,000 for western countries including the US, while a lower incidence is reported for Asian countries. If not associated with a syndrome, clinical symptoms – if present at all – are very often unspecific and abdominal pain and palpable tumor can be the only findings at the time of diagnosis.
MRI is considered the imaging modality of choice for tumor staging and subsequent treatment planning. If imaging is conclusive, often no biopsy is performed prior to initiation of therapy. Clinical treatment is according to protocols of SIOP (Society of Pediatric Oncology) in Europe or COG (Children's Oncology Group) in North America. Therapy includes primary surgery (COG), preoperative chemotherapy (SIOP), and/or adjuvant chemotherapy. If not treated, prognosis of a Wilms tumor is poor. Independent of prognostic factors such as stage and grading, the overall outcome is good and approximately 90% of all children will be cured.
Questions for imaging are: a) supporting the suspicion of a Wilms tumor for initiation of therapy, b) evaluation of tumor volume, c) contralateral tumor manifestation and d) lymph nodes metastasis or infiltration of neighboring structures e.g. diaphragm or liver.
Tumor staging has to include at least the whole abdomen and thorax (lung filiae are the most common presentation of metastatic disease). Imaging modalities used are ultrasound, MRI, and CT in case of lung metastases. Depending on final tumor histology, a bone (often scintigram) and brain MRI scan have to be performed in case of CCSK (clear cell sarcoma) and RTK (rhabdoid tumor of the kidney), too. MRI is recommended independent of the above-mentioned reasons in any case where a) a caval vein tumor thrombus, b) infiltration of liver and diaphragm, or c) continuous tumor extension into the thoraxic cavity is suspected.

Patient history

A 4-year-old girl presented with a large palpable mass in the left upper quadrant and unspecific abdominal pain. Ultrasound had already revealed a large tumor of the left hemiabdomen with mass effect towards the liver. The patient was referred to our MRI department because of suspicion of Wilms tumor.

MRI protocol

MRI was conducted using a 1.5 Tesla MAGNETOM Aera with the combination of the 18-channel body coil and the integrated spine coil. For the MRI procedure the patient received an intravenous sedation using propofol. The imaging protocol included diffusion-weighted imaging (DWI, *syngo* REVEAL), acquired during free breathing, and transversal T2w TSE and HASTE sequences with navigator triggering.
A single-shot echo planar diffusion imaging with Stejskal-Tanner diffusion encoding scheme was applied. For fat saturation, an inversion recovery technique was used. The sequence parameters were:

Continued on page 10

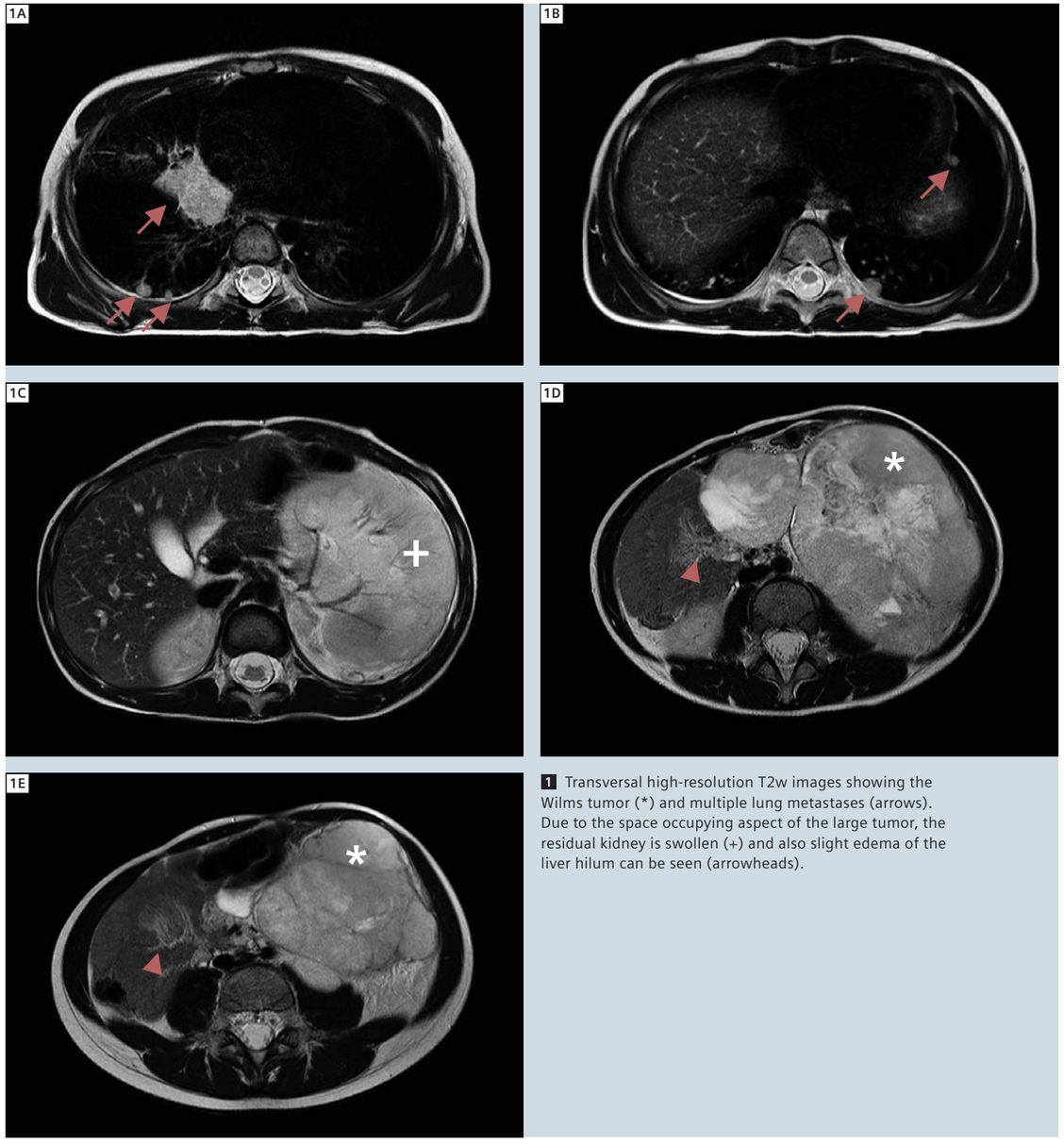

1 Transversal high-resolution T2w images showing the Wilms tumor (*) and multiple lung metastases (arrows). Due to the space occupying aspect of the large tumor, the residual kidney is swollen (+) and also slight edema of the liver hilum can be seen (arrowheads).

2 Rotating MIP based on high b-value images.

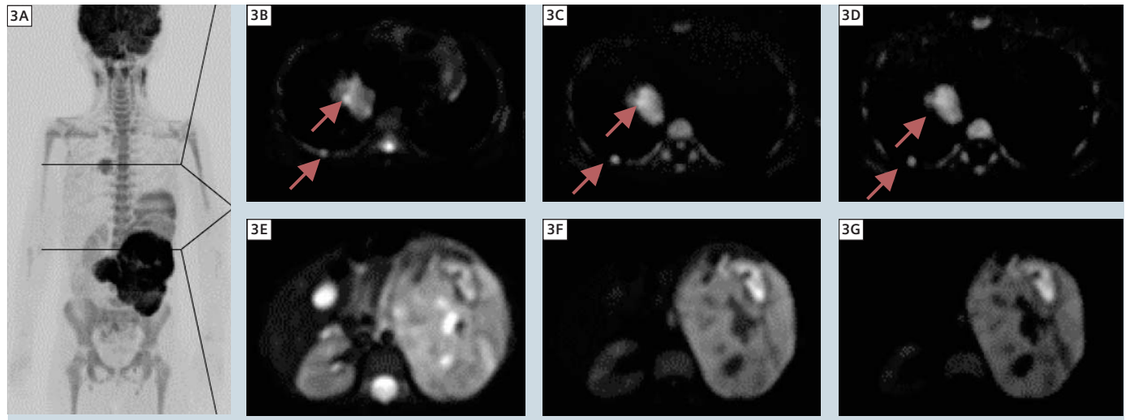

3 **(A)** Coronal DWI MIP. Original b-value images at 0 and 800 s/mm² **(B, C** and **E, F)** as well as calculated b-value at b 1400 s/mm² **(D, G)** are shown. (Arrows pointing to lung metastases.)

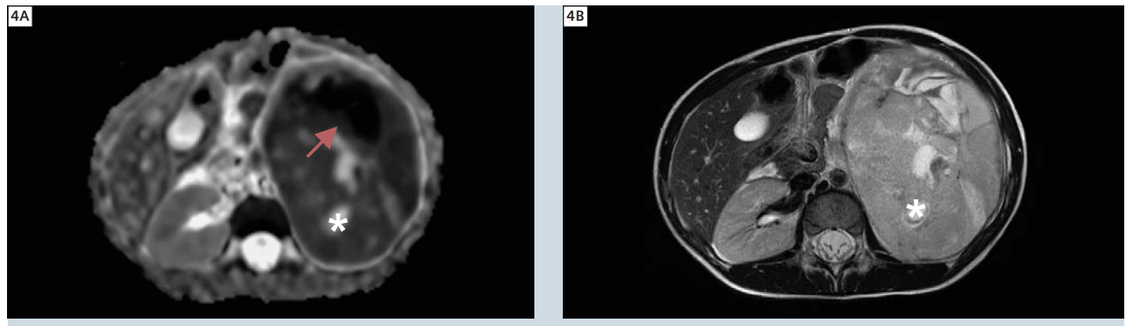

4 Calculated ADC map **(A)** and corresponding T2w image **(B)** demonstrating the tumor heterogeneity. The area marked by the arrows has a clear restriction in diffusibility but based on T2w imaging alone, no differentiation between this area and the one marked with * is possible. While the high signal area on T2w and high ADC values may represent cysts or calceal dilation, the area with the high restriction of diffusion represents a very densely packed areal e.g. mucous tumor cells.

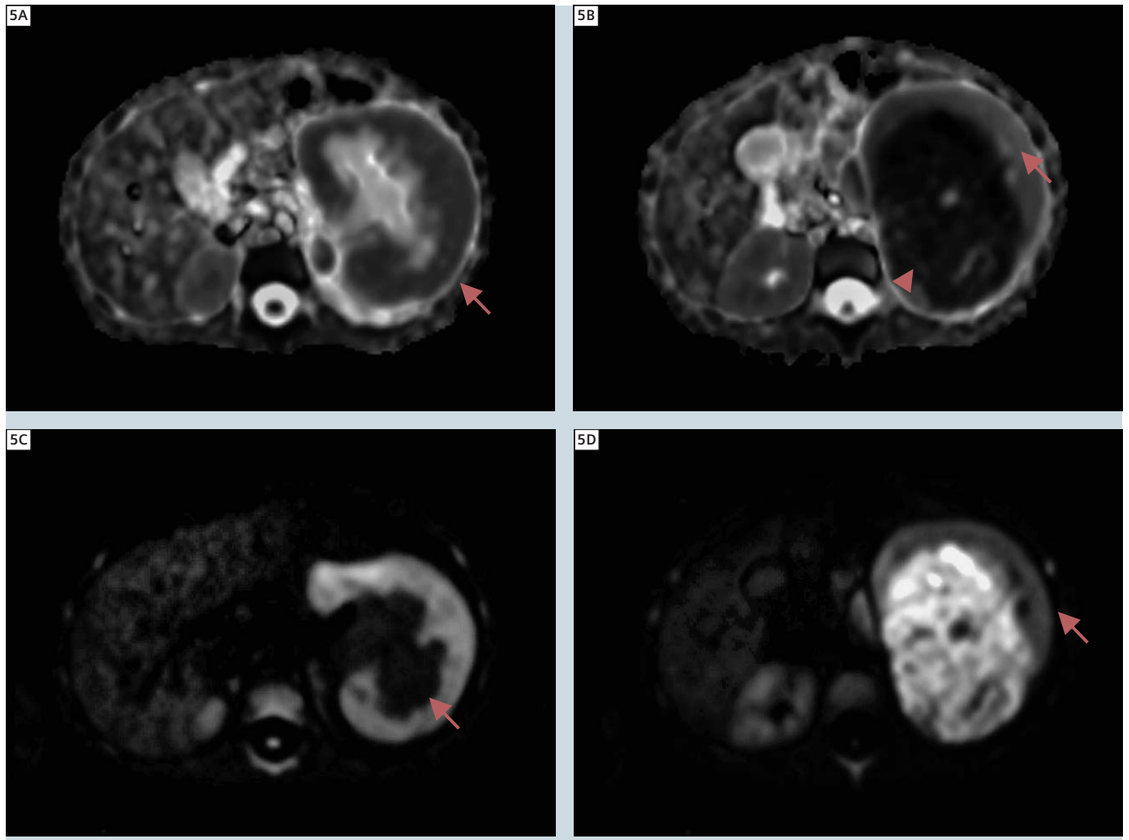

5 Based on ADC maps and high b-value images (b 1400 s/mm² is shown), a clear differentiation between residual but swollen kidney tissue (arrows) and the Wilms tumor (arrowhead) is possible. Both types of tissue differ in their cellular density, however, on T2w images no clear differentiation is possible in this case (compare Fig. 1). Nevertheless, not all areas of the tumor are characterized by high signal on the very high b-value images, demonstrating well the tumor heterogeneity. **(A, B)** ADC maps. **(C, D, E)** b 1400 s/mm² images. **(F)** Coronal thick-slice MPR based on b 1400 s/mm² images (* spleen).

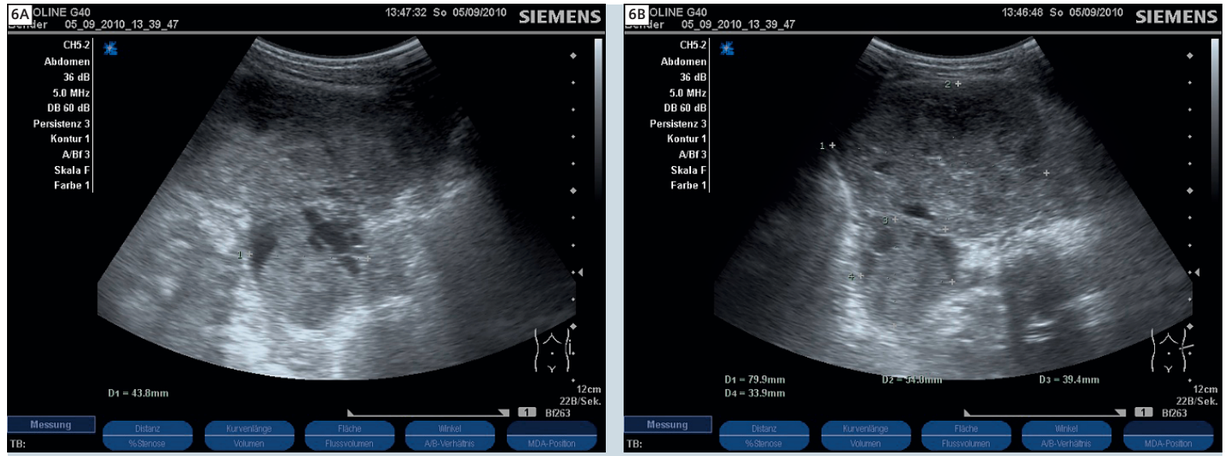

6 Corresponding images of the initial ultrasound examination of the Wilms tumor in sagittal **(A)** and transversal **(B)** orientation are shown.

Continued from page 6

TR 15400 ms, TE 75 ms, TI 180 ms, PAT factor of 2, 3-scan trace (averaged), FOV 309 x 380, matrix 208 x 128 (interpolated to 208 x 256), slice thickness 5 mm, no gap, 4 averages. Real voxel size was 1.5 x 3 x 5 mm^3. Two b-values at b 0 and b 800 s/mm^2 were acquired. ADC maps and additional high b-value images at b 1400 s/mm^2 were calculated automatically by the scanner software, based on linear signal decay. DWI covered the whole body trunk from skull base towards upper lower extremities. Acquisition time was approx. 15 min. For presentation and fast overview about tumor spread, a rotating maximum intensity projection (MIP) based on b 800 s/mm^2 was generated.
For detailed morphology and assessment of tumor infiltration, navigator triggered T2w TSE was applied for the abdomen including the lower thorax and mediastinum. Sequence parameters were TR 3508 ms, TE 102 ms, 2 averages. PAT factor 2, FOV 188 x 250 mm^2, matrix 269 x 512, slice thickness 6 mm, 20% gap, acquisition time was approx. 8 min.

Imaging findings

A large occupying tumor deriving from the lower pole of the left kidney with compression of the residual kidney and mass effect towards the liver and especially the left liver lobe is shown. Due to the mass effect, slight edema of the liver hilus can be seen. However, the border of the mass is well circumscribed and no evidence of diffuse tumor infiltration of the liver, spleen or diaphragm can be seen. Since no encasement of retroperitoneal vessels or other structures is seen DD of neuroblastoma can be ruled out. Also the lumen of the abdominal aorta is regular and neither a tumor infiltration of the large vessels nor a tumor-thrombus can be visualized. The right kidney and the other abdominal organs are free of metastases. However, already well visualized by the MIP DWI, a large tumor mass at the right lung hilum can be seen with compression of central lung structures and edema of the depending lung tissue. In addition, at least four additional lung metastases are detected.
No evidence for bone metastases. The bright signal of the bone marrow on high b-value images has to be considered as age related. The size of the displaced spleen is also within normal age-related range.
On a follow-up study after chemotherapy and before surgery a tremendous reduction of tumor size can be noticed. Only small residual tumor tissue of one lung metastases is visible on CT and MRI.

Conclusion

Whole-body imaging in staging of Wilms tumor can replace CT imaging and gives all necessary information for therapy planning. With the help of newer imaging modalities in MRI, especially DWI, the prediction of tumor response needs to be evaluated. This can easily be done by correlating histological data with imaging data from patients enrolled in prospective clinical trials. As preoperative chemotherapy is only part of the SIOP studies such investigations can predominantly be performed in Europe.

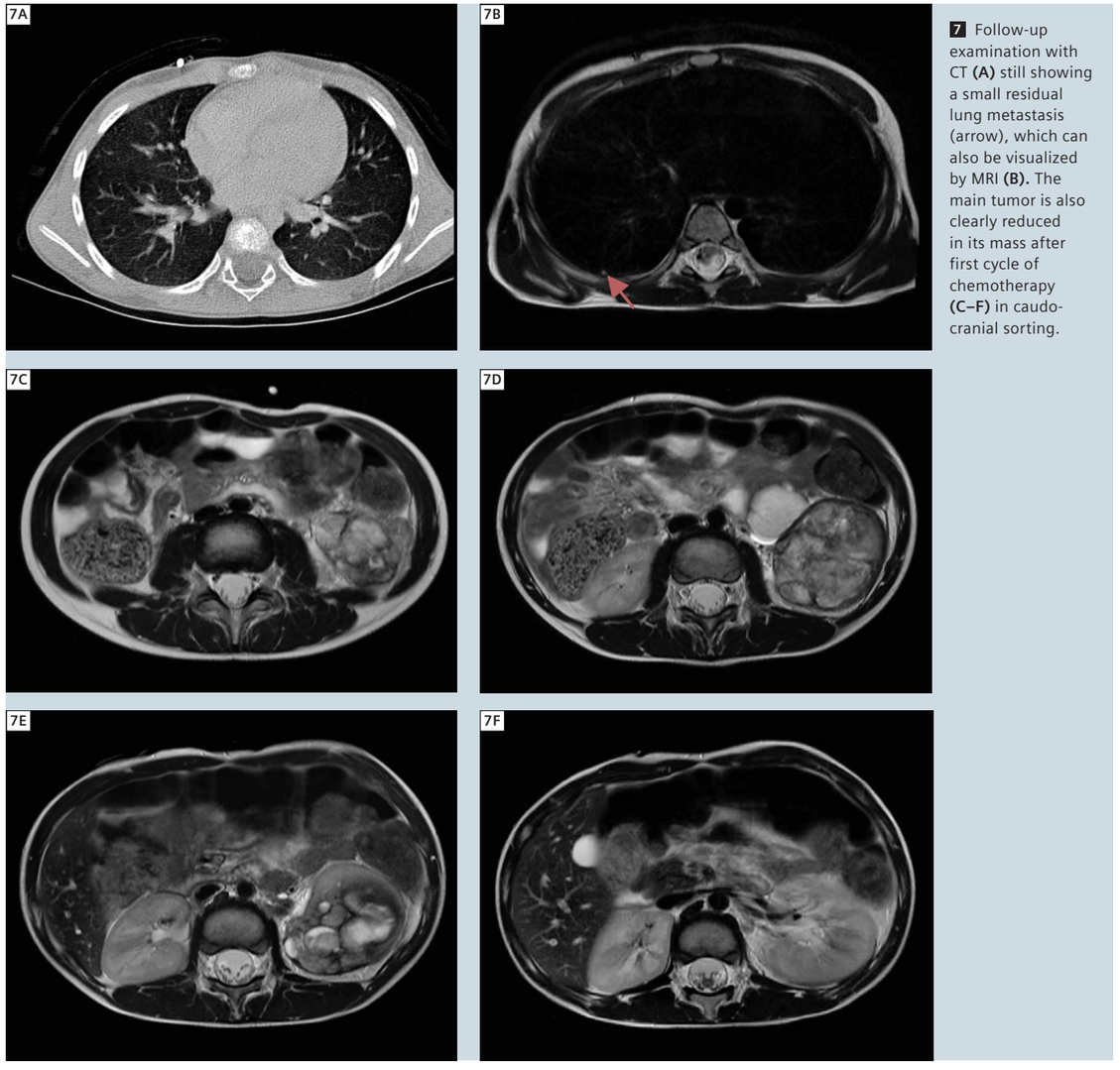

7 Follow-up examination with CT **(A)** still showing a small residual lung metastasis (arrow), which can also be visualized by MRI **(B).** The main tumor is also clearly reduced in its mass after first cycle of chemotherapy **(C–F)** in caudo-cranial sorting.

References

1 Kaste, S.C., Dome, J.S., Babyn, P.S., Graf, N.M., Grundy, P., Godzinski, J., Levitt, G.A., Jenkinson, H. 2008 Wilms tumour: Prognostic factors, staging, therapy and late effects Pediatric Radiology 38 (1), pp. 2-17.

2 Graf, N., Tournade, M.-F., De Kraker, J. 2000 The role of preoperative chemotherapy in the management of Wilms' tumor: The SIOP studies. Urologic Clinics of North America 27 (3), pp. 443-454.

Contact
PD Dr. Dr. Günther Schneider
Dept. of Diagnostic and Interventional Radiology
Saarland University Hospital
Kirrberger Strasse
66421 Homburg/Saar
Germany
dr.guenther.schneider@uks.eu

Cerebral Arterio-Venous Malformation detected by *syngo* TWIST MRA

Ali Yusuf Oner; Turgut Tali; Nil Tokgoz

Gazi University, School of Medicine, Department of Radiology, Ankara, Turkey

Patient history

A 17-year-old patient suffering from untractable epilepsy was referred to our institution for imaging evaluation. He underwent an initial brain MRI on a 3T MAGNETOM Verio, which showed a right parietal polymicrogyric focus with a suspected neighboring arterio-venous malformation (AVM) not readily depicted by time-of-flight (TOF) MR angiography (MRA). A second contrast enhanced *syngo* TWIST MRA succesfully showed the AVM nidus and the patient was referred for stereotactic radiosurgery.

Imaging findings

T2-weighted turbo spin-echo (TSE) images in the axial plane and coronal TIRM images show right pariteal shallow sulci, with indistinct gray-white matter interface, lined by polymicrogyric cortex (Fig. 1). On the T2-weighted images small vascular flow voids are noted. The AVM nidus goes undetected on a 3D TOF MRA due to its low flow status (Fig. 2), whereas a post-contrast *syngo* TWIST MRA readily shows the AVM nidus fed by the anterior system, together with the early central draining veins (Fig. 3).

Sequence details

All images were acquired using a 3T MAGNETOM Verio with software version *syngo* MR B17 and the standard head matrix coil.

Axial TSE T2W: TR 4000 ms, TE 107 ms, FOV 220 x 220 mm², matrix 410 x 512, 2 averages, iPAT factor of 2, slice thickness 5 mm, gap 1.5 mm.

Coronal T2W TIRM: TR 9000 ms, TE 94 ms, FOV 200 x 220 mm², matrix 232 x 256, 1 average, iPAT factor of 2, slice thickness 5 mm, gap 2 mm.

3D TOF MRA: TR 21 ms, TE 3.60 ms, FOV 181 x 200 mm², matrix 331 x 384, 1 average, iPAT factor of 2.

***syngo* TWIST MRA:** TR 2.79 ms, TE 1.01 ms, FOV 350 x 400 mm², matrix 245 x 384, iPAT factor of 2, slice thickness 2.5 mm, 25 measurments with a temporal resolution of 1.09 seconds per single slab.

Conclusion

Anomalies of neuronal migration and vascular malformations are two important and relatively frequent causes of epilepsy. However their coexistence, as in the presented case, is less usual. Although their diagnosis is straight forward by MRI and TOF MRA, 4D MRA techniques following contrast injection such as *syngo* TWIST can be the problem-solving tool in cases with low flow AVM's.

Contact
Ali Yusuf Oner, M.D.
Gazi University
School of Medicine
Department of Radiology
Ankara
Turkey
Phone: +90 312 202 5163
yusufoner@gazi.edu.tr

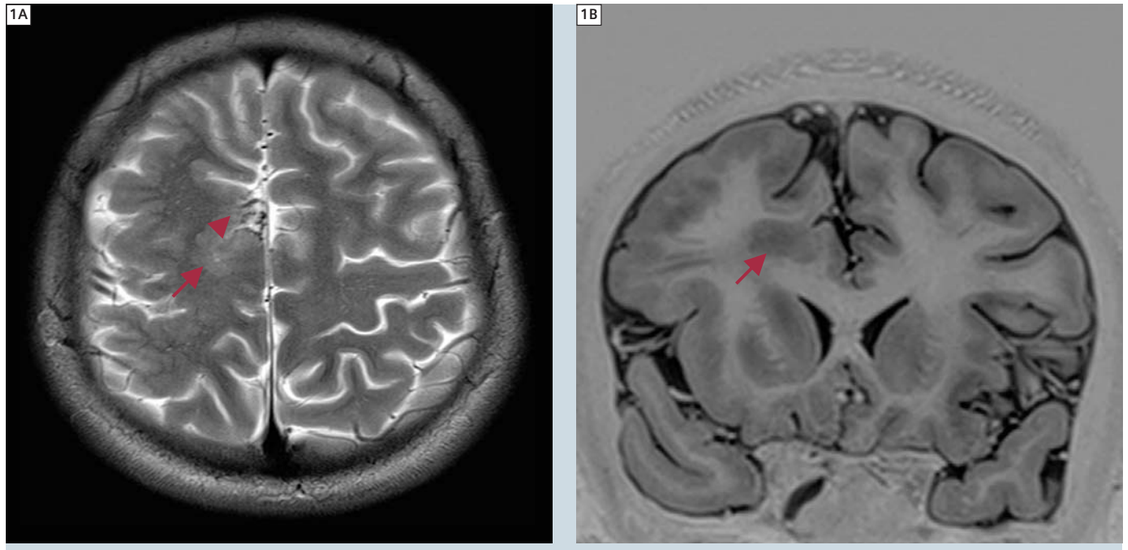

1 T2-weighted image in the axial plane **(A)** and inverted STIR image **(B)** in the coronal plane show right parietal polymicrogyric cortex (arrows) with indistinct gray-white matter interface. Note the small vascular flow voids, raising suspicion of a possible accompanying AVM arrowhead.

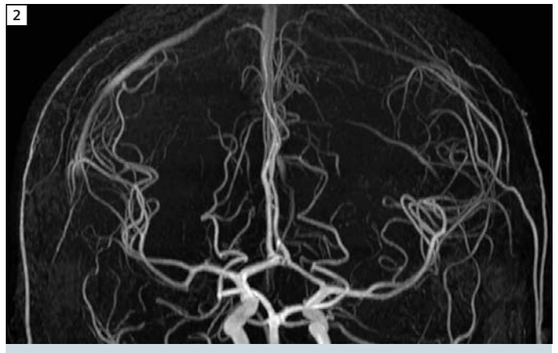

2 Coronal maximum intensity projection (MIP) of a 3D TOF MRA fails to demonstrate the AVM nidus.

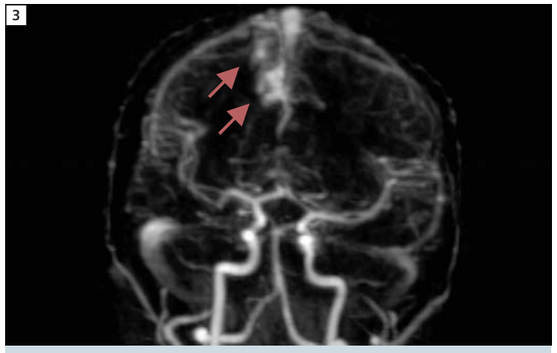

3 Highly temporal resolved post-contrast 4D MRA in the coronal plane shows a low-flow AVM mostly fed by the anterior arterial system, with a central drainage (arrows).

Case Report:
Cerebral Amyloid Angiopathy (CAA) using Susceptibility-Weighted Imaging (*syngo* SWI)

Markus Lentschig

MR, Nuclear Medicine and PET/CT Center Bremen Mitte, Bremen, Germany

Background

With the development of a 3D gradient-echo (GRE) based susceptibility-weighted imaging sequence (*syngo* SWI), a neuroimaging MR technique is now available in clinical routine which maximizes tissue magnetic susceptibility and makes use of these differences to generate a unique contrast, different from that of proton density, T1, T2, and conventional T2* imaging we are used so far in clinical routine. Compared to other imaging techniques *syngo* SWI – a long TE flow compensated gradient echo imaging providing enhanced contrast with the combination of phase and magnitude information – has already provided superior results in clinical studies in detecting intracranial bleeding but also in depicting minute intracranial vascular malformations.

Cerebral Amyloid Angiopathy

Cerebral amyloid angiopathy (CAA) is a small vessel disease which is characterized by deposition of amyloid β protein within the cerebral arterioles. It is known that there is a clear association of CAA with the following aging, dementia, Alzheimer's disease, postradiation necrosis, and spongiform encephalopathies. But so far, no in vivo imaging technique is available which enables either the direct visualization or quantification of the amyloid deposits. But as an indirect sign, typically microhemorrhages within and around the arteriole vessel wall lobar microbleeds are found and related to CAA. Usually CAA is involving the cortex and subcortical white matter within the frontal and parietal lobes. In contrast, hypertensive or atherosclerotic microangiopathy shows microhemorrhages in a deep or infratentorial location.

Sequence details

A 68-year-old patient with suspicion of TIA (transient ischemic attack) has been referred to our institution for imaging and to rule out further diseases of the brain. All images were acquired at 3 Tesla using a MAGNETOM Verio with the standard 12-channel head coil. Sequence parameters for shown images were:
T1 SE: TR 500 ms, TE 8.4 ms, FOV 230, matrix 256 / 95 % (interpolated to 512), SL 5 mm, TA 1:53 min:s, voxel size 1.0 x 0.9 x 5 mm
***syngo* SWI:** TR 27 ms, TE 20 ms, FOV 230 / 75 %, Matrix 256 / 95 % (interpolated to 512), SL 2.5 mm, TA 2:48 min:s, voxel size 0.9 x 0.9 x 2,5 mm. Phase and magnitude images and the finally post-processed SWI are available for image analysis. Also, a thick-slice MPR (multiplanar reconstruction) which is generated Inline is available.
DarkFluid (FLAIR): TR 9000 ms, TE 94 ms, FOV 230 / 84 %, Matrix 256 / 95 % (interpolated to 512), SL 5 mm, TA 2:26 min:s, voxel size 1.0 x 0.9 x 5 mm

Imaging findings

Multiple T2w hyperintense isolated foci in the periventricular white matter are shown on DarkFluid (FLAIR) images (arrows figure 1A). In addition, dorsal of the posterior horn and lateral ventricle converging hyperintense periventricular T2w hyperintense areas are shown, which can be interpreted as age-related periventricular gliosis (arrowheads figure 1). However, also in the temporal lobe cortical and subcortical T2 hyperintense spots with only slightly increased signal can be visualized by DarkFluid (FLAIR) imaging (arrows figure 1B). In addition, there is a widening of the internal and external cerebral fluid interspaces. On native T1w MRI, no hyperintense signal can be demonstrated; only in the case of the largest periventricular white-matter foci, a corresponding

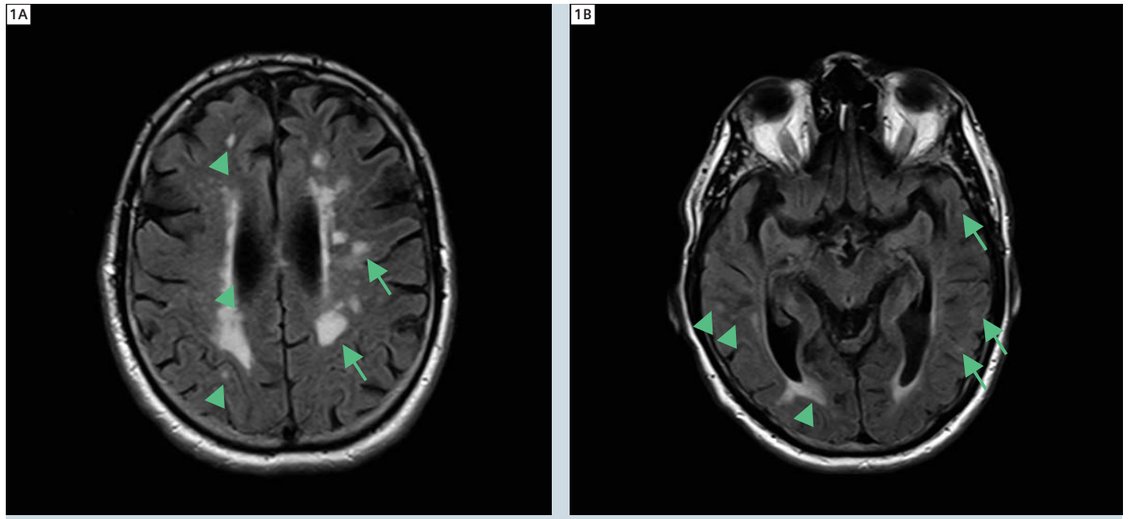

1 DarkFluid (FLAIR) images of a patient with cerebral amyloid angiopathy.

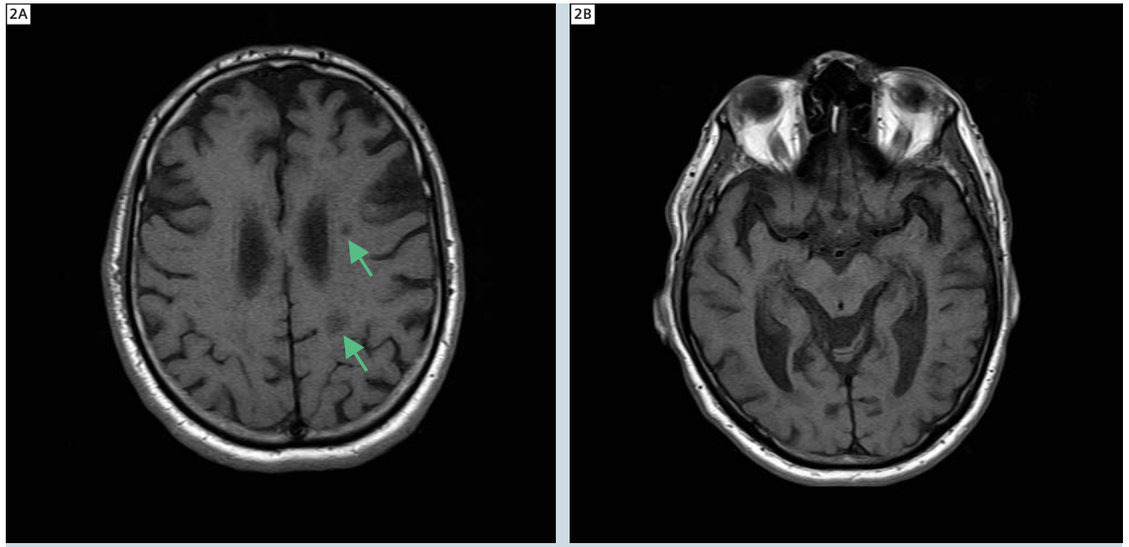

2 Corresponding native T1-weighted images.

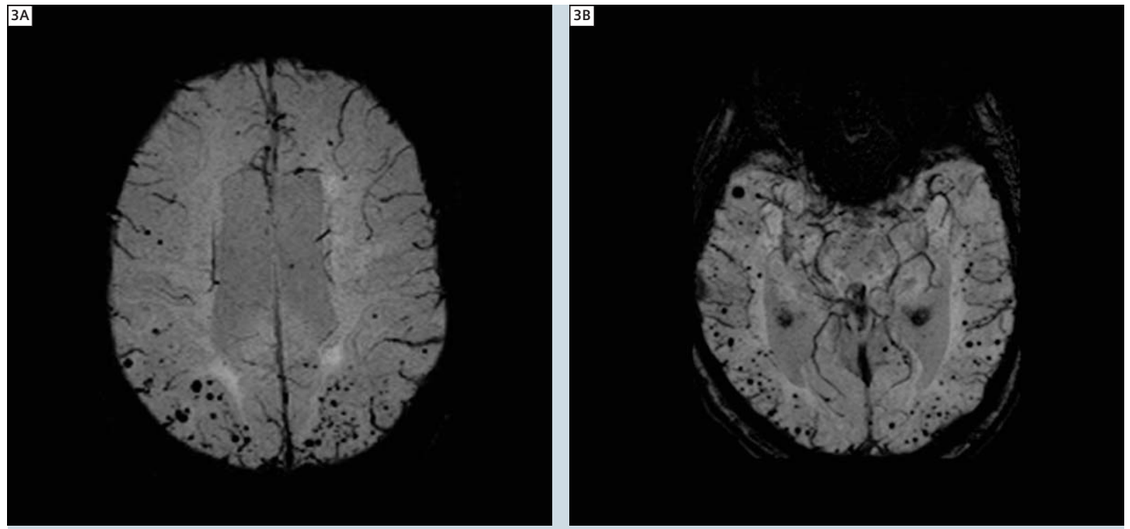

3 *syngo* SWI showing multiple cortical and subcortical bleedings.

hypointense lesion can be found. However, SWI looked completely different: multiple smallest cortical and subcortical bleedings were visualized in the temporal, parietal and less prominent in the frontal lobe (figure 3).
In conclusion the findings in our patient are a mixture of unspecific vascular / age related findings (periventricular gliosis, reduced brain volume, microinfarcts) and CAA. However, extent and severity of CAA is only visualized by *syngo* SWI in detail and would have been clearly underestimated based on conventional MRI only.

Conclusion

syngo SWI has shown in this case to be a sensitive tool for precise assessment of CAA. In general, SWI can provide useful additional information in the evaluation of various pediatric and adult neurologic conditions and can be incorporated easily into the routine imaging assessment. It is known that SWI is more sensitive in detection of small bleedings and small vascular malformations than conventional T2* imaging and that it is an imaging technique which is highly sensitive to iron accumulation in the brain; this is observed in ageing process, reflection of brain damage, diseases of iron metabolism and haemorrhages. Iron involvement is already accepted in Hallervorden-Spatz disease, neuroferritinopathy, aceruloplasminemia, Friedreich's Ataxia. However, larger studies are still needed to determine the role of SWI in iron measuring especially in neurodegenerative diseases (Alzheimer's disease, Parkinson, ALS, and in Multiple Sclerosis).

Contact
Markus G. Lentschig, M.D.
MR and PET/CT Imaging Center Bremen Mitte
Sankt-Jürgen-Str. 1
28177 Bremen
Germany
www.mr-bremen.de

References

1 Haacke EM, Mittal S, Wu Z, Neelavalli J, Cheng YC.Susceptibility-weighted imaging: technical aspects and clinical applications, part 1. AJNR Am J Neuroradiol. 2009 Jan;30(1):19-30. Epub 2008 Nov 27. Review.

2 Mittal S, Wu Z, Neelavalli J, Haacke EM. Susceptibility-weighted imaging: technical aspects and clinical applications, part 2. AJNR Am J Neuroradiol. 2009 Feb;30(2):232-52. Epub 2009 Jan 8. Review.

3 Haacke EM, DelProposto ZS, Chaturvedi S, Sehgal V, Tenzer M, Neelavalli J, Kido D. Imaging cerebral amyloid angiopathy with susceptibility-weighted imaging. AJNR Am J Neuroradiol. 2007 Feb;28(2):316-7.

4 Schrag M, McAuley G, Pomakian J, Jiffry A, Tung S, Mueller C, Vinters HV, Haacke EM, Holshouser B, Kido D, Kirsch WM. Correlation of hypointensities in susceptibility-weighted images to tissue histology in dementia patients with cerebral amyloid angiopathy: a postmortem MRI study. Acta Neuropathol. 2009 Nov 25. [Epub ahead of print]

Try them on your system

Trial licenses for most of the applications featured in this issue of MAGNETOM Flash are available free of charge for a period of 90 days: Please contact your local Siemens representative for system requirements and ordering details or visit us online* at **www.siemens.com/discoverMR** for further details, product overviews, image galleries, step-by-step videos, case studies and general requirement information.

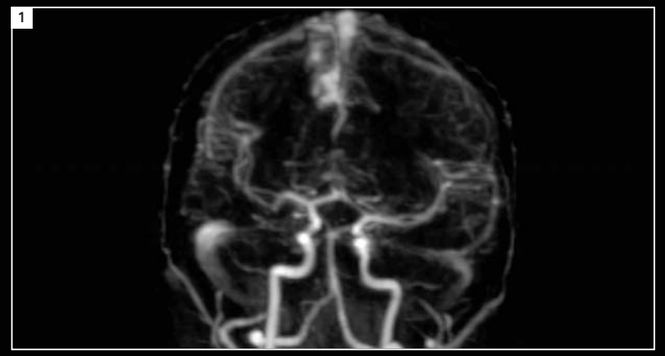

1 *syngo* TWIST (page 13).

2 *syngo* SWI, susceptibility-weighted imaging (page 23).

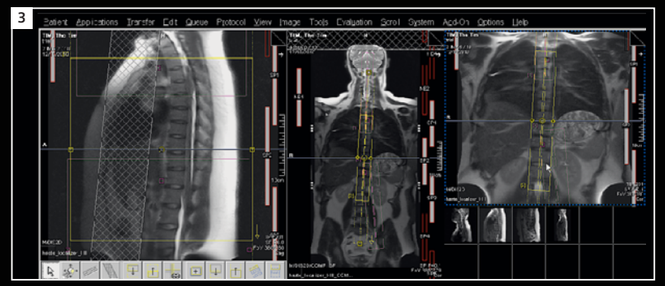

3 Tim Planning Suite (page 33).

4 *syngo* Composing (page 63).

*Direct link for US customers:
www.siemens.com/WebShop

Direct link for UK customers:
www.siemens.co.uk/mrwebshop

Case Reports: Susceptibility-Weighted Imaging (*syngo* SWI) at 3T

Kate Negus; Peter Brotchie, MBBS, Ph.D.

Barwon Medical Imaging, The Geelong Hospital, Geelong, Victoria, Australia

Introduction

This is a pictorial review of susceptibility-weighted imaging (*syngo* SWI) using a MAGNETOM Trio system with software version *syngo* MR B15 and a 32-channel head coil at The Geelong Hospital, Victoria, Australia.
syngo SWI is a 3D FLASH sequence that is flow compensated in slice, read and phase directions. The data received contains a combination of phase and magnitude information. The susceptibility-weighted images are produced by first filtering the phase images of unwanted field inhomogeneities and then weighting the magnitude images with this phase mask. Two maps are automatically calculated; phase mask multiplied magnitude images and SWI minIP (minimum intensity projection of 8 images on a sliding scale). In addition, the phase and magnitude images can also be produced by modifying the reconstruction tab card.
The SWI images are T2*-weighted and are enhanced by flow compensation and phase masking, so there is exquisite detail of areas of susceptibility due to venous blood, haemorrhage and iron storage.

The phase images can be windowed to see contrast between iron deposition and normal tissue and also to visualize gyral pattern to anatomically orientate lesions more accurately. The SWI sliding minIP is useful to visualize change in tissue susceptibility caused by structures such as veins that cross many slices.

SWI sequence details for all case studies: swi3d1r, transverse plane, TR 28 ms, TE 20 ms, flip angle 15, bandwidth 120 Hx/px, FOV 220 (FOV phase 84.4%), resolution 199 x 256, slice thickness 3 mm, 48 slices, voxel size 0.9 x 0.9 x 3 mm, 1 average, acquisition time 2:19 min.

Since SWI is more sensitive to haemorrhage than conventional T2* gradient echo imaging, we replaced the T2* gradient echo sequence with *syngo* SWI in all of our brain protocols. In order to do this without increasing scan time, the SWI sequence as provided by the standard protocol tree with the software version *syngo* MR B15 was modified by increasing the voxel size from 0.8 mm x 0.7 mm x 1.2 mm (resolution 256 x 384 and 1.2 mm slice thickness) to 0.9 mm x 0.9 mm x 3 mm (resolution 199 x 256 and slice thickness 3 mm), giving us lower resolution but allowing us to image the whole brain rather than only a section of it, in half the time of the standard sequence. The 3 mm slice thickness also correlates to our other brain sequences allowing direct comparison to be made.

The resolution is high enough to diagnose clinically relevant lesions and the sequence short enough to include in all protocols that would benefit from this new technique, without a time penalty. Whole brain coverage of our sequence means that lesions in unexpected locations would not be missed due to lack of coverage.

Case 1: Thrombosis and Associated Venous Infarct

Patient history

A 65-year-old male presented to our emergency department with dysphagia, word-finding difficulty and right sided weakness.

Imaging findings

Non-contrast CT identified a hypodense mass lesion in the left thalamus with a hyperdense border. Contrast CT and CT venogram demonstrated a segment of non-filling likely due to thrombosis in the left internal cerebral vein with associated venous infarct in the left thalamus. MRI was obtained to confirm the vein thrombosis and extent of infarction. Initial MRI on our Philips Edge 1.5T system confirmed a non-filling section of the left internal cerebral vein in keeping with thrombosis, extending to the vein of Galen. There was an area of susceptibility artefact in the gradient echo images in the left thalamus representing haemorrhage. There were 2 small foci of restricted diffusion in the left centrum semiovale likely related to the venous infarction, but no definite restricted diffusion involving the left thalamus or the left basal ganglia. MR spectroscopy of the basal ganglia region showed an increased lactate peak suggestive of ischaemia.

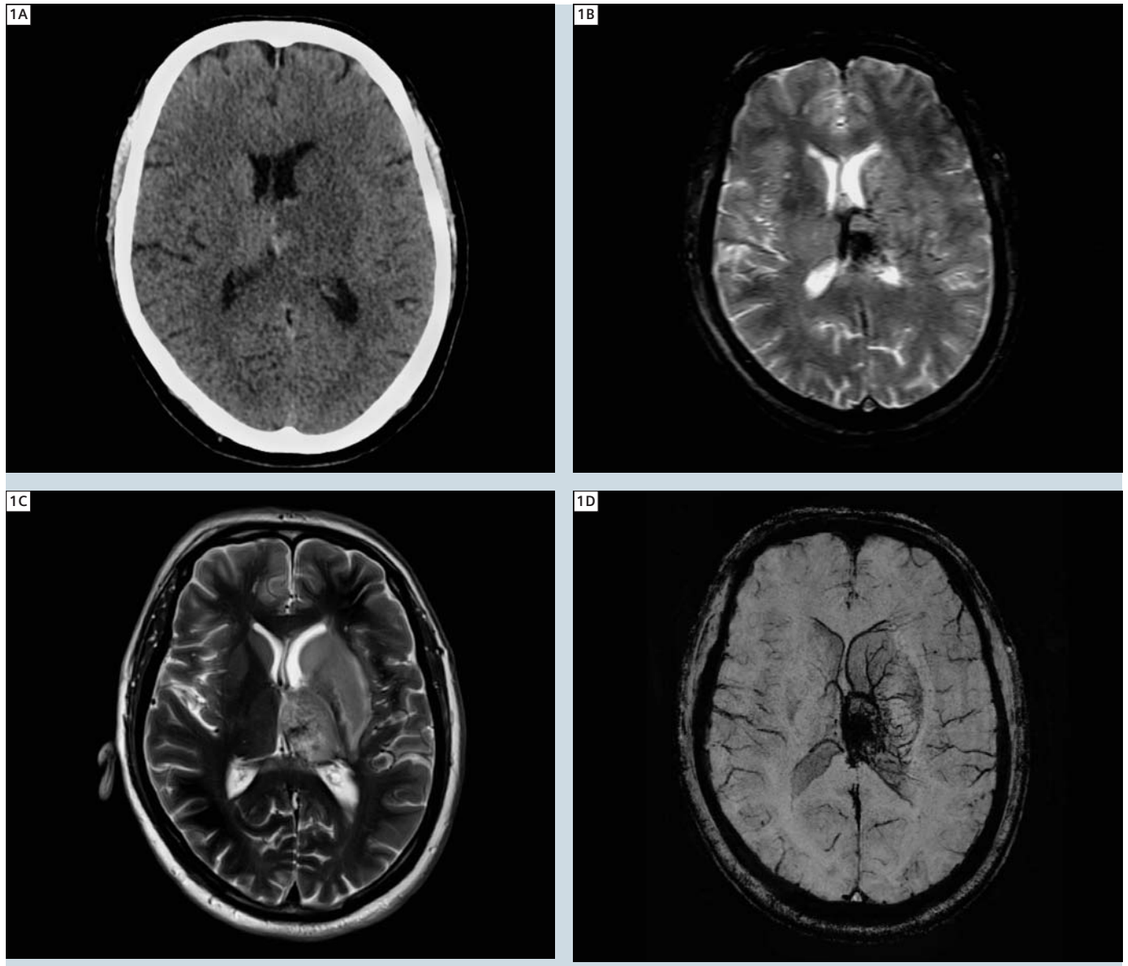

1 **A)** Native CT scan. **B)** T2* GRE at 1.5 Tesla. **C)** T2w TSE with *syngo* BLADE at 3 Tesla. **D)** Corresponding *syngo* SWI at 3 Tesla.

The patient was recalled to our Siemens 3T MAGNETOM Trio scanner the following day. The sequences performed included axial T2w, T1w, Diffusion-Weighted Imaging (DWI), Susceptibility-Weighted Imaging (*syngo* SWI) and MR venography. This imaging confirmed the left internal cerebral vein thrombosis and associated venous infarct.

Discussion

SWI nicely demonstrated the venous tributaries of the left internal cerebral vein with signal dropout due to the presence of deoxyhaemoglobin in the vessels. Signal dropout is also seen in the thrombosed internal cerebral vein and within the thalamic haemorrhage, demonstrating the high sensitivity but low specificity of this sequence.

Case 2: Amyloid Angiopathy

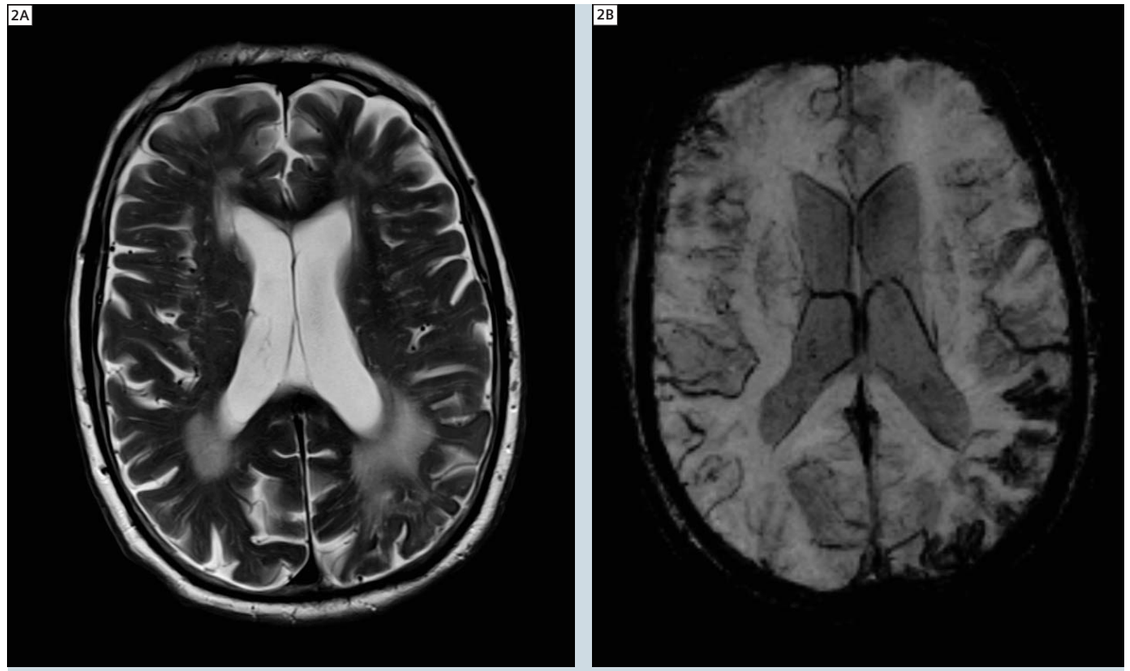

2 All images acquired at 3 Tesla. **A)** T2w TSE. **B)** *syngo* SWI.

Patient history

An 83-year-old male presented for MRI from the memory clinic query fronto-temporal dementia versus Alzheimers Disease with frontal features.

Sequence details

The standard dementia protocol was performed: T1 volume, axial T2, FLAIR, *syngo* SWI, DWI whole brain images with PRESS 30 MR spectroscopy of the parietal grey matter.

Imaging findings

Haemosiderin staining over the cortical surface of the frontal and parietal lobes was evident on the SWI, consistent with previous subarachnoid haemorrhage, most likely secondary to amyloid angiopathy.

Discussion

The SWI demonstrated signal loss due to haemorrhage which was not appreciable on the routine imaging. Micro haemorrhages in the arterioles of the grey matter may lead to vascular dementia associated with amyloid angiopathy. *syngo* SWI may provide useful information in the imaging of dementia.

Case 3: Cerebral haemorrhage in case of AVM

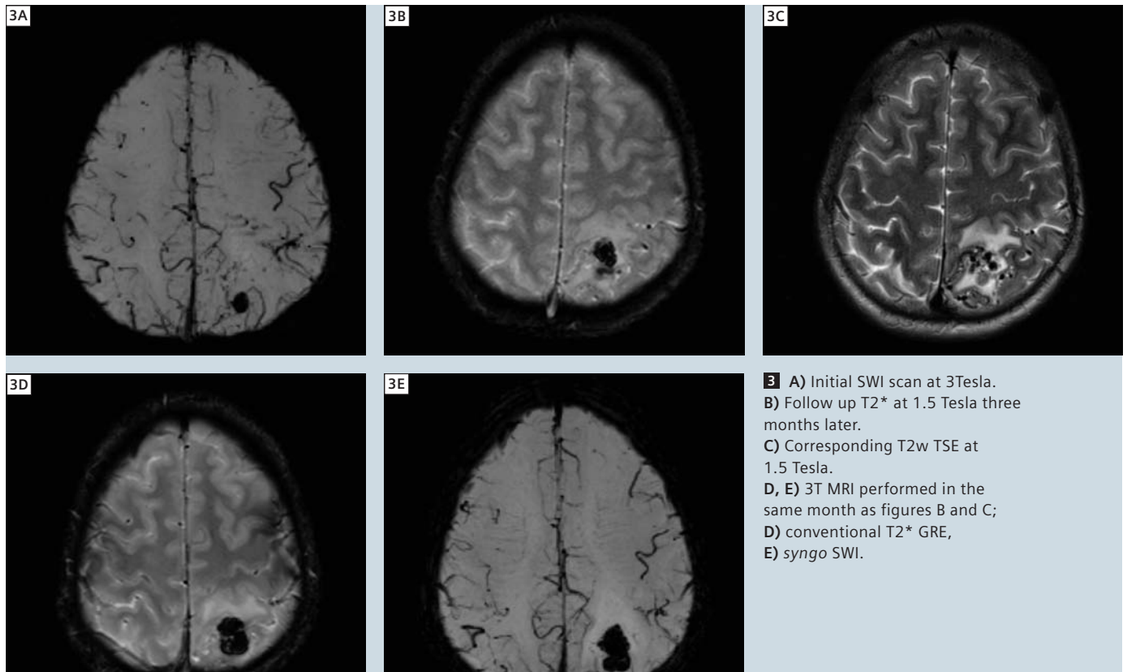

3 **A)** Initial SWI scan at 3Tesla.
B) Follow up T2* at 1.5 Tesla three months later.
C) Corresponding T2w TSE at 1.5 Tesla.
D, E) 3T MRI performed in the same month as figures B and C;
D) conventional T2* GRE,
E) *syngo* SWI.

Patient history

A 33-year-old male with a known brain arterio-venous malformation (AVM) presented to our emergency department with a history of 5 minutes of motor problems in his right hand. MRI was performed to rule out cerebral haemorrhage.

Sequence details

T1 volume, axial T2, FLAIR, field-echo whole brain images, 3D Time-of-Flight (TOF) and contrast-enhanced MR angiography and MR venography sequences were performed on our Siemens 1.5T MAGNETOM Avanto system.

Imaging findings

A collection of serpiginous flow-voids was evident within the left superior parietal lobule, similar in appearance to the patient's previous study. However there was a region of hypointense signal present within the region of the vascular malformation that was not visible on the SWI from a previous study performed on the patient 3 months prior. This was suspicious for acute haemorrhage.
The patient was recalled for SWI at 3 Tesla, so we could have a direct comparison with the previous imaging that was also performed on our 3T scanner. This demonstrated the development of a region of hypointensity situated centrally within the vascular malformation within the left parietal lobe, measuring 2.0 x 1.5 x 3.0 cm in size. On the previous imaging from 3 months prior, a small focus of hypointensity at this site was evident measuring 1 x 1 x 1 cm in diameter.

Discussion

The SWI appearance indicated the development of haemorrhage into the vascular malformation within the left parietal lobe, which had occurred since the previous study. The signal dropout on the SWI shows the margin of the haemorrhage and the associated anomalous vessels more accurately than other routine sequences.

Case 4: Traumatic haemorrhage

Patient history

48-year-old female presented to our emergency department with vomiting and headache after previously discharging herself following a diagnosis of cortical vein thrombosis.

Sequence details

Pre and post contrast T1 whole brain images, axial T2, DWI, *syngo* SWI whole brain images with MR venogram.

Imaging findings

syngo SWI demonstrated a number of hypointense foci within the sulci of the frontal lobes bilaterally and a number of extra-axial locations. These were associated with a number of small foci of restricted diffusion within the cerebral cortex. The history of recent head trauma, subsequently elicited from the patient, indicated that the appearance was most likely due to regions of extra-axial haemorrhage and small cortical contusions.

Discussion

SWI is more sensitive to very small areas of traumatic haemorrhage because of its higher resolution and better sensitivity to blood products than the routine sequences.

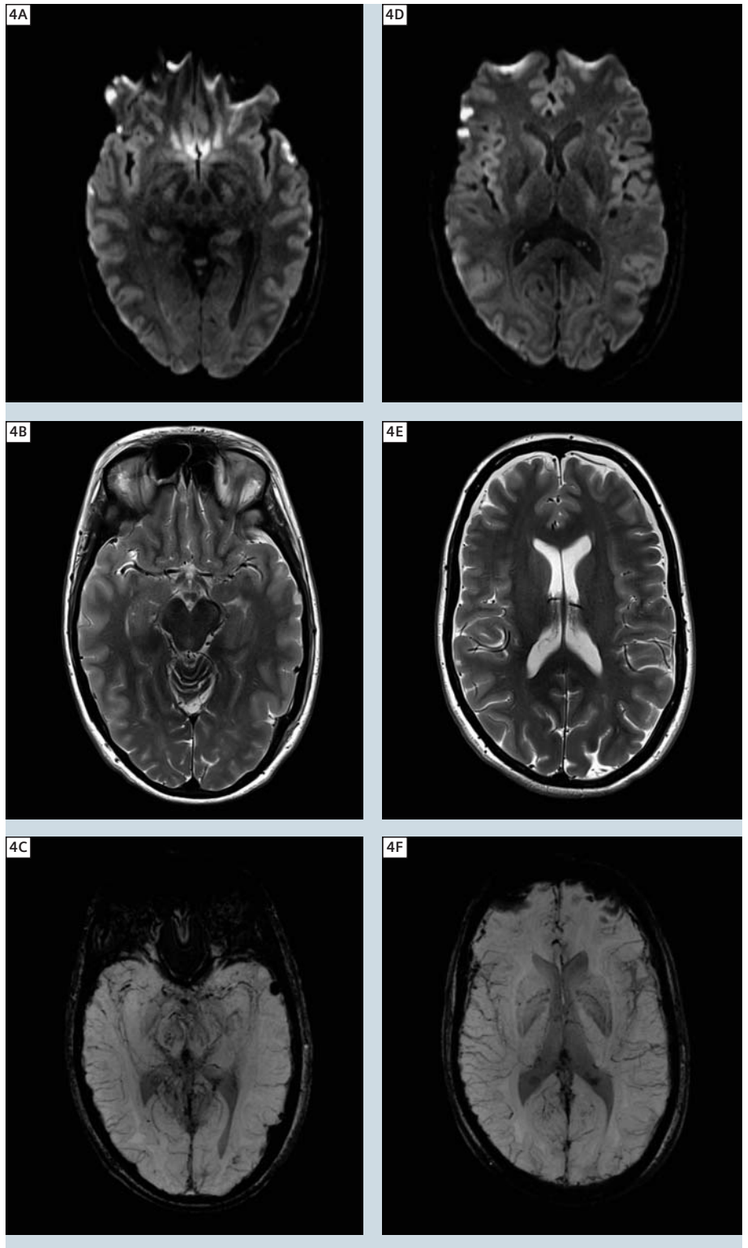

4 All images acquired at 3 Tesla. **A, D)** DWI **B, E)** T2w TSE 4 **C, F)** *syngo* SWI.

Case 5: Cerebral metastases in case of oesophageal adenocarcinoma

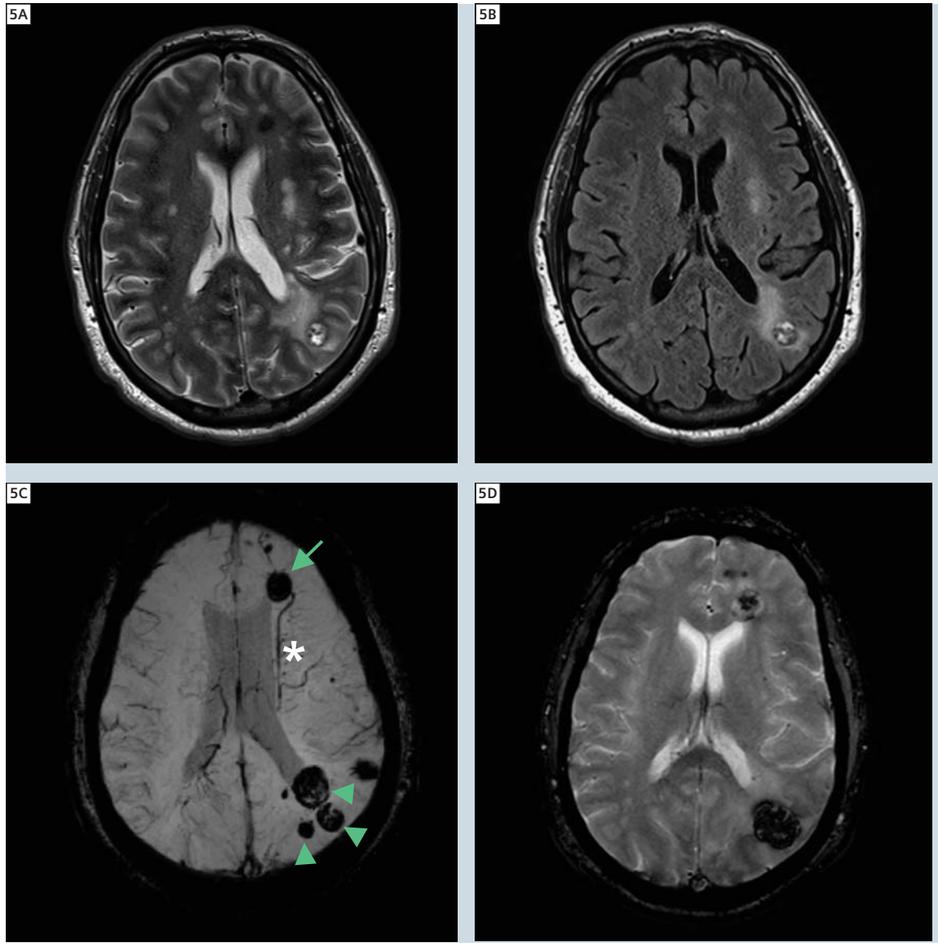

5 **A)** T2w TSE at 3 Tesla.
B) T2w FLAIR at 3 Tesla.
C) *syngo* SWI at 3 Tesla: cavernous haemangioma marked by arrow, DVA marked by asterisk, hemorrhagic metastases marked by arrowhead.
D) Follow-up after one month with a conventional T2* sequence at 1.5 Tesla.

Patient history

A 48-year-old male with oesophageal adenocarcinoma presented with right retro orbital pain for 8 weeks and was scanned for query cerebral metastases.

Sequence details

Pre- and post contrast T1 volume, axial T2, FLAIR, DWI, *syngo* SWI whole brain images, coronal T1, fat sat T2, post contrast fat sat T1 images of orbits and paranasal sinuses.

Imaging findings

No evidence of orbital mass or mass within the paranasal sinuses was demonstrated.
Numerous T2 hypointense lesions with marked signal dropout on SWI were evident throughout the left cerebral hemisphere. However, some of these were unaltered in appearance from the previous study from 2 years earlier and were consistent with cavernous haemangiomas. The others represent haemorragic metastases.

Discussion

The patient returned for a follow-up scan on our 1.5T MAGNETOM Avanto scanner 1 month later and standard T2* gradient echo imaging was performed. Compared to the 3T SWI, the standard gradient echo imaging at 1.5T is not as sensitive to the multiple haemorrhagic areas, failing to show some of the smaller lesions evident on the 3T SWI sequence.

Case 6: Haemorrhagic component of MCA infarction

6 All images acquired at 3 Tesla. **A)** DWI **B)** T2w TSE **C)** *syngo* SWI

Patient history

A 48-year-old female presented to our emergency department with sudden onset of left face, arm and leg weakness. CT brain was reported as right middle cerebellar artery infarction. MRI was performed to confirm this finding.

Sequence details

Pre- and post contrast volume T1, axial FSE T2, FLAIR, *syngo* SWI, DWI images of the whole brain and 3D TOF MRA circle of Willis.

Imaging findings

Abnormal signal was seen within the right caudate head and lentiform nucleus with significant susceptibility artefact within these structures that was most consistent with the presence of blood products. The pathology is contained within the middle cerebral artery distribution and appearances on *syngo* SWI are most consistent with a cerebral infarction with haemorrhagic transformation.

Discussion

The SWI sequence demonstrated the full extent of the haemorrhagic component of the infarction better than any of the routine sequences. The presence of haemorrhage with stroke is important to demonstrate as it changes treatment options.

Case study discussion

syngo SWI has allowed smaller susceptibility lesions to be demonstrated than previously possible, in cases of vascular malformation, tumor, stroke, trauma and dementia.
In many cases cited in the literature, SWI was the only imaging sequence to show the abnormality due to its increased sensitivity to iron content.
In all 6 of our cases the SWI sequence demonstrated increased detail of the pathology compared with the routine imaging sequences. In cases 2, 4 and 5, some lesions appeared to be too small to see on other imaging sequences, indicating how the sensitivity of *syngo* SWI may benefit diagnosis.
The increased signal and susceptibility effects at 3T enhance the use of *syngo* SWI, allowing full brain coverage in a short amount of time.

References

1 *syngo* SWI powered by Tim. Hot Topic by Siemens Healthcare. Available online at www.siemens.com/magnetom-world (go to Publications > Hot Topics).
2 Susceptibility Weighted Imaging, Opening new doors to clinical applications of Magnetic Resonance Imaging – E. Mark Haacke PhD Comment: MRM, 2004 Sep;52(3):612-618.
3 Susceptibility-weighted MR imaging: a review of clinical applications in children. Tong KA, Ashwal S, Obenaus A, Nickerson JP, Kido D, Haacke EM. AJNR Am J Neuroradiol. 2008 Jan;29(1):9-17. Epub 2007 Oct 9. Review.
4 Susceptibility-weighted imaging to visualize blood products and improve tumor contrast in the study of brain masses. Sehgal V, Delproposto Z, Haddar D, Haacke EM, Sloan AE, Zamorano LJ, Barger G, Hu J, Xu Y, Prabhakaran KP, Elangovan IR, Neelavalli J, Reichenbach JR. J Magn Reson Imaging. 2006 Jul;24(1):41-51.
5 Reliability in detection of hemorrhage in acute stroke by a new three-dimensional gradient recalled echo susceptibility-weighted imaging technique compared to computed tomography: a retrospective study. Wycliffe ND, Choe J, Holshouser B, Oyoyo UE, Haacke EM, Kido DK. J Magn Reson Imaging. 2004 Sep;20(3):372-7.

Contact
Kate Negus
MRI Supervising Technologist
Barwon Medical Imaging
The Geelong Hospital
PO Box 281
Geelong, 3220, Victoria, Australia
Phone: +61 3 5226 7070
katen@barwonhealth.org.au

Assoc. Prof. Peter Brotchie, MBBS, Ph.D.
Director MRI
Barwon Medical Imaging
The Geelong Hospital
Geelong, 3220, Victoria, Australia
Phone: +61 3 5226 7032
peterbr@barwonhealth.org.au

3T MR Imaging of Peripheral Nerves Using 3D Diffusion-Weighted PSIF Technique

Avneesh Chhabra[1], M.D.; Theodore Soldatos[1], M.D.; Aaron Flammang[1]; Wesley Gilson[1]; Abraham Padua[2]; John A Carrino[1], M.D., M.P.H.

[1]Johns Hopkins University, Baltimore, MD, USA
[2]Siemens Healthcare, MR RD Management, Malvern, PA, USA

High-resolution magnetic resonance (MR) Neurography is a novel imaging technique, which enables multiplanar imaging of peripheral nerves, as well as diagnosis and localization of entrapment and non-entrapment peripheral neuropathies related to etiologies, such as inflammation, tumor and trauma. Typically, MR Neurography techniques utilize a combination of fat-saturated T2-weighted, short inversion time recovery (STIR), or T2 spectral adiabatic inversion recovery turbo spin echo (T2 SPAIR TSE) images for the detection of the nerve signal, contour and size changes, as well as T1-weighted spin echo or fluid attenuated long inversion recovery (FLAIR) images for the anatomic assessment of the involved areas, based on the abundant intra- and perineural fat. However, the diagnostic ability of conventional MR Neurography is limited in the evaluation of smaller peripheral nerves of the axial and appendicular skeleton, where the similar caliber and T2 signal intensity of peripheral nerves and adjacent vessels render discrimination of the above structures difficult, if not impossible. Since nerve injuries and entrapments commonly lead to effacement of perineural fat in the area of involvement, T1-weighted images are often not helpful. In addition, an attempt to suppress vascular signal with saturation bands often fails in distal locations of the body, as the peripheral nerves frequently course through various obliquities.

Table 1: Acquisition parameters for 3D-PSIF at 3T

The typical acquisition parameters employed for the 3D-PSIF sequence in a Siemens 3T MAGNETOM Verio scanner. The spatial resolution of this technique yields 0.9 x 0.9 x 0.9 mm voxel sizes and, whenever possible, this dimension is preserved. When examining areas requiring larger or smaller coverage, the scan matrix and the FOV are adjusted accordingly. This and number of slices are all that is changed. Scan time is typically kept below 6 minutes 30 seconds through the use of parallel acquisition. High quality thin MIP projections are rendered for display purposes.

Acquisition parameter	Value
Slabs	1
FOV	172 mm
Slice thickness	0.9 mm
TR	12 ms
TE	4.1 ms
Averages	1
Coil	8-channel knee coil
PAT	GRAPPA 2
Flip angle	30
Fat suppression	Water Excitation Normal
Diffusion mode	Phase
Diffusion moment mT/m*ms	85
Diffusion directions	1
Dimension	3D
Elliptical scanning	On
Asymmetric echo	Off
Receiver bandwidth	230 Hz/Px
Acquisition time	4 min 37 sec

Due to recent advances in 3T MR imaging with incorporation of optimized extremity coils and new pulse sequences, 3-dimensional high-resolution and high-contrast demonstration of the peripheral nerves is possible. The 3-dimensional diffusion-weighted sequence based on reversed fast imaging with steady-state precession (3D-PSIF) has been recently implemented in high-resolution MR Neurography imaging protocols and has a potential to overcome most of the above mentioned challenges in small peripheral nerve imaging. The 3D-PSIF is a balanced gradient echo steady-state free precession (SSFP or PSIF) sequence with inherent features of a spin-echo sequence, as compared with other unbalanced spoiled or refocused gradient-echo techniques, such as fast low-angle shot (FLASH), fast field-echo, and gradient recall acquisition using steady-states (GRASS or FISP). Therefore, the 3D-PSIF sequence demonstrates less influence of local magnetic field inhomogeneities on the spin relaxation. The water-excitation technique enables uniform fat suppression and is unaffected by the chemical shift effect. Although 3D-PSIF may also be performed without fat saturation, fat-suppressed images usually provide better nerve-to-background contrast ratio. In addition, the application of diffusion moment provides suppression of water signal. In most cases, a diffusion moment value of 80–90 mT/m*ms provides an acceptable compromise in peripheral nerve-to-background contrast and image signal-to-noise ratios (SNR). Since the signal depends strongly on the steady-state condition, all moving structures, such as flowing blood, demonstrate a loss of signal intensity. As a result, the high T2 signal intensity of peripheral nerves is effectively differentiated from the nulled signal of adjacent vessels (Figs. 1, 2). Although 3D-PSIF images provide predominantly T2 contrast, there is a potential to perform post-contrast imag-

1 Sagittal 3D-PSIF image of the forearm and wrist demonstrates the median nerve (arrow) along its entire course.

2 Coronal 3D-PSIF image of the lumbosacral plexus demonstrates excellent discrimination of the nerve roots from adjacent soft-tissue structures.

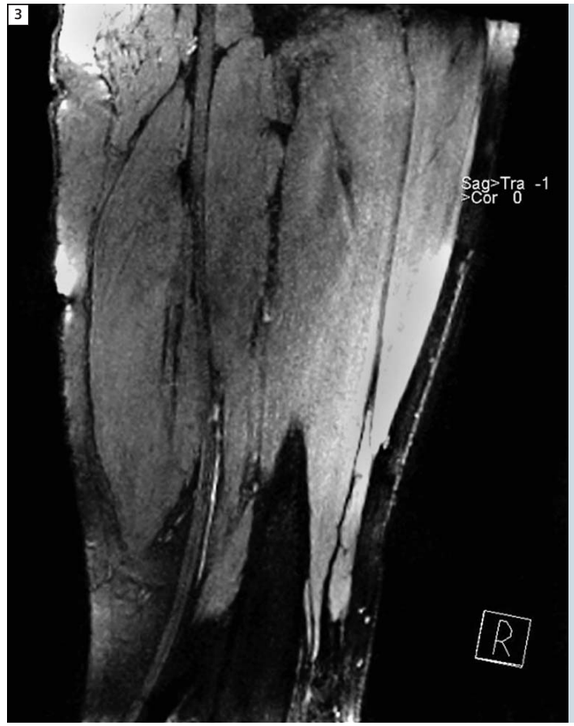

3 Coronal 3D-PSIF maximum intensity projection (MIP) of the thigh demonstrates the course of the sciatic nerve.

ing following administration of intravenous gadolinium. In 3D-PSIF imaging, the acquisition of isotropic voxels enables the data set to be reformatted into any imaging plane without significant loss of resolution. The latter feature may provide confirmation of anatomic continuity, as well as identification of branching, focal enlargement, course deviation and/or displacement of peripheral nerves. In addition, maximum intensity projections (MIPs) can be employed to further enhance the conspicuity of the nerves and provide images, which can be distributed to referring physicians for better depiction and understanding of nerve anatomy and pathology (Fig. 3). Table 1 displays the typical acquisition parameters employed for the 3D-PSIF sequence in a Siemens 3T MAGNETOM Verio scanner. In clinical practice, 3D-PSIF has proven more efficient than the conventional STIR and T2 SPAIR TSE sequences in differentiating small peripheral nerves from adjacent vessels. In the extremities, and particularly distal to the knee and elbow joints, the commonly encountered T2 hyperintense subcutaneous and/or fascial edema restricts the identification of small peripheral nerves on conventional T2-weighted sequences. In contrast, the inherent diffusion sensitive gradients of 3D-PSIF enable selective suppression of the water signal of the stationary subcutaneous and fascial edema, thus improving the conspicuity of small peripheral nerves in the above areas. On the other hand, the inherent high TE values of 3D-PSIF images result in lower SNR as compared to conventional fat-saturated T2-weighted images, which remain superior in delineating the fascicular structure of the nerves. In post-contrast imaging, as compared to the three-dimensional volumetric interpolated breathhold examination (3D VIBE) sequence, the 3D-PSIF technique provides better visualization of the nerve fascicles, as well as more adequate assessment of the anatomic relationship between fascicles and enhancing intraneural and/or extraneural tumors.
In summary, the 3D-PSIF sequence with high spatial resolution and high contrast provides reliable and objective identification of peripheral nerve anatomy and may be incorporated as part of the high-resolution MR study of peripheral nerves, whenever accurate nerve localization and/or pre-surgical evaluation are required.

→ Don't miss the talks on peripheral nerve imaging on www.siemens.com/magnetom-world

- Imaging of peripheral nerves – status quo by Mirko Pham University of Heidelberg, Germany
- Peripheral nerve imaging from head to toe by Meng Quan-Fei. The First Affiliated Hospital of Sun Yat-sen University, Guangzhou, China

Contact
John A. Carrino, M.D., M.P.H.
Associate Professor of Radiology and Orthopedic Surgery
Section Chief, Musculoskeletal Radiology
The Russel H. Morgan Department of Radiology and Radiological Science
601 North Caroline St. /JHOC 5165
Baltimore, MD 21287-0856
USA
carrino@jhmi.edu

Full Spine Imaging utilizing the Tim User Interface

James Hancock

MRI Radiographer Benson Radiology, Adelaide, South Australia

Planning a full spine with Tim

Positioning technique

- The spine coil is on the table and is plugged in.
- Place the base of the head coil on the table and plug it in.
- Place the base of the C-spine coil on the table and plug it in.
- Position the patient on the examination table with the head comfortably placed in the head coil. Shoulders against the neck coil.
- The triangular leg pad should be placed to reduce back strain.
- Place the top half of the c-spine coil on and clip it into place (this depends on patient size).
- Use the laser to centre on the indicated position on the neck coil.
- Press the isocenter button to move the patient into the magnet bore.

1 Patient positioning.

Tim planning

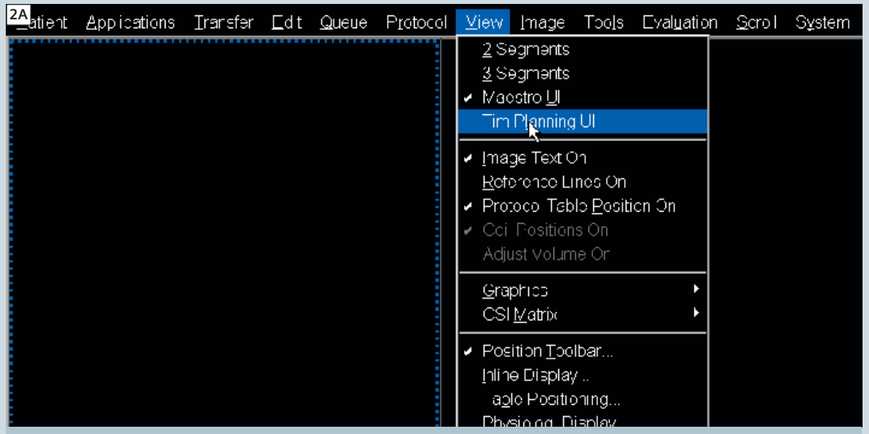

2A Open the Tim Planning Suite from the drop-down menu.

- When performing a full spine examination you need to activate the Tim Planning Suite user interface.

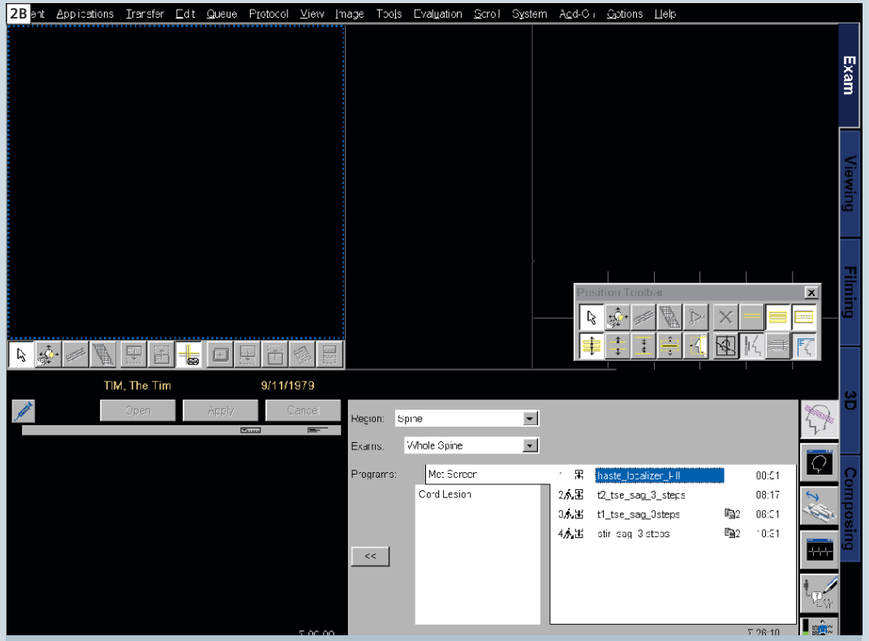

2B The Tim user interface.

- Figure 2B shows the layout for the Tim User Interface. Depending on the clinical indication, at our institution we have two basic protocols saved for full spine imaging: The "Met Screen" protocol can be used for all full spine examinations except in the presence of a potential cord lesion when the "Cord Lesion" protocol should be used instead, as the sagittal slices are thinner and there are more of them.

Running the localizers

- First step to planning is to run the localizers. Drag the appropriate HASTE localizer into the queue for running. This localizer begins in the cervical spine then moves the table before running localizers in the thoracic and lumbar spine. We end up with three localizers in the running queue. Thus it covers three stations. Once complete, Tim composes these three stations into one complete image for the entire spinal cord in both sagittal and coronal planes. These images allow us to plan the setup for the rest of the scans.

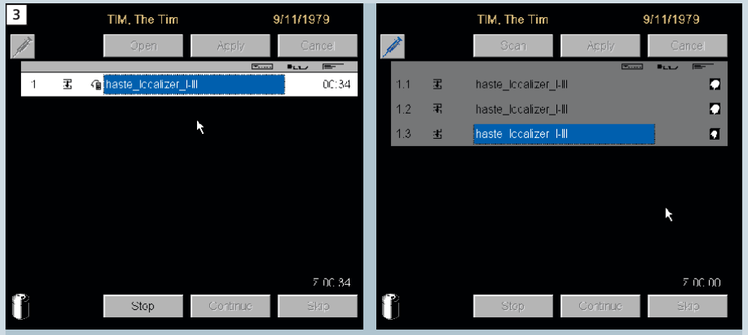

3 The measurement queue with the 3 localizers.

Setting up the correct fields-of-view

- Drag the T2 sagittal sequences across into the queue and open it. This sequence displays three separate sub protocols one for each region of the spine.
- When setting up for a full spine it is best to take a systematic approach.
- Initially set up your FOV to ensure that you are going to cover the entire spine. This involves placing a composed sagittal image of the full spine into the middle rectangular window.
- When setting up your FOV coverage, ensure that "coupled graphics" is on. This can be achieved by right clicking in any of the three boxes and selecting the option.
- With "coupled graphics" on you can then move your FOV and position it appropriately for the correct coverage. See the example in figure 4.

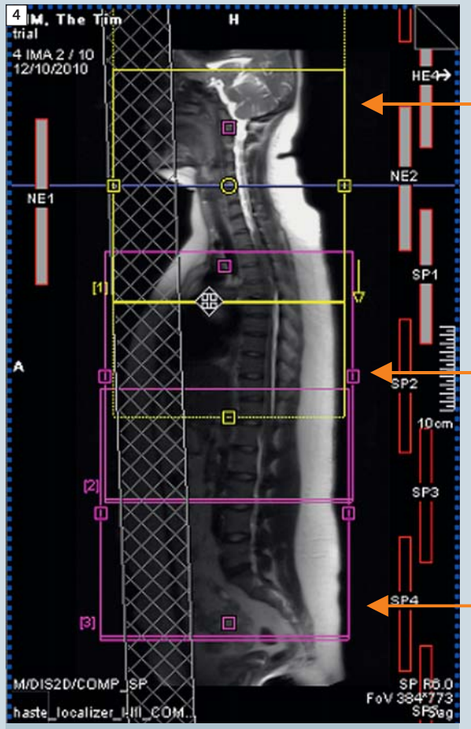

Note the three separate FOV boxes. The upper FOV is yellow, indicating that it is currently active. By utilising "coupled graphics" you can grab and drag all of the three and move them as one. This makes setting up your coverage very easy. Each FOV is also numbered and you can select them by clicking on the little numbers.

4 Easy FOV set up to cover the whole spine.

Setting up the slice positions
C-Spine

- Once the FOV has been set you need to set the slice group locations for each of the subgroups. Applying a systematic approach, begin with the cervical spine.
- The best way to do this is to load your individual C-Spine station localizer and place it into the two square windows. One of these should be a sagittal and the other should be a coronal.
- In the rectangular window place the composed full spine image and choose the coronal orientation.
- Position the C-Spine slice group. Before moving any of the slice groups take "coupled graphics" off. This will allow you to work with and angle an individual group of slices.

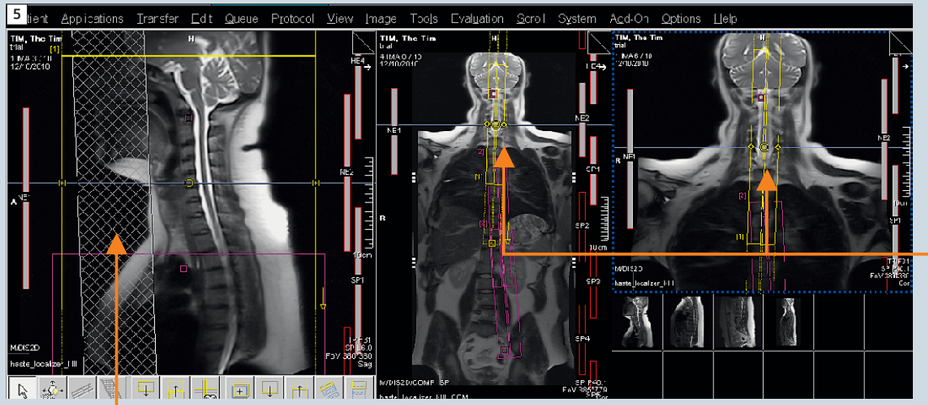

Using the Coronal localizer in these boxes lets you locate your slice group and angle appropriately. With "coupled graphics" off, the changes you make only affect this individual slice group.

By having a sagittal localizer in this box you can keep an eye on your FOV.

T-Spine

- Once you are happy with the C-Spine slice group location you can move on to the T-Spine. Again to set this up follow the same systematic approach.
- Load a sagittal and coronal T-Spine localizer image into the square windows.
- Keep the Full Spine coronal image in the rectangular window.
- To select the thoracic spine subgroup click on the small number 2 displayed next to the second subgroup. You will know you have the group selected as it will turn yellow.
- With "coupled graphics" off you can now proceed to angle the slice group to follow the thoracic spine. You will note that there is some overlap between groups 1 and 2 – this is needed for the composing process later on.

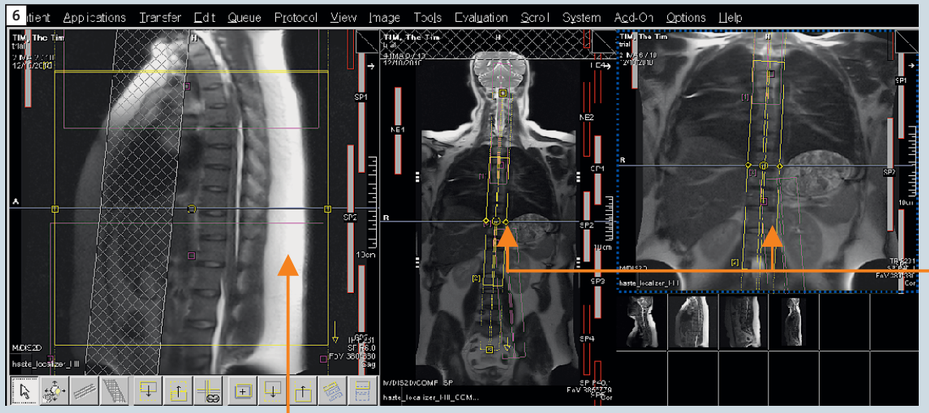

Using the coronal localizer in these boxes lets you locate your slice group and angle appropriately. With "coupled graphics" off, the changes you make only affect this individual slice group.

By having a sagittal localizer in this box you can keep an eye on your FOV.

L-Spine

- Once you are happy with the T-Spine slice group location you can move on to the L-Spine. Again to set this up follow the same systematic approach.
- Load a sagittal and coronal L-Spine localizer image into the square windows.
- Keep the full spine coronal image in the rectangular window.
- To select the lumbar spine subgroup click on the small number 3 displayed next to the third subgroup. You will know you have the group selected as it will turn yellow.
- With “coupled graphics” off you can now proceed to angle the slice group to follow the lumbar spine. You will note that there is some overlap between groups 2 and 3 – this is needed for the composing process later on.

By having a sagittal localizer in this box you can keep an eye on your FOV.

Using the coronal localizer in these boxes lets you locate your slice group and angle appropriately. With “coupled graphics” off, the changes you make only affect this individual slice group.

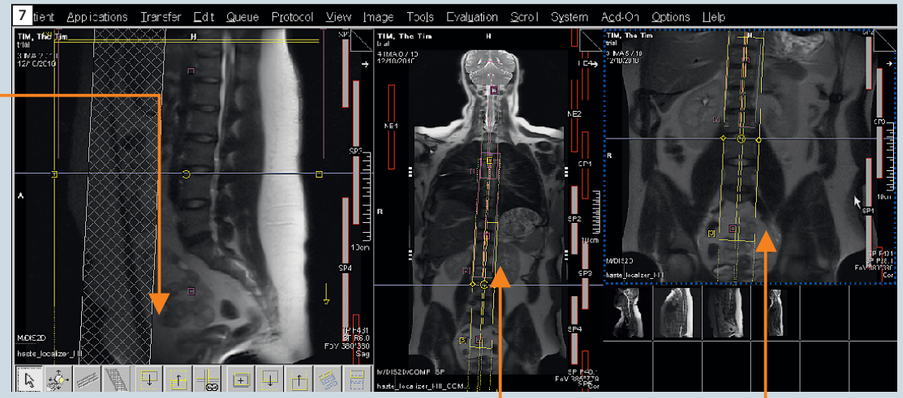

Important notes

- Any presets that you position will affect all three subgroups.
- Changes made to one subgroup will not affect the other groups, so never assume!
- Overlaps are built into the protocols. Be careful when setting up your FOV. Keep these overlaps in place to ensure smooth composing of final images. Thus, when setting up your FOV leave “coupled graphics” on.
- When setting up your slices for the sagittal sequences you will often be angling in the A-P (coronal) plane to follow the spine. Avoid using big differences in angle between one group and another. Too much angle will affect the composing software.
- If the patient is very scoliotic then you can try adding more slices to allow you to cover the region.
- Worst case scenario: Choose your angles for each region of the spine, but you will not be able to compose a full spine image. This may be necessary if the patient is very scoliotic.
- Avoid in-plane rotation as this will cause composing to fail.
- Rotation of subprotocols in the F-H (axial) plane should be avoided. A difference of just 1 degree between subprotocols will cause composing to fail.
- If you need to repeat a region of the spine due to patient movement then you only need to select the region affected by the movement and rerun that particular subgroup. See the example in figure 8.

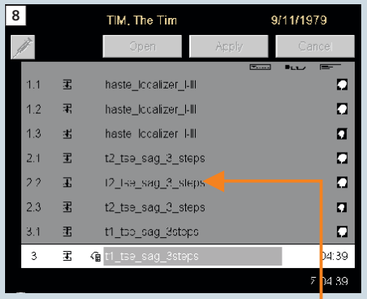

You can see how each subgroup for the T2 sagittals has its own number: 2.1, 2.2, 2.3 etc. Thus if you need to rerun a region simply hold shift and click the one you need to repeat. Drag and drop that region back into the queue. A cross will run through the compose indicator, showing that it is only going to run that one region again.

Performing your axial scanning

- Axial scans can be planned for each individual region as per normal.
- Make use of a nicely composed full spine sagittal image in the rectangular window and an individual region coronal image in one of the square windows to aid in planning.
- With “autocoil select” on wherever you move a slice group, the appropriate coils will be switched on.
- Run the required axial sequences which can be taken from the individual spine protocols as needed.

Using the Compose Task Card

- All full spine sagittal images need to be sent to the composing task card where they are filtered and stitched together. To do this we access the individual sequences from the browser and send them to be composed.

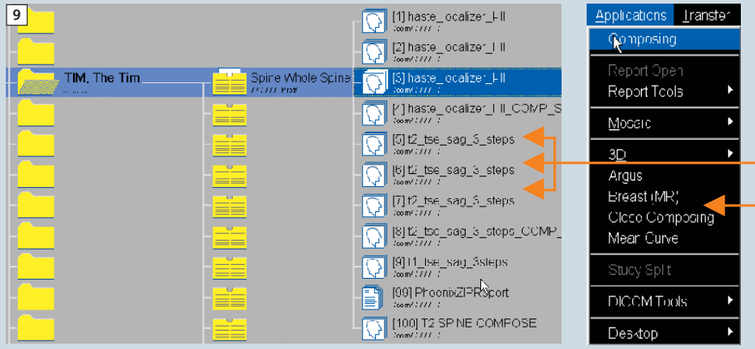

In the browser you select each individual step by holding control and clicking each step with the mouse. This process is performed individually for each type of contrast be it T2, T1 or STIR.

Once you have selected the individual sequences the composing function is found under the Applications menu. Click this and it will open composing.

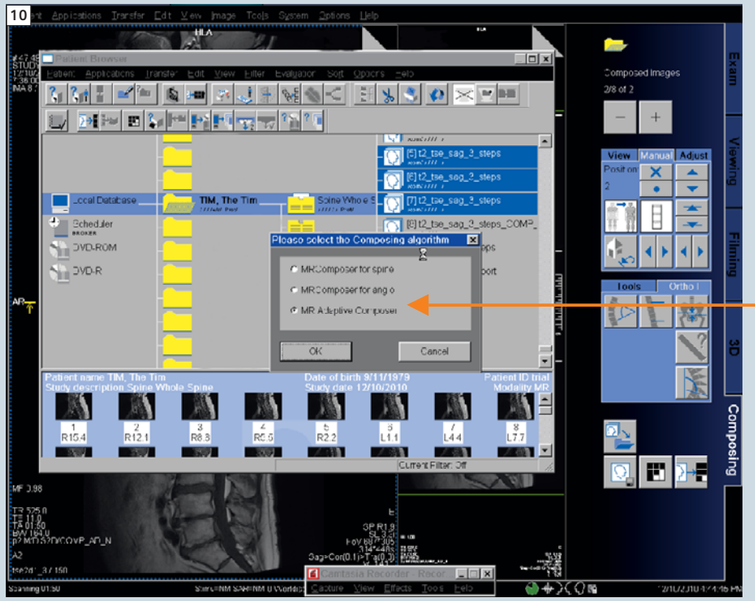

When composing, the software will open and ask you which algorithm you wish to use. Always choose “Adaptive”.

Initially your composed images will look like those opposite. We run a normalize filter across the images which helps to smooth out the signal and stitching points.

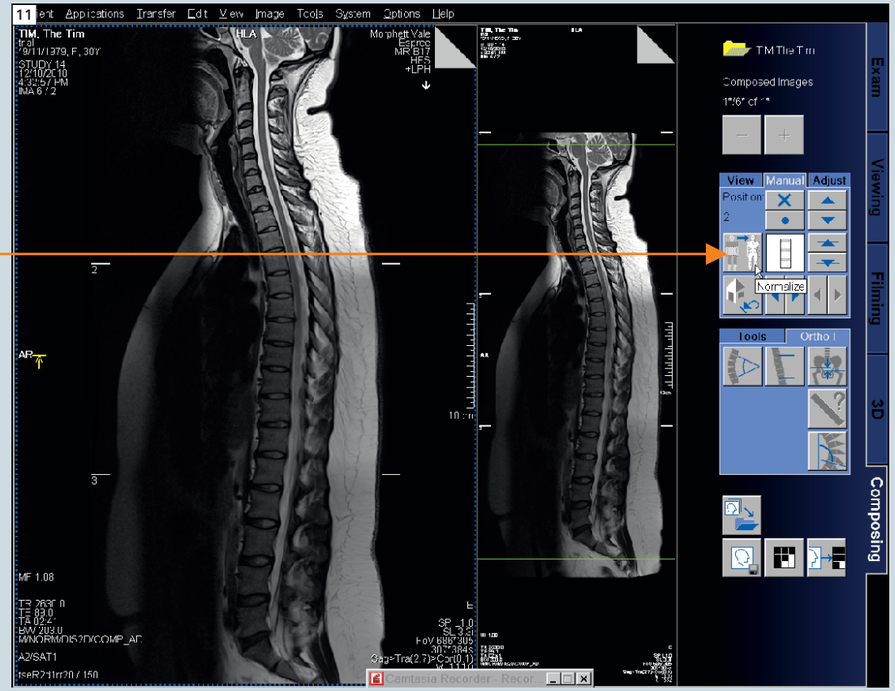

Once the images have been normalized you need to save the entire series, thus select "Save all As" as shown. Give the sequence a name such as T2 SAG Compose, etc. Ensure you save them as a new series. Repeat the process for the other sagittal contrast weightings.

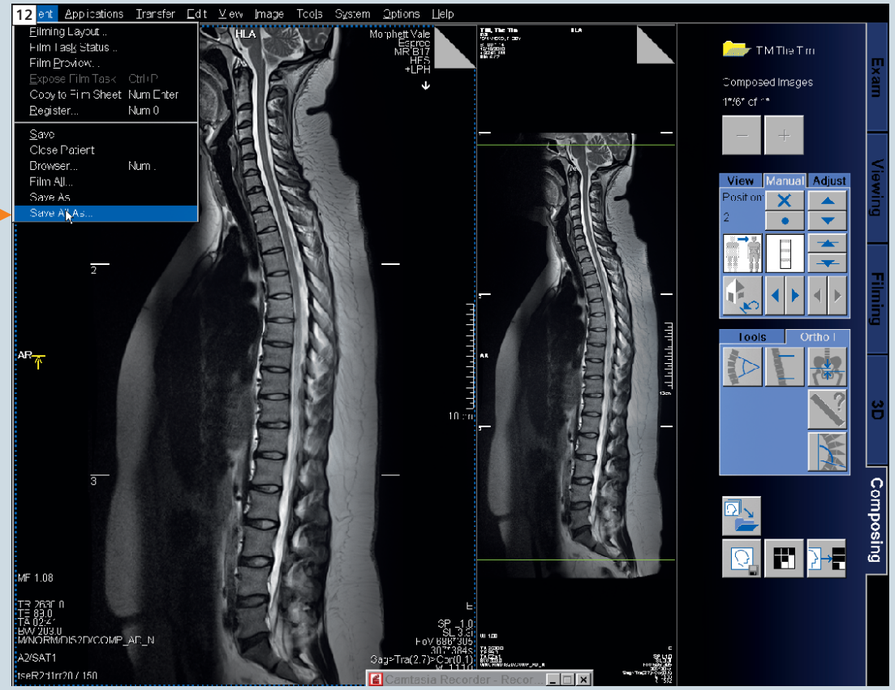

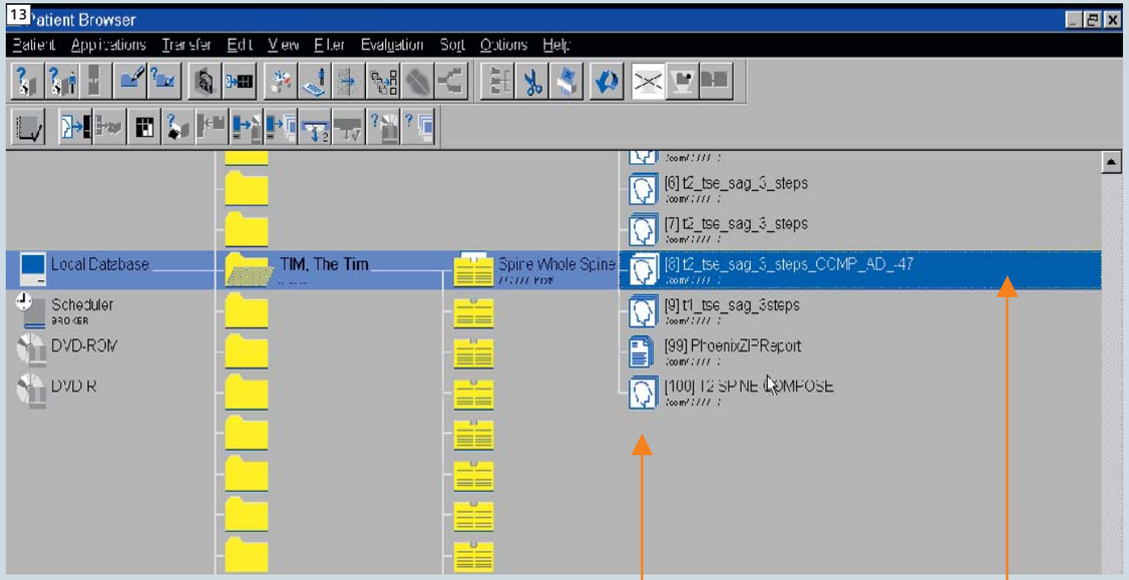

The saved series will appear in the browser and you can then send it to viewing and film it. The initial compose images are highlighted in blue (long red arrow) with our saved series appearing at the bottom of the list (short red arrow). Your composed series can be sent to PACS from here also.

Contact
James Hancock
Benson Radiology
Adelaide
South Australia
James.Hancock@bensonradiology.com.au

Knee Imaging with 4-Channel Flex Coils. The Influence of Patient Positioning and Coil Selection on Image Quality

Birgit Hasselberg; Marion Hellinger

Siemens Healthcare, Erlangen, Germany

2

2 Patient positioned for an examination of the right knee. Both knees are positioned in one plane.

3

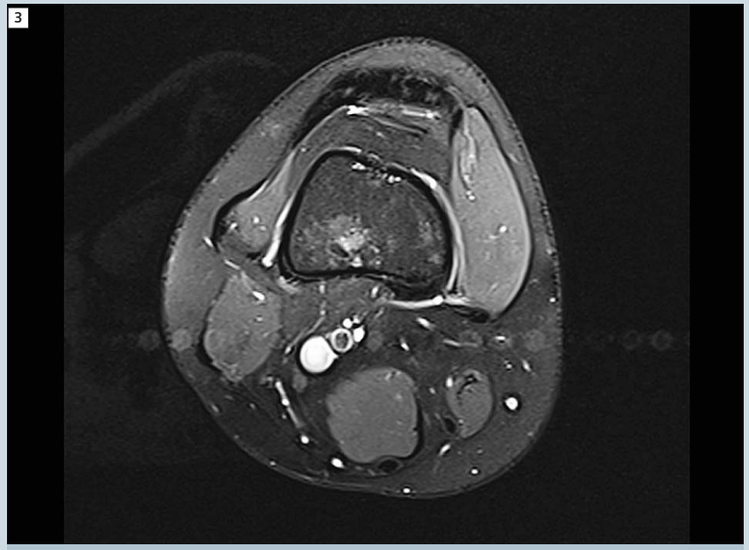

3 Using the Siemens protocol from clinical library arthrography Pd_tse_fs_tra_320, due to incorrect patient positioning, infolding effects of the not examined left knee are visible.

− Wrong

Correct patient positioning and the selection of the right coil have a huge influence on image quality as the following examples clearly show.

The patient is positioned supine on the table in feet-first orientation.
In the first case, the patient lies straight on the table; both knees are positioned in one plane.
The resulting transversal clinical image shows aliasing effects from the left knee (which is not being examined) in the left-right phase-encoding direction.

4

4 Patient correctly positioned for knee exam. The knee not being examined is positioned on a cushion.

5

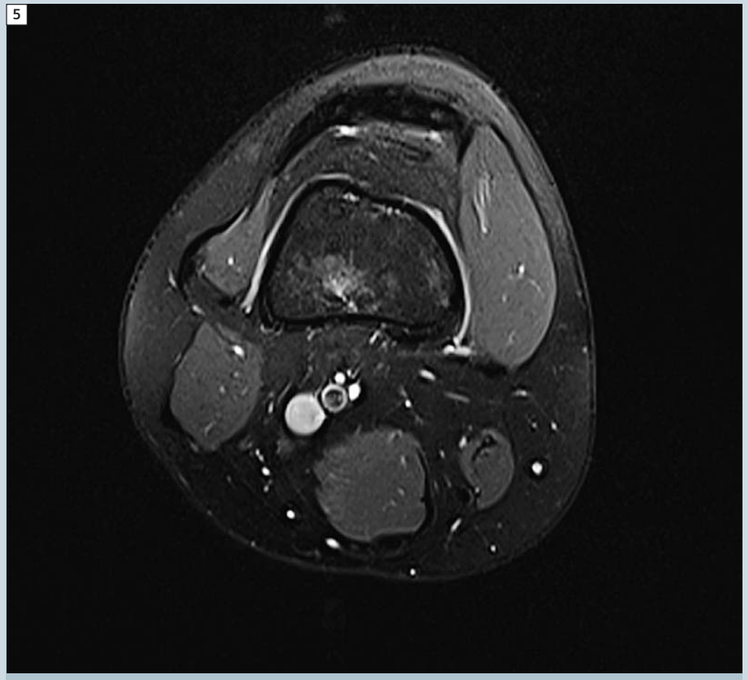

5 Again using the Siemens protocol from the clinical library arthrography Pd_tse_fs_tra_320. No infoldings due to correct patient positioning.

+ Right

Done right, the patient is again positioned supine on the table in feet first orientation. However, in this case the left knee is raised by a cushion in order to avoid the aliasing effect. The knee which is not examined is positioned higher than the examined knee.
The resulting transversal image shows no aliasing effects.

6 A small knee positioned in a large 4-channel flex coil.

Wrong

Besides correct patient positioning, the size of the knee in combination with the chosen coil has an effect on the image quality. The so-called “coil filling-factor” is demonstrated below. When you choose a coil which is too large for the examined body part, you get less overall signal which results in a minor image quality.

In the first case, the large 4-channel flex coil is used for the examination of a small knee.
The resulting sagittal series shows minor image quality: apart from minor signal-to-noise ratio, this also results in inhomogeneous signal distribution as well as fat suppression.

7 T1_tse_fs_sag_256 of a small knee in a large 4-channel flex coil, resulting in minor image quality.

8 A small knee positioned correctly in a small 4-channel flex coil.

Right

In the second case, the small 4-channel flex coil is used for the examination of a small knee. At the popliteal fossa we left the coil open
The resulting sagittal image shows a good SNR with an adequate image quality.

9 T1_tse_fs_sag_256 of a small knee examined with a small 4-channel flex coil, resulting in good SNR, good image quality. Compared to figure 7 there is good contrast and homogenous fat saturation in the bone.

1 4-Channel Flex coil large and small

Finally, remember to position the patient in the isocenter of the magnet. The flexibility of the large and small 4-channel flex coils gives perfect support in optimal left-right positioning. As shown above, the 4-channel flex coils come in 2 sizes and are part of the standard system configuration. They provide superior signal-to-noise-ratio (SNR) and can be used for the examination of various body parts. The wrap around coil is made of soft and flexible material. Due to its 4-channel design it is iPAT-compatible. The coil can easily be combined with other coils such as Spine 32 and Body 18.

In summary, we can state that in knee examinations correct patient positioning and the selection of the right coil have a huge influence on the resulting clinical images.

Contact
Marion Hellinger
Siemens Healthcare
H IM MR PLM AW T Workflow
Allee am Roethelheimpark 2
D-91052 Erlangen
Germany
marion.hellinger@siemens.com

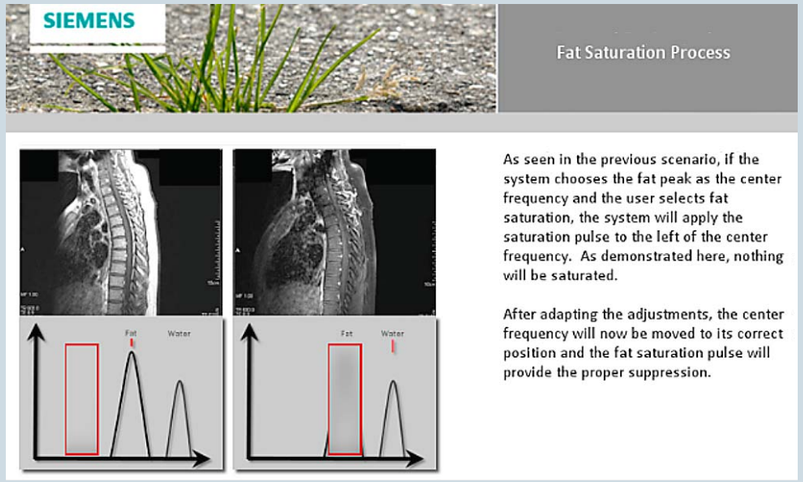

→ **Get free-of-charge application training at www.siemens.com/magnetom-world**

In this 8 min online training on fat saturation you will learn

- how to identify the fat and water peaks
- to calculate fat and water separation
- to perform the optimal fat saturation process

→ **Visit us at www.usa.siemens.com/fatsat-video**

Case Report:
Knee MR Imaging of Haemarthrosis in a case of Haemophilia A

M. A. Weber; J. K. Kloth

University Hospital Heidelberg, Department of Diagnostic and Interventional Radiology, Heidelberg, Germany

Background

In daily patient-care imaging of joints in childhood is often still a domain of x-ray and ultrasound. However, the application of MRI in pediatric imaging is of growing importance not only because of the excellent soft tissue contrast and the superior capacity of this technique to visualize and evaluate the extension of involvement of soft tissues but also because of its capability to early and precisely detect bone destruction. In addition to its high sensitivity, MRI is also an invaluable tool to rule out differential diagnoses e.g. malignancies. However, MR in pediatrics requires different imaging approaches to those for adults. Imaging speed and high resolution are key elements. And since these two requirements are in direct conflict, several working groups recommend the usage of 3Tesla MR in combination with multi-channel coils to overcome at least partially the contradiction of fast and highly resolved MR scans in children.

Patient history

In this case we report on the imaging findings of a 14-year-old male adolescent with known haemophilia A. Very often these patients present after an initial traumatic event with recurrent bleedings into the large joints, dominantly in the knees but also hips, shoulders etc. Bleeding into muscles can also occur, but this is less common than in the joints. Recurrent haemarthrosis causes early destruction of the joints. Severe pain and disability are the most

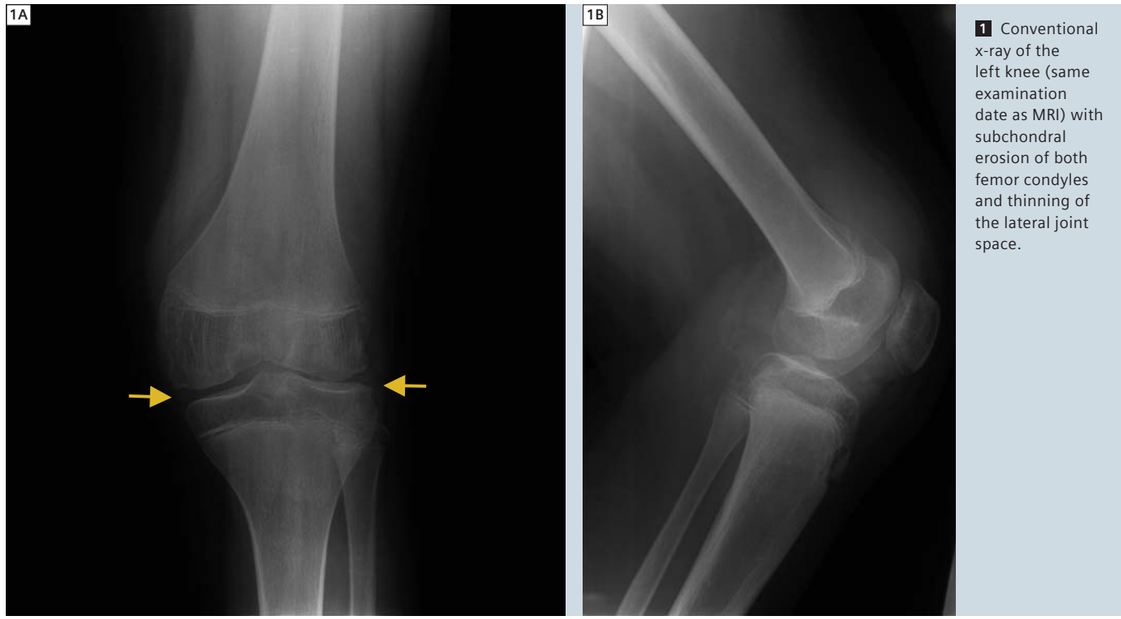

1 Conventional x-ray of the left knee (same examination date as MRI) with subchondral erosion of both femor condyles and thinning of the lateral joint space.

2 Sagittal PD-weigthed TSE MRI. Erosion of the anteriomedial femur condyle is shown (arrow).

common but also very unspecific clinical symptoms and can have different causes in childhood and adolescence (e.g. aseptic osteonecrosis).
The said patient presented with these unspecific symptoms in the ambulance of our orthopedics department. Haemophilia A was already known und multiple events of haemarthrosis documented. Conventional x-ray showed effusion and discrete signs of arthrosis with smallest lateral and medial osteophytes. With the suspicion of a new event of intraartricular bleeding, the patient was immediately referred to the MRI department for further evaluation.

Sequence details

Examination was performed on a 3T open-bore MR system (MAGNETOM Verio), equipped with 18-channels (Tim [102 x 18] configuration) in combination with a dedicated 15-channel knee coil.

Imaging protocol included:

- Sagittal PDw TSE without fat saturation (TR 6090 ms, TE 88 ms, FOV (186 x 220) mm^2, matrix (346 x 512) px^2, slice thickness 3 mm, parallel imaging factor of 2, bandwidth 181 Hz/px, two averages, TA 3:21 min).
- Coronal T2w TIRM (TR 6690 ms, TE 53 ms, TI 210 ms, FOV (218 x 220) mm^2, matrix (400 x 448) px^2, slice thickness 3 mm, parallel imaging factor of 2, bandwidth 280 Hz/px, no averaging, TA 3:41 min).
- Transversal PDw TSE with spectral fat saturation (TR 3420 ms, TE 77 ms, FOV (197 x 220) mm^2, matrix (804 x 896, interpolated) px^2, slice thickness 4 mm, parallel imaging factor of 2, bandwidth 162 Hz/px, no averaging, TA 2:38 min).
- Coronal native T1w SE without fat saturation (TR 872 ms, TE 11 ms, FOV (165 x 220) mm^2, matrix (384 x 512) px^2, slice thickness 3 mm, no parallel imaging, bandwidth 150 Hz/px, no averaging, TA 3:19 min).
- Transversal enhanced T1w TSE without fat saturation (TR 458 ms, TE 12 ms, FOV (194 x 220) mm^2, matrix (396 x 448) px^2, slice thickness 4 mm, parallel imaging factor of 2, bandwidth 180 Hz/px, two averages, TA 5:30 min).
- Coronal enhanced T1w TSE with spectral fat saturation (TR 1210 ms. TE 13 ms, FOV (165 x 220) mm^2, matrix (326 x 512) px^2, slice thickness 3 mm, parallel imaging factor of 3, bandwidth 181 Hz/px, no averaging, TA 2:50 min).

Total imaging time was approximately 25 minutes.

Imaging findings

Findings of severe haemarthrosis include clear synovial thickening and enhancement as a sign of intense proliferation of the synovia. Effusion contains also solid-appearing containments as well as T1w iso- and slightly hyperintense areas. These findings are consistent with older haematoma. Erosions of the cartilage can be found in both joint compartments including thinning of the tibial cartilage. In addition, erosion of the cartilage and bone can also be found in the retropatellar joint. Epiphyseal fusion and bone marrow are age-related and without suspicious findings. No signs of fracture are visible and ligaments as well as menisci are within normal range. However, as already suspected through conventional x-ray, MRI shows also small osteophytes as sign of secondary arthrotic osseous changes.

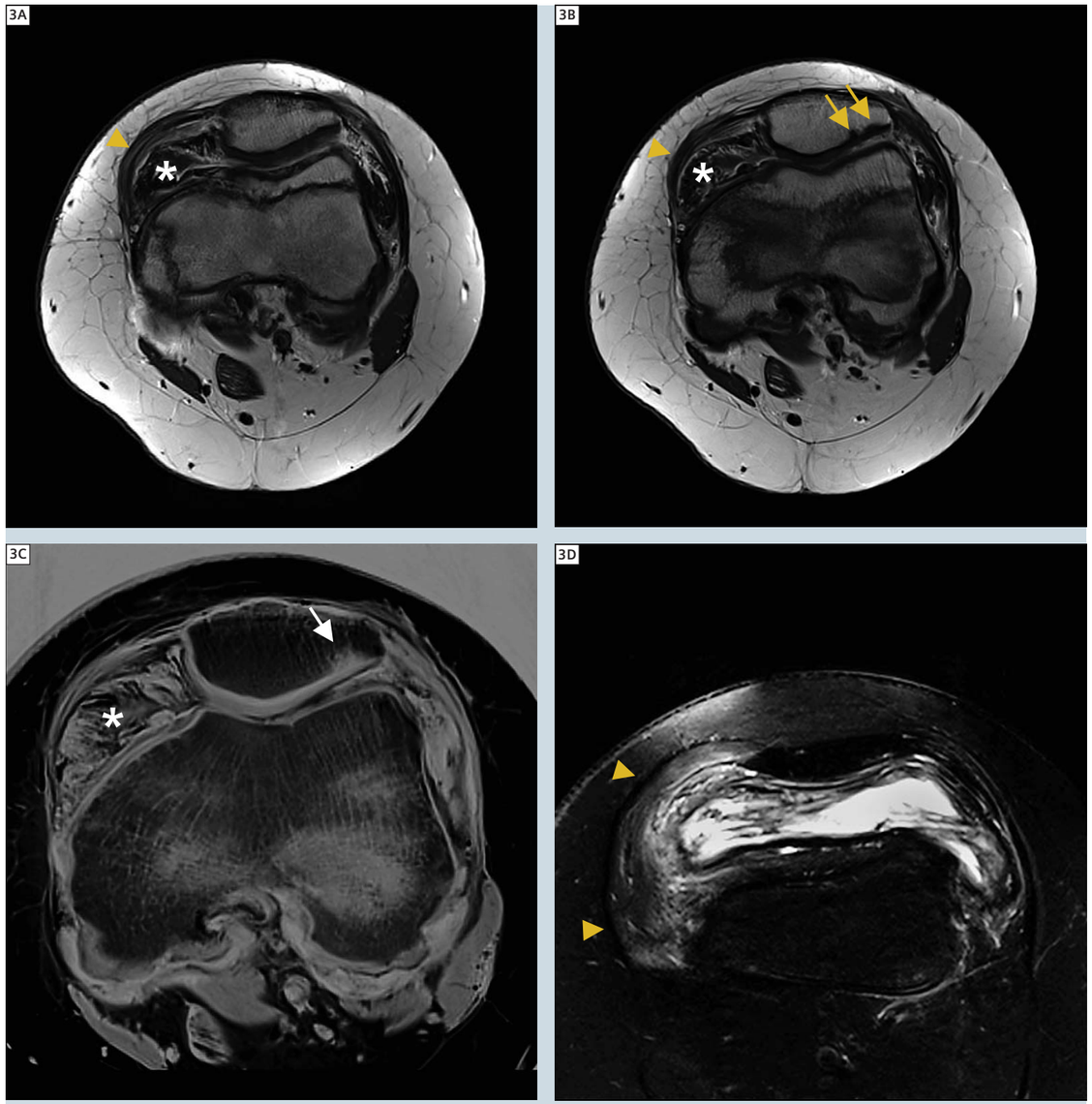

3 **A–C:** Enhanced T1w axial MRI. **3B:** Inverted. **D:** Transversal T2w TSE with spectral fat saturation. Arrows: Erosion of cartilage and bone destructions, arrow heads: synovial thickening and synovialitis, asterisk: effusion with haematoma.

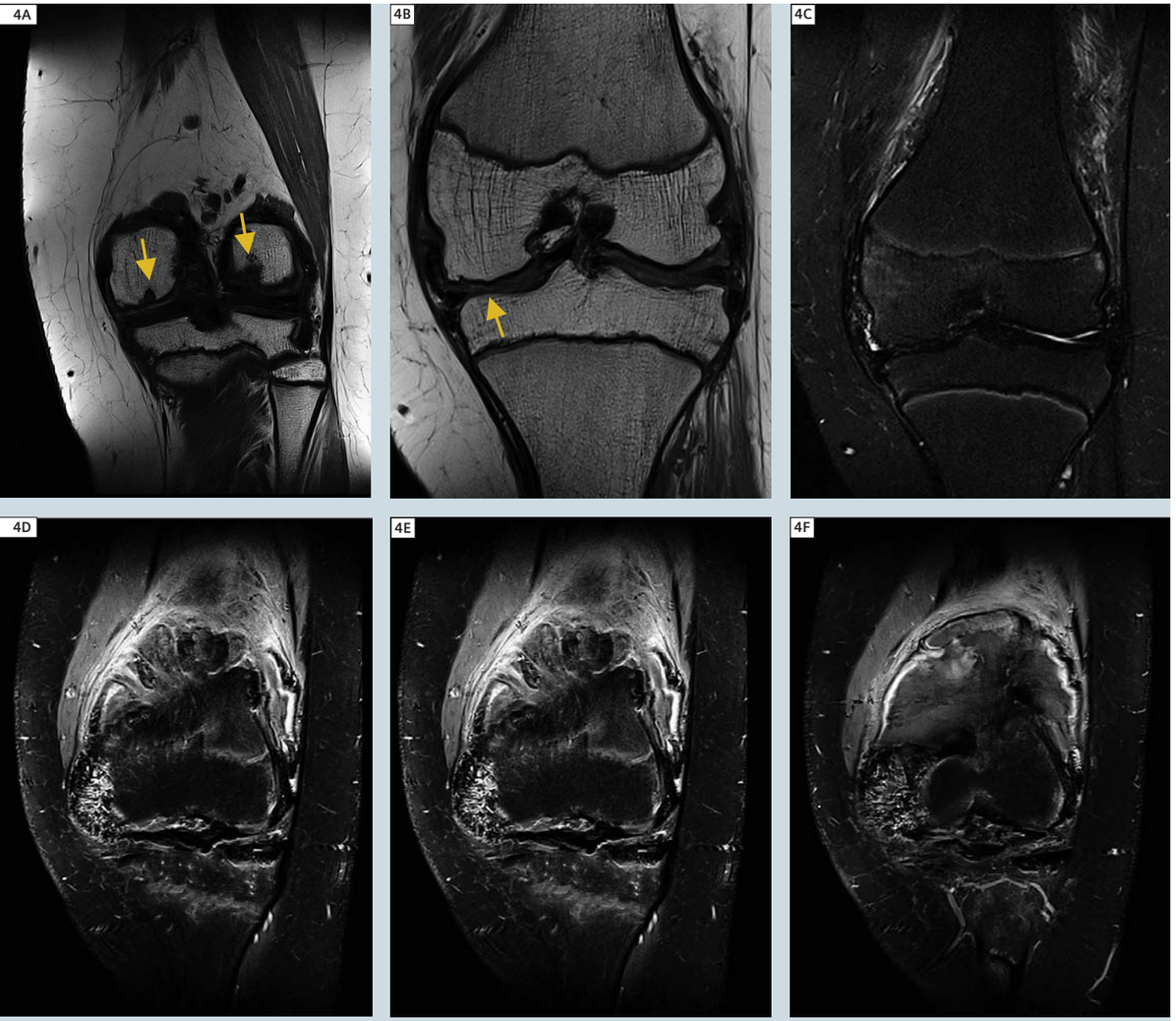

4 **A:** Coronal T1w SE showing erosion of the femur condyles. **B:** Thinning of tibial cartilage (arrow). **C:** Coronal TIRM showing regular bone marrow and epiphyseal fusion within normal age-related range. **D–F:** Enhanced T1w with fat saturation revealing extensive synovialitis.

Conclusion

In this case of haemarthrosis in a patient with recurrent bleedings, MRI at high field-strength (3T) and in combination with dedicated high-density coils is an invaluable tool for the evaluation of joints in childhood and adolescence within a reasonable time-frame and with superb image resolution, resulting in most accurate assessment of joint damage and extension of synovialitis. It is already known that in cases of haemophilia implementing MRI for assessment of joint involvement changes the patient management [Pergantou et al.]. However, the appropriate selection of MR imaging techniques as well as the appropriate translation of MRI findings into scoring systems are subject of ongoing debate [Doria et al., Lundin et al.]. In clinical routine the availability of MR scan time and the requirements for fast and highly-resolved imaging hampers the wide usage of MRI. So the implementation of a 3T open-bore system in our department and as a consequence shorter scan times at higher quality has significantly improved the acceptance of MR by patients and referring physicians.

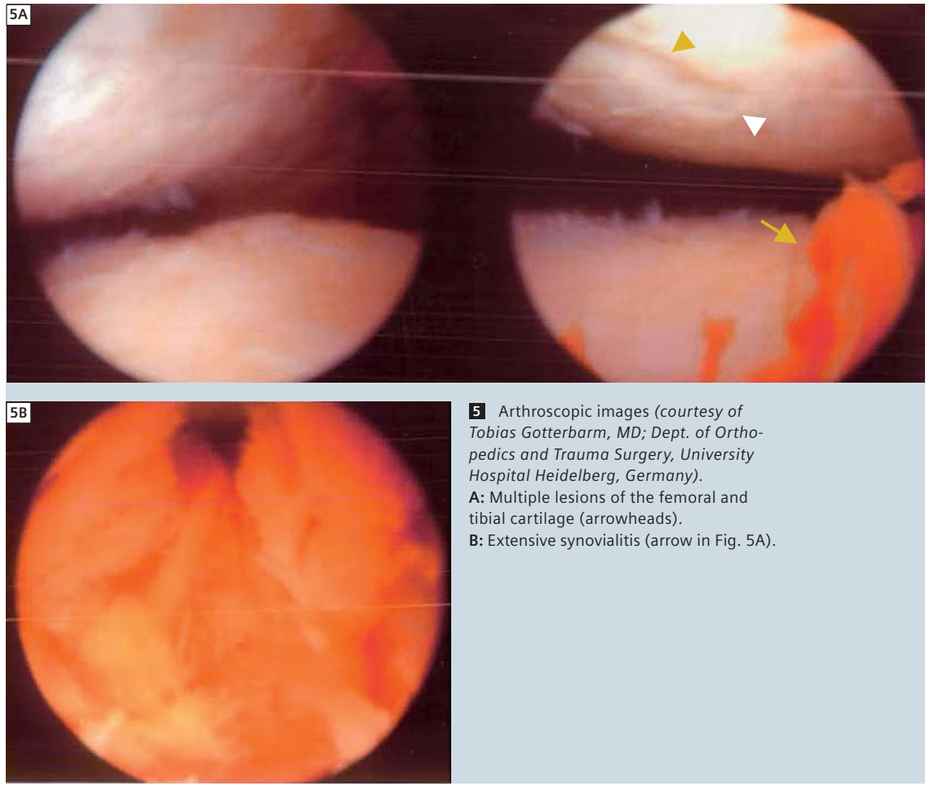

5 Arthroscopic images *(courtesy of Tobias Gotterbarm, MD; Dept. of Orthopedics and Trauma Surgery, University Hospital Heidelberg, Germany)*.
A: Multiple lesions of the femoral and tibial cartilage (arrowheads).
B: Extensive synovialitis (arrow in Fig. 5A).

References

1 Pergantou H, Matsinos G, Papadopoulos A, Platokouki H, Aronis S. Comparative study of validity of clinical, X-ray and magnetic resonance imaging scores in evaluation and management of haemophilic arthropathy in children. Haemophilia. 2006 May;12(3):241-7.

2 Doria AS, Babyn PS, Lundin B, Kilcoyne RF, Miller S, Rivard GE, Moineddin R, Pettersson H; Expert MRI Working Group of the International Prophylaxis Study Group. Reliability and construct validity of the compatible MRI scoring system for evaluation of haemophilic knees and ankles of haemophilic children. Expert MRI working group of the international prophylaxis study group. Haemophilia. 2006 Sep;12(5):503-13.

3 Lundin B, Berntorp E, Pettersson H, Wirestam R, Jonsson K, Ståhlberg F, Ljung R. Gadolinium contrast agent is of limited value for magnetic resonance imaging assessment of synovial hypertrophy in hemophiliacs. Acta Radiol. 2007 Jun;48(5):520-30.

M.-A. Weber J. K. Kloth

Contact
Marc-André Weber, M.D., M.Sc.
Heidelberg University
Professor of Radiology
Diagnostic and Interventional Radiology
Im Neuenheimer Feld 110
69120 Heidelberg
Germany
MarcAndre.Weber@med.uni-heidelberg.de

Advantages of MSK Imaging at 3 Tesla with special focus on Spine and Tumor Imaging

Marc-André Weber, M.D., M.Sc.

Diagnostic and Interventional Radiology, University Hospital Heidelberg, Germany

Background

In 2009, our institution, the Department of Diagnostic and Interventional Radiology, had to decide for a replacement of an existing 1.0 Tesla MR system with conventional coil technology and a bore-size of 60 cm at the Department of Orthopedics with the main departments Orthopedics and Traumatology as well as Paraplegiology and Rehabilitation Medicine. While the clinicians were satisfied with the robustness of imaging in case of metal implants with the old scanner, compromises in image resolution and relatively long examination times as well as the missing capabilities of the old system for scanning multiple regions of interest within one examination without the need for patient repositioning did limit the usage of MRI. In addition, due to the limited signal-to-noise ratio (SNR) as a result of the low field strength and old coil technology implemented in this system, the increasing clinical demand for widening the application of MRI to include, for example, molecular assessment of cartilage repair or multi-region tumor staging in children and adults could not be fulfilled sufficiently in a clinical environment.
The advantages of 3 Tesla especially for orthopedic imaging are well known: increase in SNR (proportional increase of the SNR with the increase of the field strength) and less prominent effect of B1 inhomogeneity on image quality for most areas of interest in musculoskeletal (MSK) imaging (knee, shoulder, ankle, wrist etc.) results in clearly improved image quality (resolution wise) and / or faster scan times. However, for advanced spine imaging as well as tumor staging, the "dielectric shading" effects would again have limited the usability of the MRI scanner. But with the development of anatomy optimized amplitude and phase transmission settings for homogenous B1 radio-frequency (RF) transmission and in combination with further optimizations of the magnet and gradient design (TrueForm technology), local signal drop out at 3T can be reduced significantly if not even eliminated practically. Another limitation of higher field strength is the higher energy deposit within tissue, resulting in higher specific absorption rate (SAR). And finally, metallic implants will result also in increased signal drop due to pronounced susceptibility artifacts [Fries 2008, Baudendistel 2004]. But these effects with negative impact on the image quality and examination time can again significantly be reduced if not compensated by new MR technology (e.g. adopting sequence techniques and application of parallel imaging techniques). Finally, we were convinced that the advantages of the 3T technology available with the new scanner generation do outweigh the disadvantages significantly. In spring 2009 we therefore decided for replacement of our old 1T scanner by a 3T MAGNETOM Verio.
We would like to present below some interesting cases out of our daily clinical routine which demonstrate the advantages of MSK imaging at 3T with special focus on spine and tumor imaging.

Case 1

As a center dealing with a high number of patients with hemi-/ paraplegia, cerebral palsy as well as scoliosis, the 70 cm open-bore system has the advantage of a very flexible patient positioning. As demonstrated in figure 1B, especially severe contractions of the extremities often seen in these patients do require sufficient space in the anterior-posterior direction. In figure 1A our MR-compatible wheelchair is shown, which enables an easy and relative fast patient transport into the scanner.

1 Patient with contractions of the lower extremities. MR-compatible wheelchair for easy patient transport.

Flexible patient positioning in the 70 cm open-bore system.

2 **A)** T1w TSE sagittal
B) T2w TSE sagittal

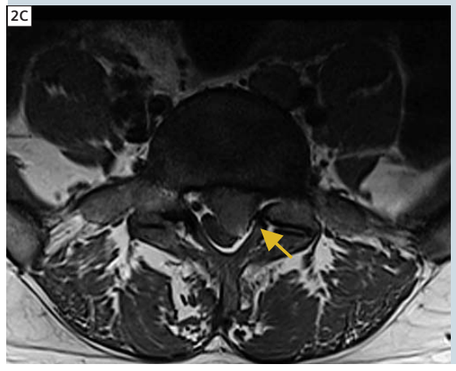

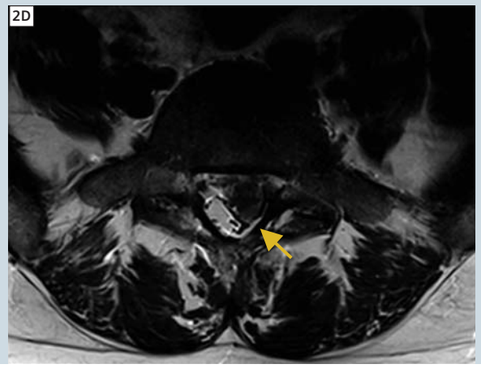

C) T1w TSE axial (oblique)
D) T2w TSE axial (oblique)

Case 2

This case demonstrates our standard imaging strategy in case of lower back pain. We apply mainly turbo spin-echo (TSE) sequences for this purpose. Sequence parameters for the shown images are:
T1w TSE sagittal: resolution (0.7 x 0.7 x 3.0) mm^3, TR 684 ms, TE 12 ms, TA 2:48 min (fig. 2A).
T2w TSE sagittal: resolution (0.7 x 0.7 x 3.0) mm^3, TR 3650 ms, TE 113 ms, TA 3:00 min (fig. 2B).
T1w TSE axial (oblique): resolution (0.7 x 0.7 x 3.0) mm^3, TR 969 ms, TE 12 ms, TA 3:09 min (fig. 2C).
T2w TSE axial (oblique): resolution (0.7 x 0.7 x 4.0) mm^3, TR 5060, TE 115 ms, TA 2:59 min (fig. 2D).
With a total scan time of less than 15 minutes, this protocol focuses on a fast assessment of the lumbar spine. However, because of the higher signal-to-noise contribution of the 3 Tesla system in combination with the integrated multi-channel spine coil, also a relatively high sub-millimeter in-plane resolution at slice thicknesses of 3 mm for sagittal and transversal planes is achieved.
In this particular case, a medio-lateral large hernia of the intervertebral disc of L5/S1 with compression of the left nerve root is seen (arrows).

Case 3

In case of malignancies or inflammation, however, we have to expand our clinical routine protocol. This case shows selected images of a 63-year-old male patient with known spinal astrocytoma WHO grade III. This patient underwent chemo- and radiotherapy and presented at our institution with clinically stable paraplegia at the level of Th5. A swollen myelon can be seen in this follow-up exam at the height of the irradiated tumor at the height of thoracic vertebra 6–8. On post-contrast T1w MRI, an inhomogeneous medullar enhancement can be seen (arrow). Note that the patient also underwent laminectomy and that a residual seroma can be detected. Enhancement within the vertebra was stable over a long period of time and based also on CT imaging, this finding has to be classified as a hemangioma of the 9th thoracic vertebra.

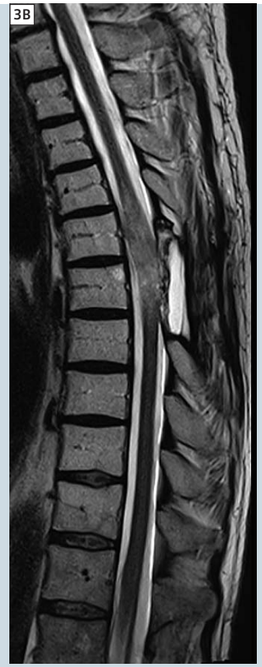

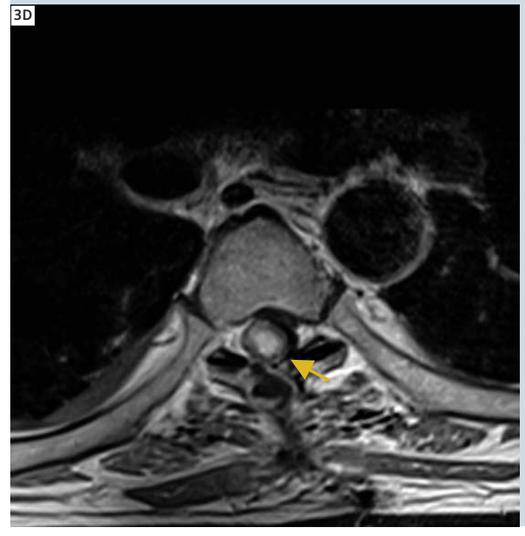

3 **A)** T1w TSE sagittal
B) T2w TSE sagittal
C) ce T1w sagittal with fat-saturation
D) ce T1w axial (oblique)

Case 4

43-year-old male patient, who underwent a dorsal stabilization after traumatic fracture of vertebra Th10 and had complete paraplegia below this segment. On conventional x-ray, the spine fusion from Th9 to Th11 is shown (fig. 4A). Figure 4B shows an MRI which was performed at our institution with our old 1 Tesla scanner. While artifacts caused by metallic implants on the 1T exam with the chosen sequences are less prominent compared to imaging at 3T (compare Fig. 4C), SNR and therefore in-plane resolution was low in the 1T exam and a further evaluation of the tethering of the myelon was not possible. The high SNR of the 3T scan allowed for a high in-plane resolution (Fig. 4C, D) and also for T2w 3D imaging (*syngo* SPACE, Fig. 4E).The capability of evaluating the whole area of interest with the SPACE sequence at highest resolution and contrast in any orientation allowed further evaluation of the reason for the dorsal dislocation of the myelon starting at the height of Th6.

Based on this MRI exam, the suspicion of an arachnoidal cyst was supported leading to a dorsal dislocation and compression of the myelon. Even the slight arachnoidal web could be detected on the SPACE sequence (red arrow in Fig. 4D).
Slice thickness for sagittal T2w images were 3 mm for both examinations at 1 and 3 Tesla, respectively. Resolution of the *syngo* SPACE exam was (0.7 x 0.7 x 0.7) mm^3.

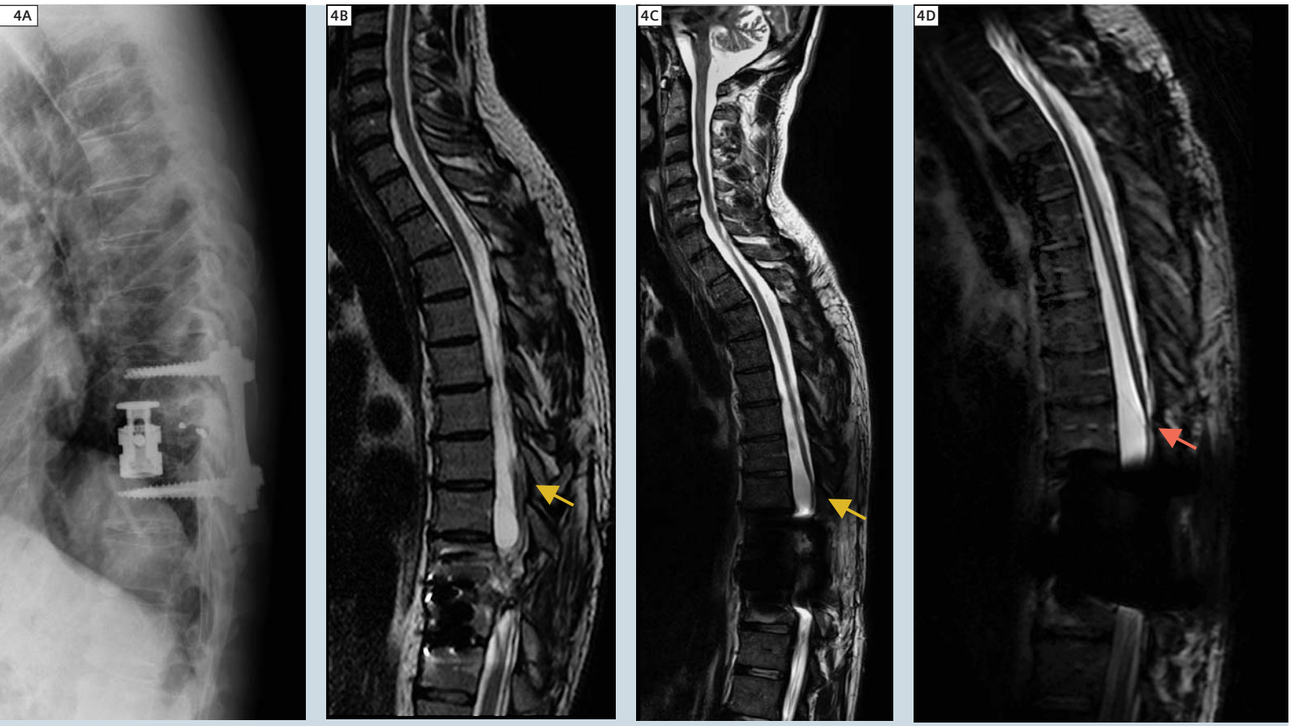

4 **A)** Conventional x-ray **B)** T2w sagittal at 1T **C)** T2w sagittal at 3T **D)** T2w *syngo* SPACE at 3T

Case 5

66-year-old female patient with molecular pathology confirmed Ewing sarcoma of the right humerus. After initial tumor excision in 2009 and osteosynthesis, the patient presented with an extensive recurrence of the tumor within four months. Figure 5A demonstrates the large tumor with infiltration also of the bone marrow. In addition, diffuse oedema is shown (arrowhead in 5A). Figure 5B also shows a large lymph node metastasis (arrow). Therefore, before again operating on the humerus, the orthopaedic tumor surgeon wants to know whether more lesions are present. Thus, a whole-body scan was added (Fig. 5C), demonstrating also multiple osseous filiae (arrows in 5C) of the pelvis and spine. No evidence of high risk or presence of a pathologic fracture was found.
By selecting appropriate imaging techniques, imaging at 3T even with metal implants present and off-center positioning can result in excellent image quality. The achievable superior resolution clearly increases confidence about extension of a tumor and impairment of anatomical structures. In addition, the capability of scanning large areas of interest up to whole-body without compromise in image quality and within a clinical acceptable setting (time and patient-comfort wise) is a prerequisite for any sufficient oncologic decision making and is highly esteemed by our tumor surgeons, especially to detect skip lesions that would distinctly influence the therapeutic concept. The superior capability of evaluating changes within the bone marrow including diffuse tumor infiltration is a particularly big advantage in our patient cohort.

5 **A)** Coronal ce T1w with fat saturation.

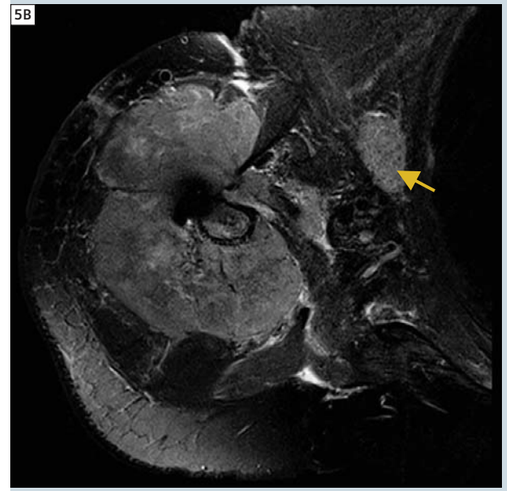

B) Axial ce T1w with fat saturation.

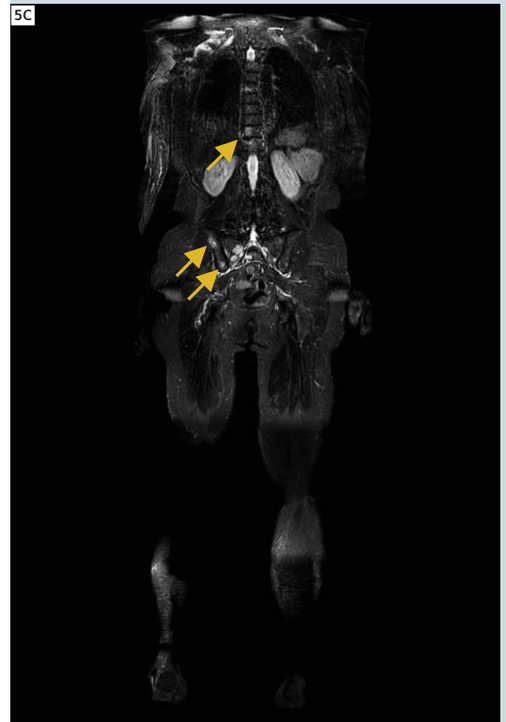

C) Coronal T2w whole-body with fat saturation.

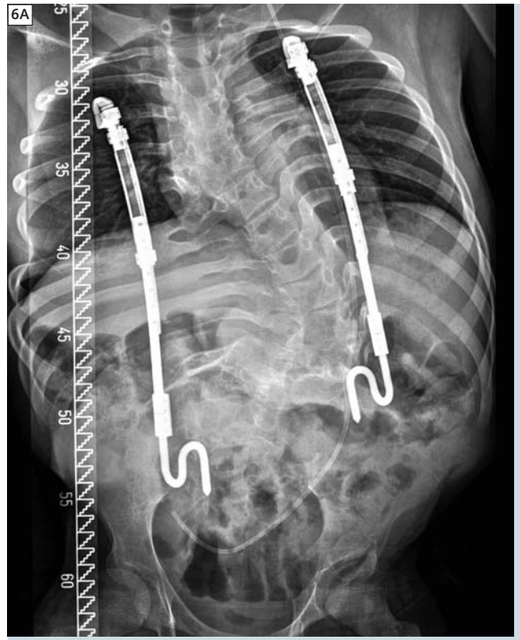

6 **A)** Conventional x-ray **B)** T2w sagittal at 1T

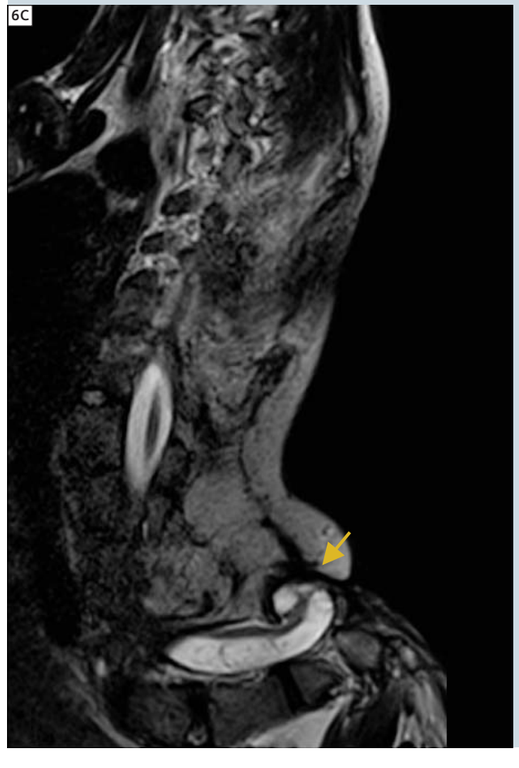

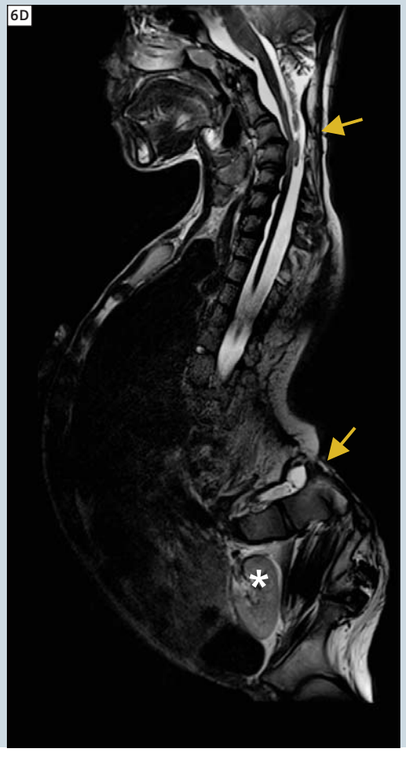

C) T2w sagittal at 3T **D)** T2w *syngo* SPACE at 3T

7 **A)** T2w sagittal at 3T **B)** T1w sagittal at 3T **C)** T2w sagittal at 1T

Case 6

Complex congenital malformation of the central nervous system, as well as the spine, requires also evaluation of the whole systemic aspect of disease. In this case, we show images from a 15-year-old boy with Arnold Chiari II malformation and lumbal meningomyelocele (closed by surgery after birth). Because of severe and progedient complex scoliosis, this patient also underwent a dorsal spine fusion of Th9 downwards to the pelvis with VEPTR instruments and underwent multiple extensions (conventional x-ray Fig. 6A).
Figures 6B and C do show the image quality difference between 1 and 3T exam (both 3 mm slice thickness). Again, the superior SNR and in-plane resolution allows for a more detailed assessment of the meningomyelocele (arrows). Especially T2w 3D imaging allows for a detailed assessment of all aspects of the impairment of the central nervous system including the myelon and nerve roots. Figure 6D shows the results of a *syngo* SPACE exam of the whole spine. The meningomyelocele is resolved in detail (arrow) as well as the displacement of the cerebellum as part of the Arnold Chiari malformation. Also tethering of the myelon, which is important for the orthopaedic surgeons to know about because it must be resolved before any operation to the spine, is well depicted. Note also the displacement of inner organs in this case (asterisk marks one of the kidneys).

Case 7

Exam of a 59-year-old male patient with complete tetraplagia at the level of C5 and secondary syringobulbia starting at the vermis down to the 6th thoracic vertebra as a consequence of a bathing accident in 1968. The patient received arachnolysis and dural plastic as specific therapy, as well as a wound examination because of a liquor pad. The *syngo* SPACE exam (Fig. 7A) shows multiple horizontal septae, which divide the syrinx and might hinder CSF exchange and thus might cause extension of the syrinx. The 3 Tesla T2-weighted image (Fig. 7A) better delineates the septae than the 1 Tesla T2-weighted image (Fig. 7C). In this case, a complete suppression of the liquor was seen on FLAIR images (not shown), suggesting communication of the multiple cystic lesions and the subarachnoid space.

8 **A)** Coronal and **B, C)** sagittal reconstructions based on 3D T2w imaging.

Case 8

Intramedullar formation of cavities can often be found as a consequence of widening of the central canal (hydro myelia) or outside the central canal (syringomyelia) as result of traumatic events or space occupying lesions / tumors or as a malformation. T2w images of a 7-year-old boy are shown, showing a syringomyelia affecting the whole myelon (holocord syrinx).

Case 9

10-year-old girl with meningomyelo-cele, paraparesis, spina bifida and rotation skoliosis is shown. In addition, partial fusion of the first and second lumbar vertebra is present as well as dysplasia of the 12th thoracic vertebra. Imaging was conducted for planning of specific therapy including instrumented dorsal spine fusion and decompression of the spinal canal. For optimal outcome and for best risk stratification of such a therapy, detailed information not only about the complexity of the disorders of the spine but also of the myelon and nerve roots is essential. CT (volume rendering shown in Fig. 9A) as well as 3T MRI demonstrated in detail the known left convex rotation scoliosis of the thoraco-lumbal spine. Syrinx from level Th3 down to the conus is visualized by MRI (arrows in Figs. 9B–D). In addition, starting at the height of Th6, a T2w hypointense, T1w isointense to the myelon, linear and parallel to the myelon running structure can be delineated that might resemble a scarred cord. Most probably this structure represents split cord malformation e.g. diastemato-myelia.

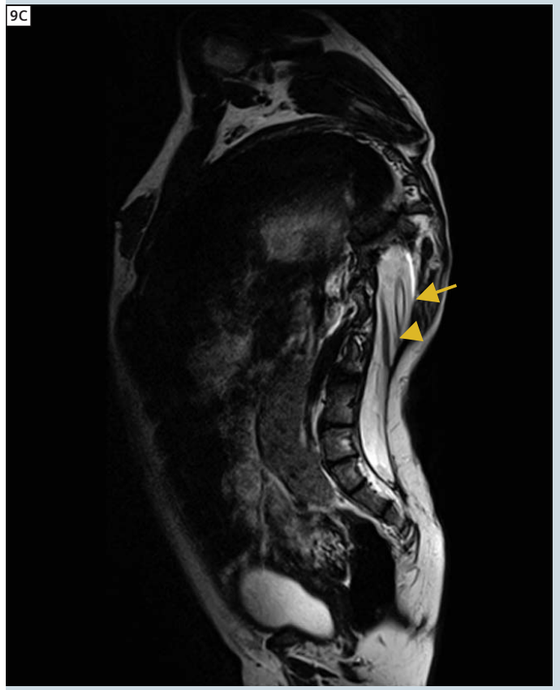

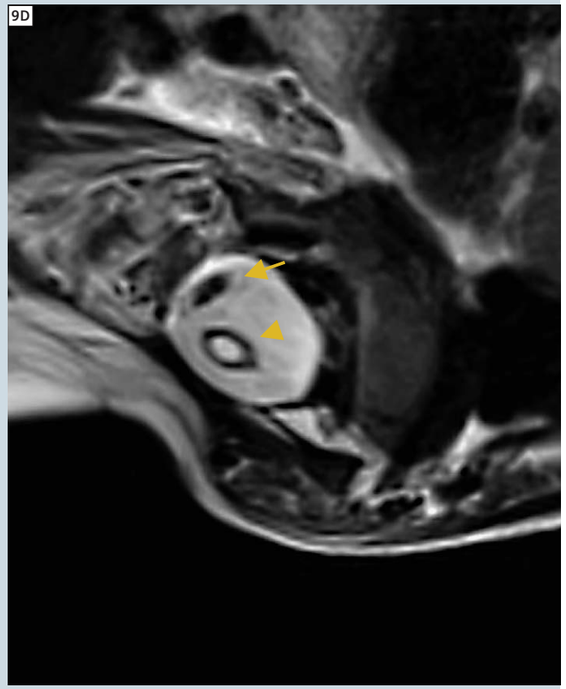

8 **A)** Volume Rendering Technique (VRT) of a CT scan. **B)** Coronal, **C)** sagittal and **D)** oblique reconstructions based on 3D T2w imaging.

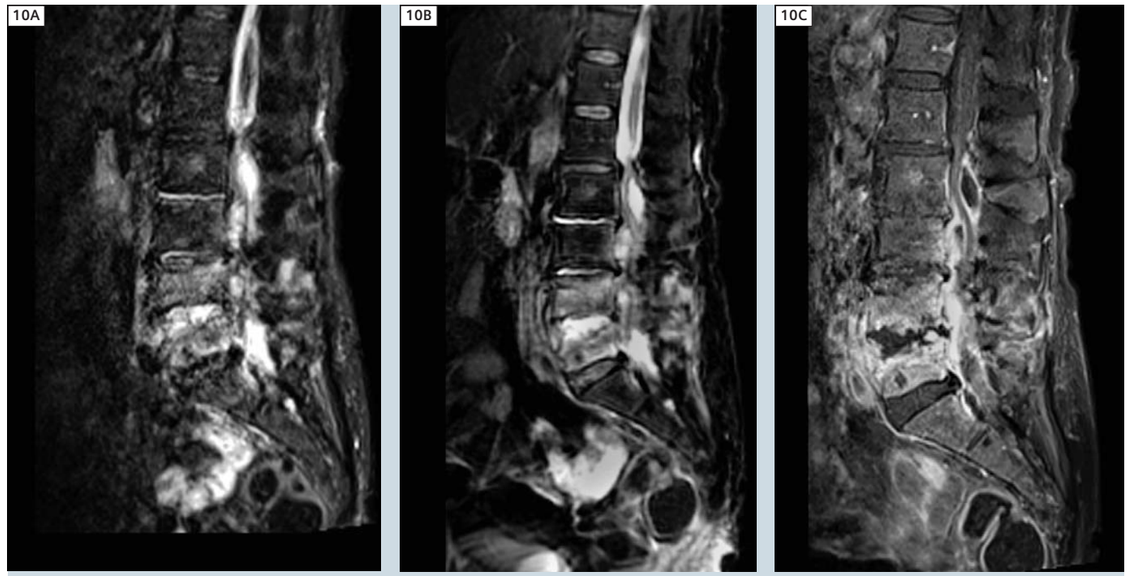

10 **A)** T2w sagittal with severe motion artifacts. **B)** T2w sagittal with *syngo* BLADE technique. **C)** ce T1w sagittal with fat saturation.

Case 10

Results of an MRI scan of an 87-year-old female patient with dementia and severe back pain are shown. Severe motion artifacts were present (Fig. 10A) but could be compensated by applying motion-insensitive (*syngo* BLADE; Fig. 10B) MR sequences and fast sequences with parallel imaging (post-contrast T1w image; Fig. 10C). Spondylodiscitis and complete destruction of the intervertebral space of L5/4 is seen. In addition, multiple epidural abscesses can be seen. The patient underwent surgery with dorsal and ventral spine fusion, open discectomy and laminectomy as well as drainage.

Conclusion

Although the adoption to the higher field strength of 3T, new coil technology and multi-region exams were challenges to radiologists, technologist and referring clinicians and do require a (short) transition phase, the clinical advantages are significant, as shown with this case series. After approximately one year of operation, the installation of the 3T open bore system with TrueForm technology has clearly improved our diagnostic potential as well as widened the indications for MRI and has lead to improved patient care. The system is therefore well received among our clinical colleagues, resulting also in a significant increase of referrals during the last year. In addition, the patient comfort of the open bore system has resulted in a higher acceptance of MRI by patients.

Acknowledgements

The excellent cooperation regarding brain and spine imaging with Prof. Dr. Stefan Hähnel and Dr. Leonie Jestaedt from the Department of Neuroradiology at the University Hospital Heidelberg (Head: Prof. Dr. Martin Bendszus) is gratefully acknowledged.

References

1 Fries P, Runge VM, Kirchin MA, Watkins DM, Buecker A, Schneider G. Magnetic resonance imaging of the spine at 3 Tesla. Semin Musculoskelet Radiol. 2008 Sep;12(3):238-52.

2 Baudendistel KT, Heverhagen JT, Knopp MV. Clinical MR at 3 Tesla: current status. Radiologe 2004;44(1):11-8.

Contact
Marc-André Weber, M.D., M.Sc.
Professor of Radiology
Head of Musculoskeletal Radiology
Department of Diagnostic and Interventional Radiology
University Hospital Heidelberg
Im Neuenheimer Feld 110
69120 Heidelberg
Germany
Phone: +49 6221-966601
Fax: +49 6221-966640
MarcAndre.Weber@med.uni-heidelberg.de

Image Quality Improvement of Composed MR Images by Applying a Modified Homomorphic Filter

Vladimir Jellus; Wilhelm Horger; Berthold Kiefer

Siemens Healthcare, Erlangen, Germany

With the development of MR machines that offer the capability to examine large regions of the body without patient and/or coil repositioning [1], MRI can now be used for imaging systemic aspects of diseases e.g. in oncology [1-6]. But documentation of complex pathologies requires a fast and easy assessment of all findings. For this purpose, image-composing techniques may be helpful [1]. To acquire information from large body regions, large fields-of-view (FOV) and multi-channel coils have to be applied [1, 5, 6]. Unfortunately, images with large FOV are often characterized by inhomogeneous illumination. At 1.5T this is caused mainly by local variations of coil sensitivities. This problem can be pronounced at higher field strength by dielectric resonances, causing local B_1 inhomogeneities [7]. Consequently, manual adjustments have to be performed including for small areas of interest, negating the potential advantage of large FOV images for fast and easy access to pathologic findings. This problem will be aggravated regarding composed images.
Therefore, a simple applicable and robust post-processing approach is required to improve signal homogeneity for composing large FOV MR images in clinical routine.

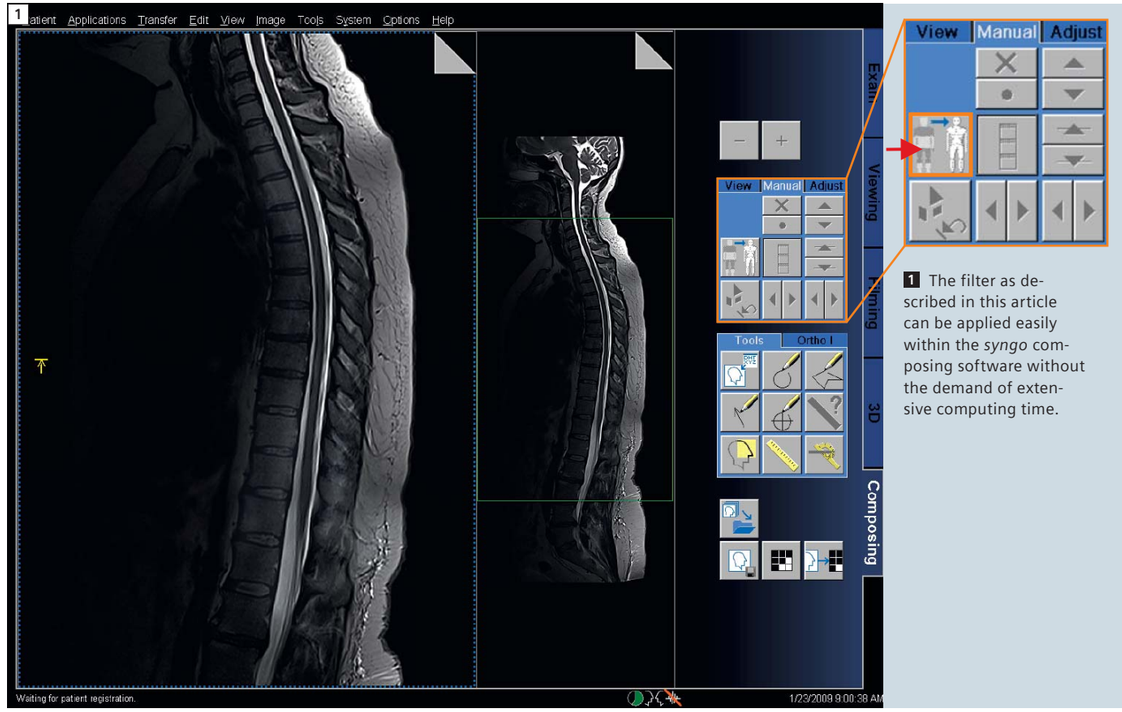

1 The filter as described in this article can be applied easily within the *syngo* composing software without the demand of extensive computing time.

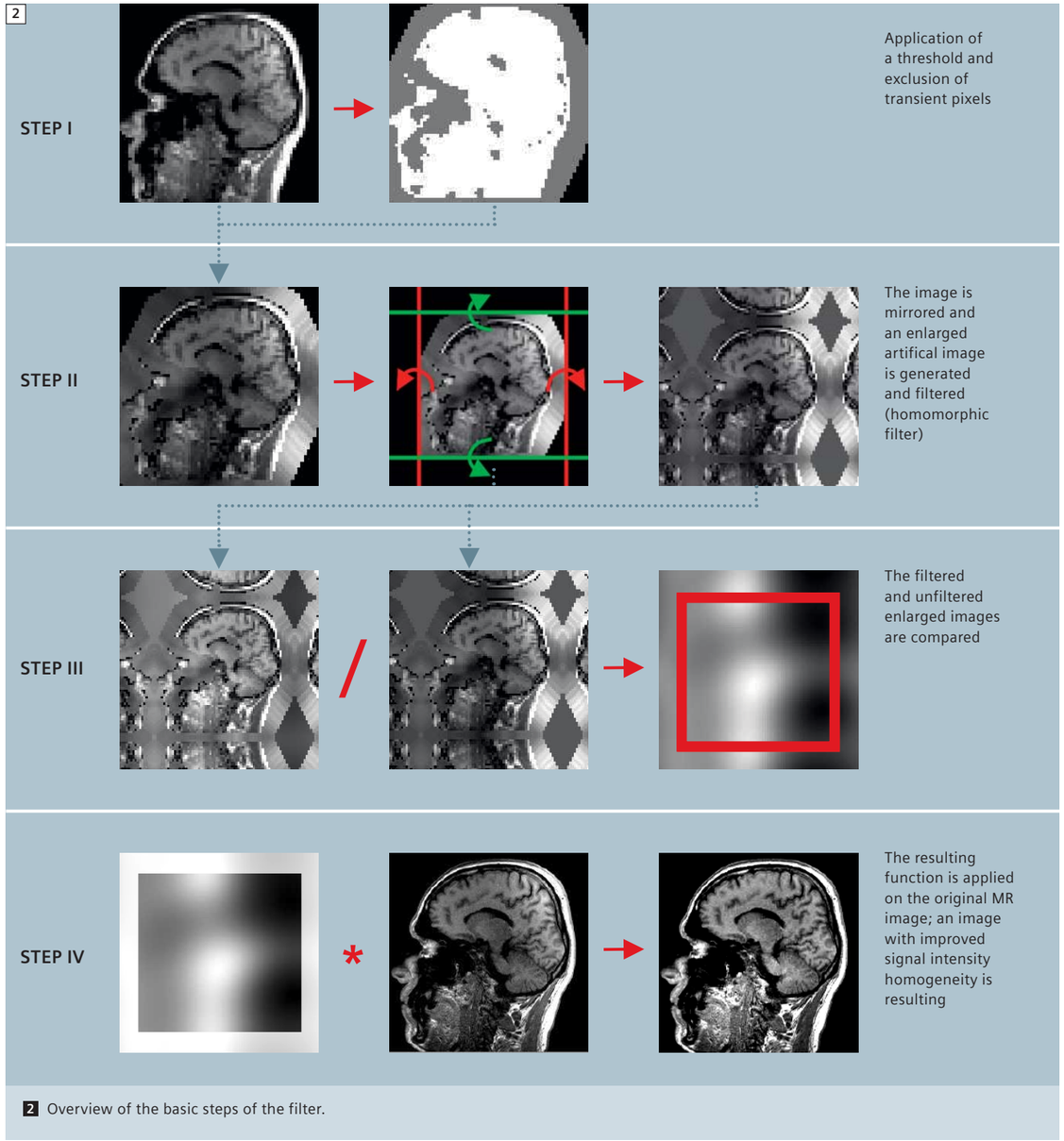

2 Overview of the basic steps of the filter.

The modified homomorphic filter in the *syngo* composing software (Fig. 1) was initially developed to reduce artifacts caused by dielectric resonances [8]. The purpose of the filter is to remove signal inhomogeneities introduced into the image by various phenomena, at 1.5T this is mainly caused by sensitivity variations of the RF-coils.
The method is based on the homomorphic filter as described in reference [9]. Homomorphic filters assume that the acquired image is a multiplication of the ideal homogenous image and the inhomogeneity. Therefore, inhomogeneity can be suppressed by a notch filter (removes low frequency components) applied to the spectrum of the logarithm of the image. In comparison to a standard homomorphic filter, the developed filter includes algorithms to exclude

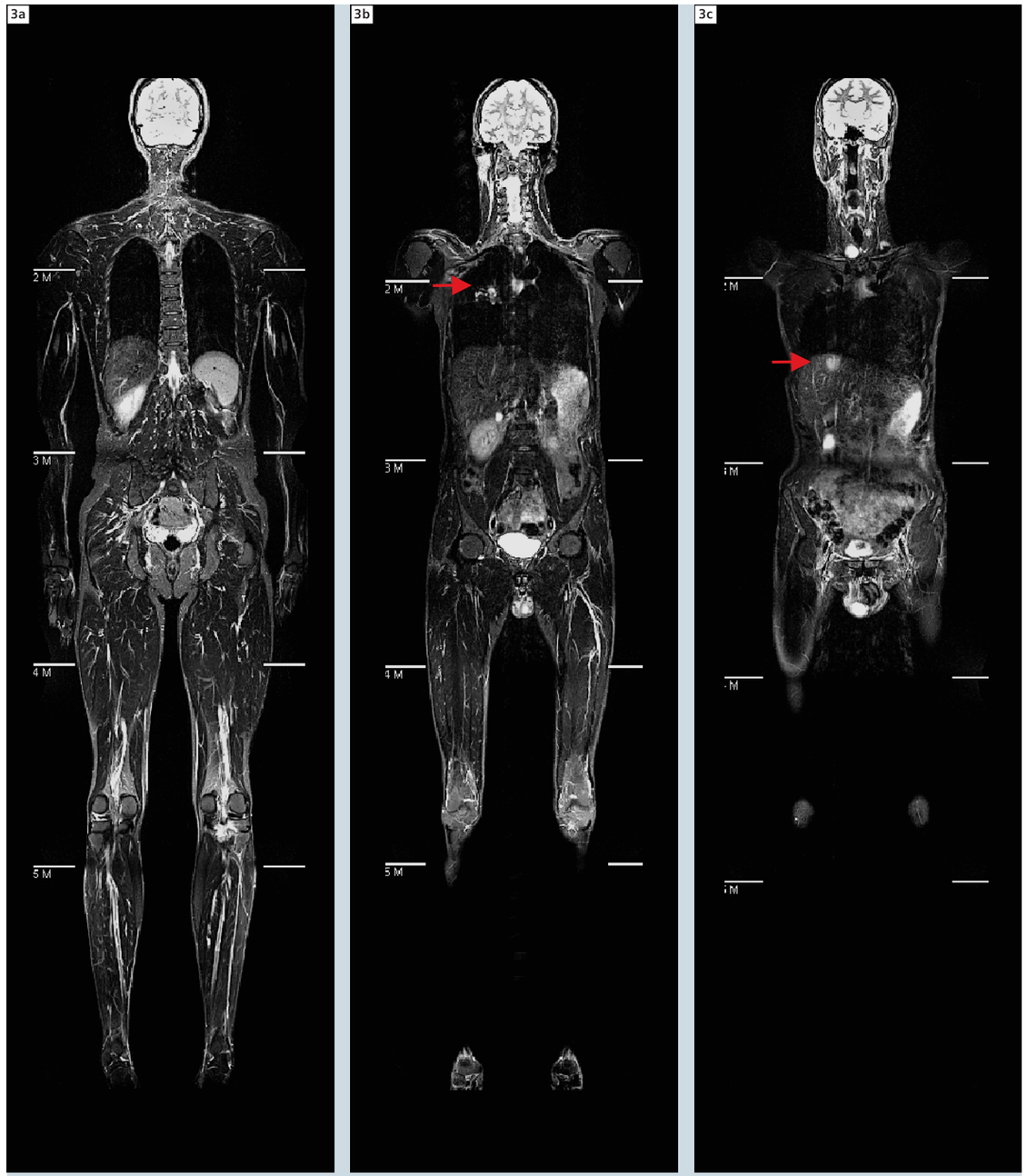

3 This case demonstrates the improved signal uniformity in whole-body MRI, when the homomorphic filter is applied.
Original composed T2-weighted STIR images are given in figures **3 a**, **b** and **c**; filtered images are given in figures **3 (A)**, **(B)** and **(C)**. While signal uniformity is clearly improved by the homomorphic filter especially for the brain, the metastases (marked by arrows) of the kidney cell cancer are well delineated without loss of contrast to their surrounding tissues. (Note: all images have the same window levels for contrast and brightness.)

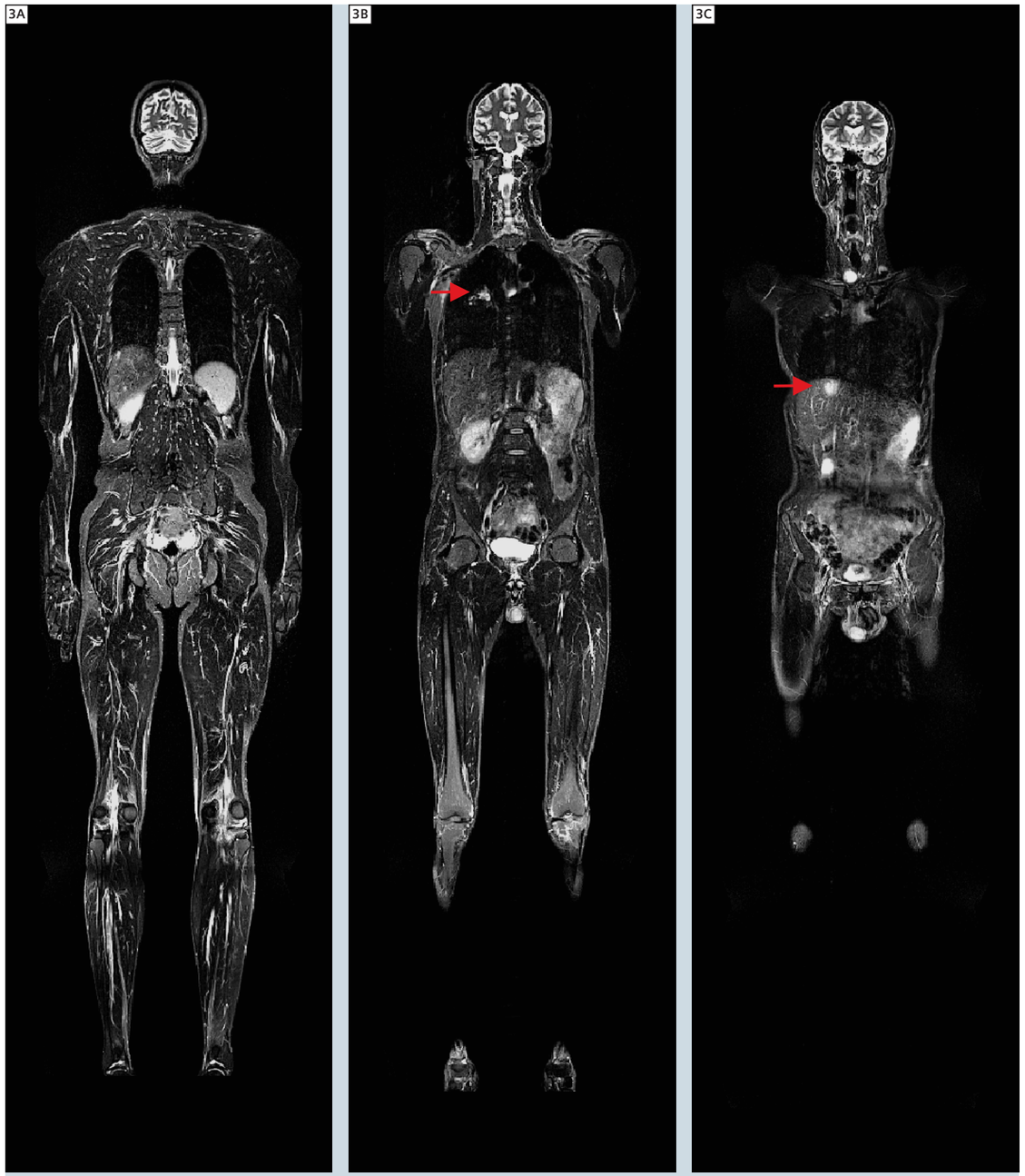

3 Filtered images are given in figures **3 (A)**, **(B)** and **(C)**.
Case courtesy of Heinz-Peter Schlemmer and Matthias Lichy, University of Tuebingen, Department of Diagnostic and Interventional Radiology, Tuebingen, Germany.

influences of areas with very low signal intensity inside the object and in the background. A “cepstrum” (spectrum of the logarithm of the image) is calculated from this prepared image and a notch filter is applied on the cepstrum (Fig. 2). The filter can be applied on all kinds of MR images, and is very valuable on composed images. It includes different steps. Firstly, the image resolution is reduced. One effect is that the effective signal-to-noise ratio (SNR) is increased in this new image and, additionally, computing performance is improved. Secondly, areas with low signal intensity are detected by setting of a threshold; isolated pixels in the background and inside the object are removed, including pixels with possible partial volume effects (via erosion). In the next step the initial signal intensities of the removed pixels are replaced by the mean value of N neighboring volume elements (with N~10–100) (compare step 1, Fig. 2). To minimize problems with extreme signal changes (especially present at the image border), the filter mirrors these parts to the outside. For this purpose, the dimensions of the image are enlarged to avoid problems caused by circular convolutions at the borders, which can cause a leap in the sensitivity. Now the standard homomorphic filter algorithm is applied on this new and artificial image with low resolution (compare step 2, Fig. 2). The ratio of the filtered image and the input artificial image provide the correction function (compare step 3, Fig. 2). Finally, the filter interpolates this correction function from the central part of the artificial, low-resolution image to full resolution (this area is corresponding to the non-mirrored central part of the initial image). After a multiplication with the values of the initial fully resolved image, a corrected image with improved signal uniformity is resulting (compare step 4, Fig. 2).
Further information about the function of the filter can be found in reference [8]. A clinical example of the improvement of the signal homogeneity can be found in figure 3, in which it is also shown that there is no compromise in the detection of suspicious lesions introduced by filtering. Further information about the influence of the filter with special regards to diagnostic safety and clinical value for whole-spine imaging in patients with multiple myeloma can be found in [10].

Contact
Vladimir Jellus, Ph.D.
Siemens Healthcare
IM MR PLM AW Orthopedics
Allee am Roethelheimpark 2
91052 Erlangen
Germany
vladimir.jellus@siemens.com

References

1 Schlemmer HP, Schafer J, Pfannenberg C, Radny P, Korchidi S, Muller-Horvat C, Nagele T, Tomaschko K, Fenchel M, Claussen CD (2005) Fast whole-body assessment of metastatic disease using a novel magnetic resonance imaging system: initial experiences. Invest Radiol. 40(2):64–71.
2 Ghanem N, Lohrmann C, Engelhardt M, Pache G, Uhl M, Saueressig U, Kotter E, Langer M (2006) Whole-body MRI in the detection of bone marrow infiltration in patients with plasma cell neoplasms in comparison to the radiological skeletal survey. Eur Radiol. 16(5):1005–14.
3 Mentzel HJ, Kentouche K, Sauner D, Fleischmann C, Vogt S, Gottschild D, Zintl F, Kaiser WA (2004). Comparison of whole-body STIR-MRI and 99mTc-methylene-diphosphonate scintigraphy in children with suspected multifocal bone lesions. Eur Radiol. 14(12):2297–302.
4 Iizuka-Mikami M, Nagai K, Yoshida K, Sugihara T, Suetsugu Y, Mikami M, Tamada T, Imai S, Kajihara Y, Fukunaga M (2004). Detection of bone marrow and extramedullary involvement in patients with non-Hodgkin’s lymphoma by whole-body MRI: comparison with bone and 67Ga scintigraphies. Eur Radiol. 14(6):1074–81.
5 Lichy MP, Wietek BM, Mugler JP 3rd, Horger W, Menzel MI, Anastasiadis A, Siegmann K, Niemeyer T, Konigsrainer A, Kiefer B, Schick F, Claussen CD, Schlemmer HP (2005). Magnetic resonance imaging of the body trunk using a single-slab, 3-dimensional, T2-weighted turbo-spin-echo sequence with high sampling efficiency (SPACE) for high spatial resolution imaging: initial clinical experiences. Invest Radiol. 40(12):754–60.
6 Rodegerdts EA, Boss A, Riemarzik K, Lichy M, Schick F, Claussen CD, Schlemmer HP (2006) 3D imaging of the whole spine at 3T compared to 1.5T: initial experiences. Acta Radiol. 47(5): 488–93.
7 Van de Moortele PF, Akgun C, Adriany G, Moeller S, Ritter J, Collins CM, Smith MB, Vaughan JT, Ugurbil K (2005). B(1) destructive interferences and spatial phase patterns at 7 T with a head transceiver array coil. Magn Reson Med. 54(6):1503–18.
8 Jellúš V, Kiefer B (2005). New Modification of the Homomorphic Filter for Bias Field Correction. Proc. Intl. Soc. Mag. Reson. Med. 13: 2247
9 Gonzales RC, Woods RE (1992). Digital Image Processing, Reading, Addison-Wesley
10 Lichy MP, Mueller-Horvat C, Jellus V, Horger W, Horger M, Pfannenberg C, Kiefer B, Claussen CD, Schlemmer HP (2008). Image quality improvement of composed whole-spine MR images by applying a modified homomorphic filter – first results in cases of multiple myeloma. Eur Radiol. 18(10):2274–82.

Value of Automated Retrospective Correction of Contrast-Enhanced Dynamic Liver MRI. Initial Clinical Experience

H.-P. Schlemmer[1,4]; M.P. Lichy[1,2]; C. Plathow[1]; W. Horger[2]; B. Geiger[3]; B. Kiefer[2]; C. Chefdhotel[3]; C. D. Claussen[1]; U. Kramer[1]

[1]*University of Tübingen, Department of Diagnostic and Interventional Radiology, Tübingen, Germany*
[2]*Siemens Healthcare, Erlangen, Germany*
[3]*Siemens Corporate Research, Princeton, USA*
[4]*German Cancer Research Center (DKFZ) Heidelberg, Germany*

Introduction

Multiphase three-dimensional contrast-enhanced dynamic liver scans (3D DCE MRI) are of high diagnostic relevance in the characterization of liver lesions, especially in the detection of primary liver malignancies, e.g. the hepato-cellular carcinoma (HCC). But detection of smaller HCC nodules within fibrotic liver tissue is especially challenging [1–7]. Not only because of the lesion size and the requirements for exact timing of the arterial phase but also because these nodules can already have bright native signal intensity, and potential contrast-media enhancement is therefore not easy to detect just by qualitative image reading. But precise (and in the clinical routine also fast) assessment of 3D DCE MRI data requires an exact anatomical match of the 3D DCE MRI data sets. However, breathing artifacts are a common observation, resulting very often in a clear anatomical offset of the different phases of liver 3D DCE MRI. In theory, a simple subtraction of images derived from different phases would highlight pathologic enhancement including signal changes of smallest and already on native images bright lesions. But this simple approach is not feasible anymore if offsets between the different phases are present. Not only offset in cranio-caudal direction can occur; under pathologic conditions especially, e.g. presence of ascites or after liver segment resection, one can observe deformations especially of the liver and as a consequence inplane shift of individual voxels are present. To enable a fast and accurate reading of liver DCE MRI, a non-rigid correction algorithm has therefore to be applied. The purpose of our study was therefore to evaluate the clinical value of a retrospective anatomical correction of multi-breath hold 3D DCE MRI.

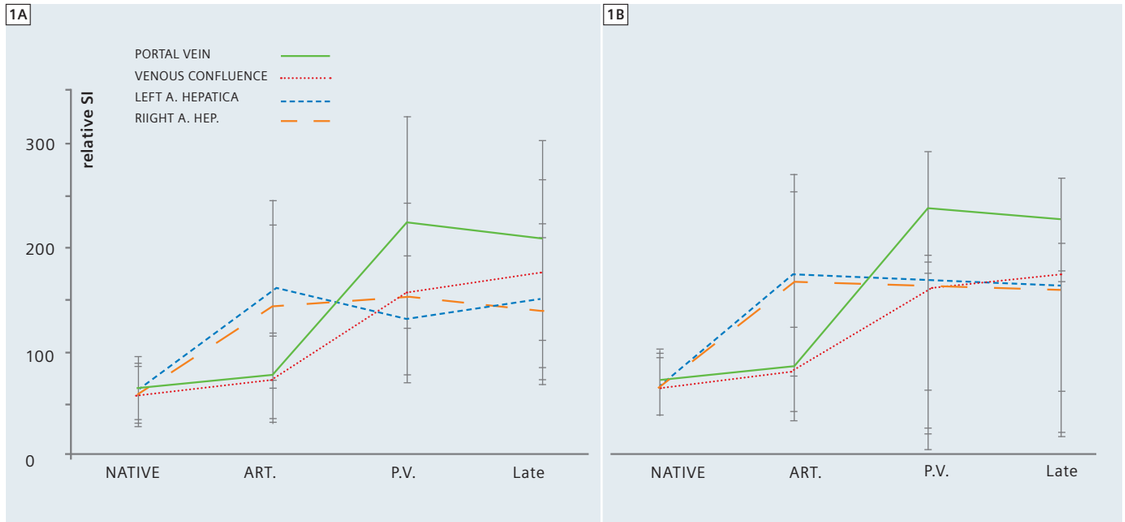

1 Relative changes of the signal intensities in patients with HCC measured by an ROI analysis. **A)** Uncorrected and **B)** corrected DCE liver data sets. SI changes of the left/right hepatic artery were found to be significantly different in the corrected and uncorrected data sets and were the most sensitive quantitative parameter for evaluation of image mismatch and therefore the function of the correction algorithm.

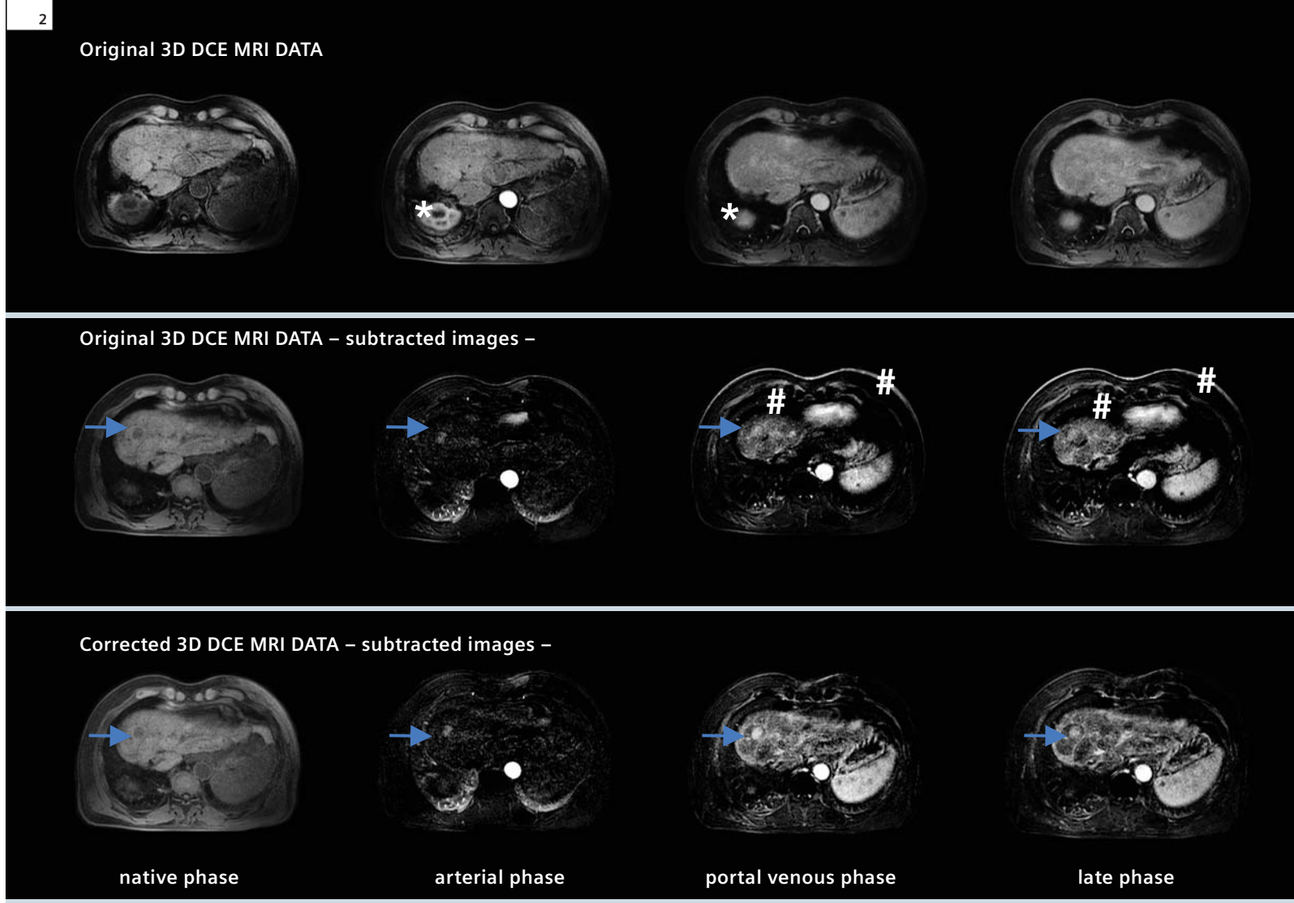

2 Example of a patient with a small HCC (lesion marked by arrows). Caused by a mismatch of the arterial and p.v. as well as late phase, subtraction artifacts are clearly visible (marked by #) in the original data sets and subtracted images are of no diagnostic value. In the case of the subtraction of the corrected images, these artifacts are not present and the lesion is well defined.

Patients and methods

For non-rigid image registration, a newly developed algorithm was adapted to the special needs of liver DCE MRI. This algorithm is based on maximization of statistical similarity criteria (global as well as local) in a variational framework. It uses corresponding gradients to drive a flow of diffeomorphisms allowing large deformations. This flow is introduced through a template propagation method, by composition of small displacements. Regularization is performed using fast filtering techniques. This approach combines the robustness of statistical similarity measures with the flexibility of diffeomorphic matching techniques [8]. In addition, the required computational power for such a non-rigid image registration algorithm can be delivered by standard hardware as implemented in today's MR scanner platforms.
For evaluation of this algorithm in a clinical setting, a prototype software platform was developed which is fully integrated in a standard *syngo* based workstation (*syngo* MMWP). This implemented prototype allows the automated retrospective correction of multi-breath-hold DCE-MRI data sets. It is also capable of synchronizing the display of the native, arterial, portal-venous (p.v.) and late liver phase. These data sets can also be processed to obtain subtraction images. In addition, corrected data derived from different phases can be

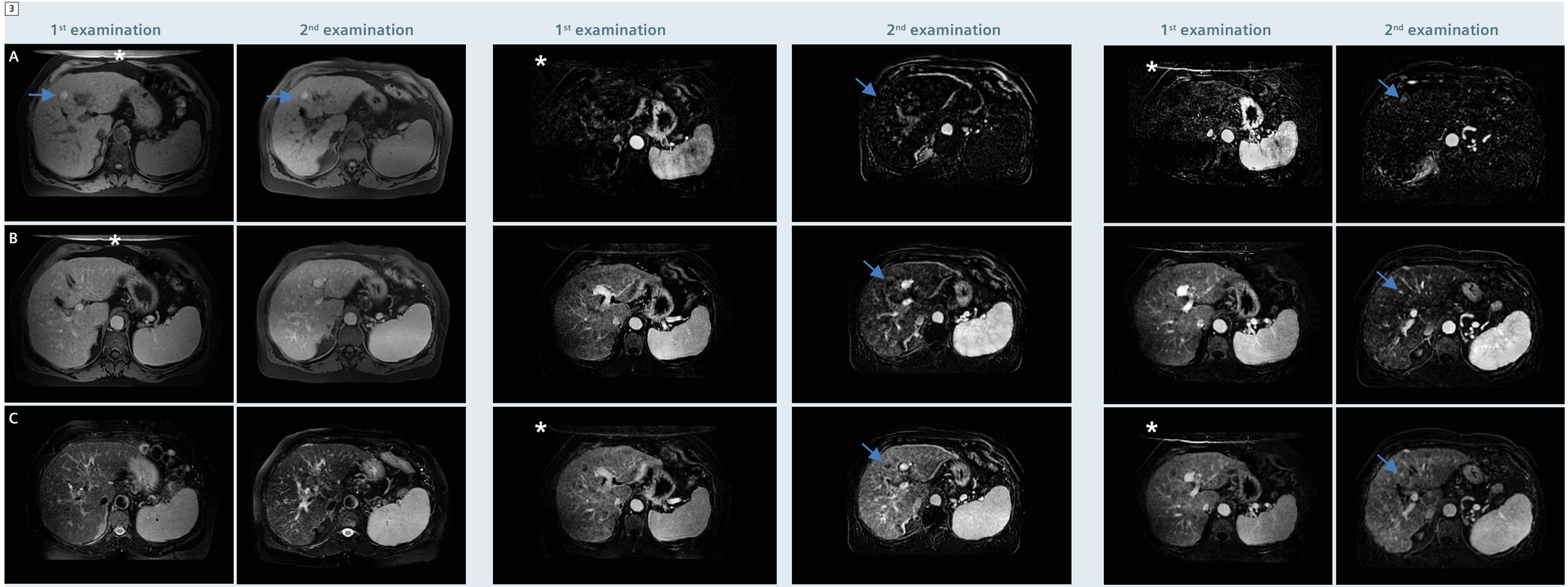

3 Example of a patient with follow-up examination in case of a dysplastic nodule (lesion marked by arrows). The lesion is already hyperintense on native T1w MRI. A slight mismatch is obvious especially for the DCE data sets at the second examination. The discrete contrast media enhancement of the lesion at the follow-up MRI only visualized on the corrected, subtracted images consequently.
A) Native T1w 3D VIBE B) post CM T1w FLASH 2D C) T2w 2D TSE *fold-in artifacts

displayed as checker boxes for qualitative analysis of the proper functionality of the algorithm. Corrected DCE MRI data can be stored as separate image sequences and these images can than be analyzed further e.g. with the Mean Curve functionality the enhancement patterns were evaluated in more detail. A total of 22 patients were evaluated in retrospect. In all cases, malignancies were proven by histology and at least one follow-up MRI was available as reference. In 17 patients a HCC was present (mean age 66 years, range 55 to 65 years). In 12/17 patients, a liver cirrhosis Child A / B was additionally reported. Additionally, 6 patients with focal nodular hyperplasia (FNH), 5 with an adenoma and 5 with liver metastases of a mamma carcinoma were evaluated. In all cases, at least one further MRI follow-up examination was available for further classification of additional suspicious lesions. All 3D DCE MRI were performed at 1.5 Tesla. For the acquisition of the dynamic data a T1w gradient-echo (either a 3D FLASH or VIBE) sequence was used. Acquisition time was approximately 20 s, resulting resolution was (2.0 x 1.5 x 2.5) mm^3. Data evaluation was performed by two experienced radiologists for the original and corrected data sets (with and without subtraction). It included qualitative (presence of artifacts, degree of anatomical mismatch) and semi-qualitative (number of lesions per liver segment, lesions diameters) criterions. For quantitative data analysis, changes of signal intensities (SI) at the native, arterial, p.v. and late (equilibrium) phase were evaluated by a region-of-interest (ROI) analysis. Therefore, ROIs were placed within the aorta, left / right hepatic arteries, tumor lesions, liver parenchyma and portal vein. The required total time for assessment of all livers lesions was documented, too.

Results

In all cases, the retrospective correction of 3D DCE MRI data sets was performed successfully. Quality rating was significantly higher for the corrected, subtracted images (statistically significant). SI changes of the left/right hepatic artery were found to be the most sensitive quantitative parameters to evaluate the function of the correction algorithm (compare graph 1). However, a significant mismatch of 3D DCE MRI data sets was only obvious in tumor patients (HCC and metastases). No artificial lesions were introduced by the correction algorithm and no additional lesions were observed in the cases with FNH (lesions per patient: n = 1.3), adenoma (n = 1.4) and metastases (n = 1.8). While not statistically different, however, in patients with a HCC numbers of detected lesions differed (original data sets: n = 4.4; corrected and subtracted DCE MRI data: n = 4.7). The total reporting time was significantly reduced by the synchronous display of the corrected DCE MRI data sets in all cases. This was most obvious in patients with HCC: 597 s (mean) for the report with the original data sets and the conventional clinically used image viewer; 231 s (mean) for the corrected and subtracted examinations.

Discussion and conclusion

As shown in this clinical feasibility study, the implementation of a non-rigid liver registration for DCE MRI can clearly improve the overall quality of DCE liver MRI especially in patients with limited breathhold capabilities. Based

on the evaluated patient cohort, a tendency towards a more accurate detection of liver lesions especially in case of HCC was observed. However, whether this fact can be reproduced in larger patient groups is still a question to be answered. In general, it should be mentioned that the detection of suspicious contrast media enhancement within the liver tissue is not relying on the most accurate coregistration and image subtraction. Reading of inaccurately registered DCE MRI is time-consuming and complex but not the reason why lesions within the liver tissue are missed. Optimal timing of image acquisition with the perfusion cycle of the liver, correct contrast media application as well as high resolution and optimal contrast behavior of the selected DCE MRI sequences are the key elements towards highest detection rates*. Therefore, a statistically significant difference in diagnostic accuracy between original and registered as well as subtracted images was neither expected nor was it observed in our patient cohort. But what is most important is that by the algorithm no artificial lesions were introduced into the registered DCE liver MRI exams. However, in daily routine, one has to read large amount of image data and for this purpose the accurate display of findings over different phases is required. Efficient reading (this means accurate detection and classification of suspicious lesions within a short time frame) of liver lesions relies on the side-by-side display of the different phases and based on our experience, a clear profit by providing registered as well as subtracted DCE liver images is obvious. In addition, the usage of the implemented algorithm is not limited to liver DCE MRI and in theory it is capable of handling a theoretically unlimited number of data points derived from any dynamic MR exam.

Based on the clinical experiences with the above applied first implementation of the algorithm, the next step was to integrate it as an easy to handle and robust procedure in the clinical workflow. In addition, several consulting radiologists requested that this functionality should be available as an inline tool; the implementation of a liver registration based on dedicated postprocessing software would have limited its wide clinical usage. Independent from this request, however, retrospective non-rigid registration of dynamic data is required for multiple purposes and already implemented for advanced image reading software.

The non-rigid registration of a four-phase liver DCE MRI exam (*syngo* dynaVIBE) is already available for all MR scanners equipped with the software versions *syngo* MR B 15 and 17. As described in "Non Rigid 3D-Registration for Accurate Subtraction of Dynamic Liver Images for Improved Visualization of Liver Lesions with *syngo* dynaVIBE" on page 71 of this issue, these implementations of *syngo* dynaVIBE require that the liver DCE MRI is set up as one single sequence with four measurements (covering the four liver phases: native, arterial, (portal-)venous and late (or equilibrium) phase). While this approach assures perfect match and correct assignment of the different phases for the correction algorithm, in clinical routine a more flexible handling may be required e.g. one could apply a single-shot HASTE MRCP between the (portal-) venous and late phase.

*See also Eric Hatfield et al. "Revisiting liver imaging with VIBE" in MAGNETOM Flash #39, 2/2008 available online at www.siemens.com/magnetom-world

Further reading: Diego R. Martin et al. "Challenges and clinical value of automated and patient-specific dynamically timed contrast-enhanced liver MRI examination" in MAGNETOM Flash #42, 3/2009 available online at www.siemens.com/magnetom-world

References

1 Van den Bos IC, Hussain SM, Dwarkasing RS, Hop WC, Zondervan PE, de Man RA, IJzermans JN, Walker CW, Krestin GP. MR imaging of hepatocellular carcinoma: relationship between lesion size and imaging findings, including signal intensity and dynamic enhancement patterns. J Magn Reson Imaging. 2007 Dec;26(6):1548-55.

2 Van den Bos IC, Hussain SM, Terkivatan T, Zondervan PE, de Man RA. Stepwise carcinogenesis of hepatocellular carcinoma in the cirrhotic liver: demonstration on serial MR imaging. J Magn Reson Imaging. 2006 Nov;24(5):1071-80.

3 Terkivatan T, van den Bos IC, Hussain SM, Wielopolski PA, de Man RA, IJzermans JN. Focal nodular hyperplasia: lesion characteristics on state-of-the-art MRI including dynamic gadolinium-enhanced and superparamagnetic iron-oxide-uptake sequences in a prospective study. J Magn Reson Imaging. 2006 Oct;24(4):864-72.

4 Yu JS, Chung JJ, Kim JH, Kim KW. Hypervascular focus in the nonhypervascular nodule ("nodule-in-nodule") on dynamic computed tomography: imaging evidence of aggressive progression in hepatocellular carcinoma. J Comput Assist Tomogr. 2009 Jan-Feb;33(1):131-5.

5 Yu JS, Kim YH, Rofsky NM. Dynamic subtraction magnetic resonance imaging of cirrhotic liver: assessment of high signal intensity lesions on nonenhanced T1-weighted images. J Comput Assist Tomogr. 2005 Jan-Feb;29(1):51-8.

6 Hecht EM, Holland AE, Israel GM, Hahn WY, Kim DC, West AB, Babb JS, Taouli B, Lee VS, Krinsky GA. Hepatocellular carcinoma in the cirrhotic liver: gadolinium-enhanced 3D T1-weighted MR imaging as a stand-alone sequence for diagnosis. Radiology. 2006 May;239(2):438-47.

7 Holland AE, Hecht EM, Hahn WY, Kim DC, Babb JS, Lee VS, West AB, Krinsky GA. Importance of small (< or = 20-mm) enhancing lesions seen only during the hepatic arterial phase at MR imaging of the cirrhotic liver: evaluation and comparison with whole explanted liver. Radiology. 2005 Dec;237(3):938-44.

8 Chefd'hotel C, Hermosillo G, Faugeras O Flow of Diffeomorphisms for Multimodal Image Registration Proc IEEE Int S Bio Im, 2002.

Contact
Ulrich Kramer, M.D.
Diagnostic and Interventional Radiology
University Hospital Tübingen
Hoppe-Seyler-Str. 3
72076 Tübingen
Germany
Ulrich.Kramer@med.uni-tuebingen.de

Non Rigid 3D-Registration for Accurate Subtraction of Dynamic Liver Images for Improved Visualization of Liver Lesions with *syngo* dynaVIBE

Matthias P. Lichy, M.D.; Wilhelm Horger; Berthold Kiefer, Ph.D.

Siemens Healthcare, Magnetic Resonance, Erlangen, Germany

Background

The arterial phase derived from T1w contrast-enhanced liver dynamics (liver DCE) is perhaps one of the most important diagnostic tools for the assessment of liver disease. However, true enhancement of liver lesions is hard to judge in several conditions such as liver fibroses or tumor necroses. In addition, even under optimal conditions, the patient might hold his breath in slightly different respiratory phases during the multiple breathholds of a multi-phase DCE liver exam (native, arterial, portal-venous and equilibrium phase) which can result in a clear offset of the anatomical position over the different phases. This has disadvantages for the reading of liver DCE data: firstly, the position has to be aligned manually (in the worst case three out of the four data sets) and secondly, the subtraction of different phases will generate severe artifacts and may falsely hint to an enhancement. But for a precise anatomical alignment it is also insufficient to adjust just the mismatch over time for the liver in the craniocaudal direction; under certain conditions e.g. severe ascites or liver resection, movement within the plane including deformation of the tissue can also be observed.

With *syngo* dynaVIBE, however, it is easy to set up liver DCE scans with retrospective non-rigid registration of the different liver phases (Figure 1) and also to generate subtracted images which can be used for improved demonstration of contrast-enhancement of the different phases without the need of

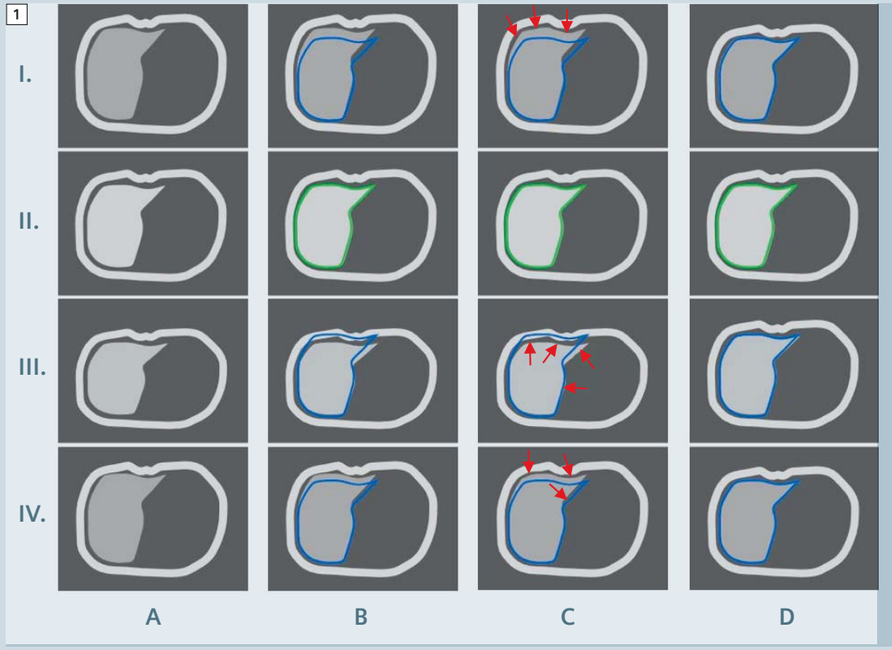

1 Scheme of the functionality of a non-rigid liver registration. In general, a dynamic liver scan consists of four phases (native (row I), arterial (row II), venous (row III) and equilibrium, row IV)). Colum **A** displays the original results from such a MR exam. However, an anatomical mismatch between the different phases can be observed (reference scan is shown in light grey). The dynaVIBE algorithm analyses the deformation of the tissue in all three dimensions and performs an elastic correction of the voxel shift (columns **B** and **C**). Resulting (column **D**) is an exact match of the anatomical structures over space and time allowing a voxel-based analysis of the liver.

How-I-do-it

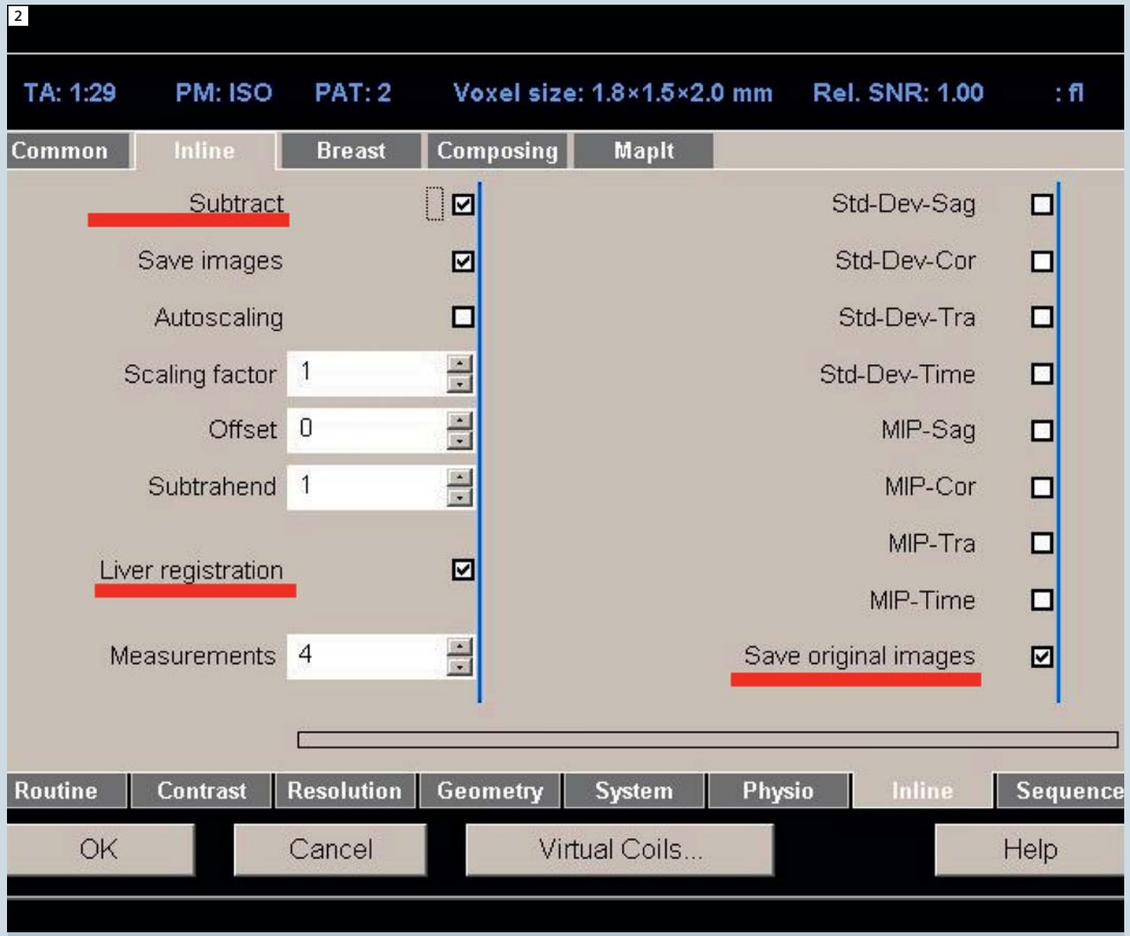

2 Easy set up of *syngo* dynaVIBE.

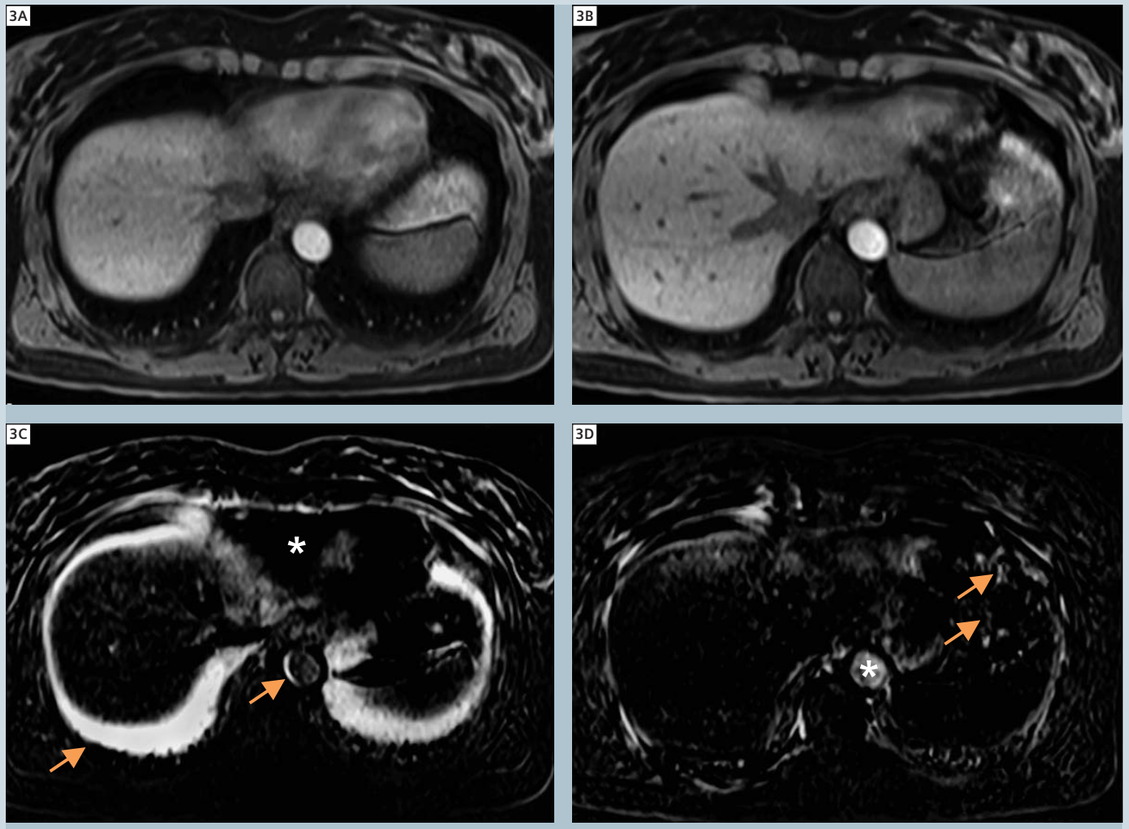

3 Example of an insufficient match between two phases (**A** and **B**) of a dynamic liver scan at identical z-axis position. In this example, no contrast-media was applied. A subtraction of two completely identical data sets would therefore result in a black screen. **3C** shows how a simple subtraction of these two data sets results in severe artifacts, either artificial enhancement (arrows) or signal void (asterisk). After applying the liver registration algorithm, a nearly perfect subtraction is achieved. However, this does not compensate for signal intensity changes introduced e.g. by pulsation / movement within one acquisition (arrows) or non contrast-media related signal changes as present in this example within the aorta (asterisk).

further post-processing steps.
This technology is available for all MAGNETOM systems running on *syngo* MR B15, 17 and for the *syngo* MR D software versions.

How to set up a *syngo* dynaVIBE liver DCE

A *syngo* dynaVIBE liver DCE examination requires four phases:
a) Native
b) Arterial
c) (Portal-) Venous
d) Equilibrium phase.
As MR sequence, a T1w 3D VIBE with fat saturation is used. It is important for the Inline calculation of the non-rigid liver registration and for the subtraction of the different phases that the scanner can clearly identify the coherent measurements which define the liver DCE. It is also a prerequisite for the algorithm that the number of slices within the slab, FOV and matrix are not changed for the separate phases of a liver DCE exam. Therefore all the above four measurements must be linked. This can easily be achieved by selecting "multiple measurements" in the "Inline" menu when adjusting the 3D VIBE sequence parameters. This parameter has to be set to "4". By activating the "Liver registration" feature (simply check the box, cf. figure 2), the non-rigid liver registration will be performed after the completion of the liver DCE.
By default, the second phase (which should represent the arterial phase) will be used as reference for the liver registration and the other three measurements will be adjusted accordingly to the position and shape of the liver as present in the reference phase. Based on this registration one can easily generate subtracted images by simply activating the "Subtraction" feature. This produces three series, showing the arterial, (portal-) venous and equilibrium enhancement patterns.
In the past the computational requirements for non-rigid registration algorithms clearly limited their usage in clinical routine. However, by optimizing the algorithm and applying the computer power available with Siemens MR scanners, the final results of a *syngo* dynaVIBE exam will be available very quickly. It is also important to note that the MR exam can be continued without need for pausing. Original data sets can be stored and also presented to the radiologist who is reporting the exam. In this case "Save original images" should be activated.

Further considerations

The liver registration algorithm is independent from the time intervals between the different measurements. These pauses between the different phases can be defined by fixed values but it is also possible to start a measurement manually (Inline display feature). However, it is not possible to combine independent 3D VIBE scans, and additional scans added for example with the "append" command accessed with the right button menu will not be integrated.
In daily routine it may be useful to set up a few variations of the liver DCE VIBE sequence with special regard to breath-hold capabilities of the patients (adopted resolution, scan duration and slab thickness) and with the features described above activated. This would further reduce the required interaction for the Radiographer in adopting the liver DCE and also avoid the risk of forgetting to activate the *syngo* dynaVIBE features.
Figure 3 shows an insufficient match of

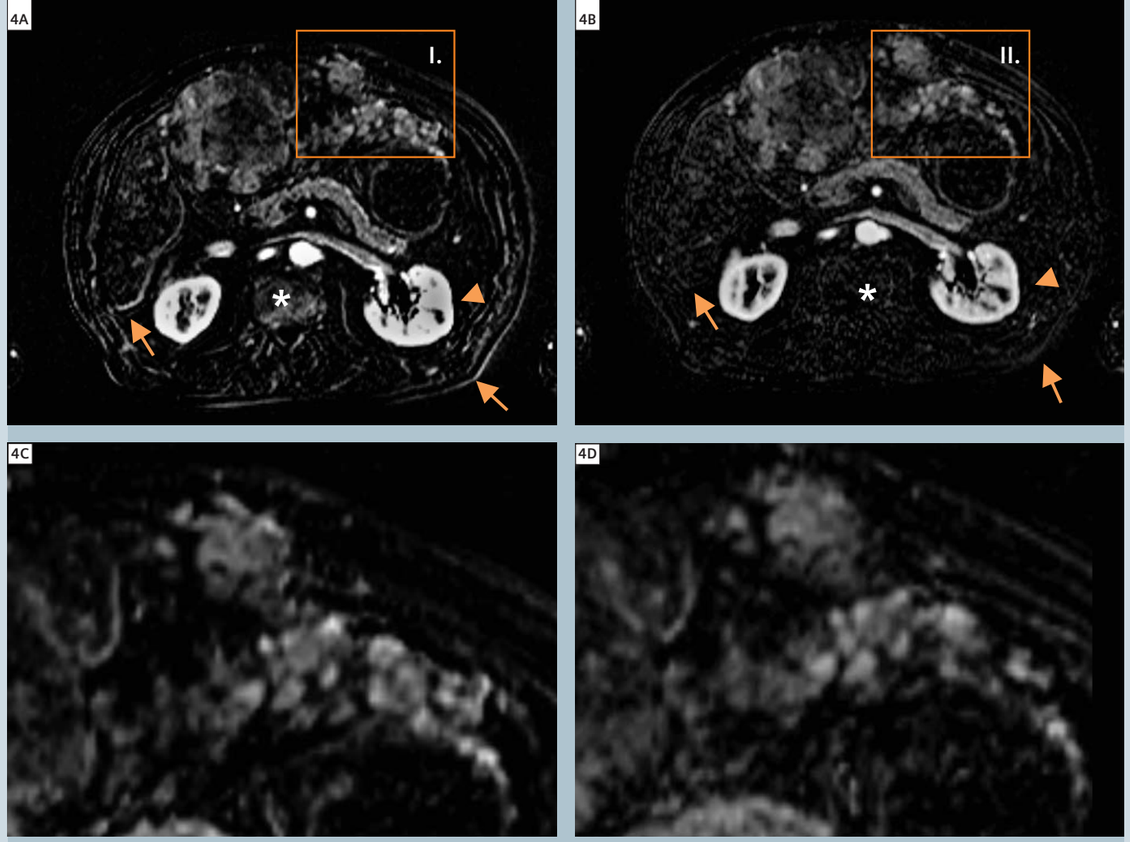

4 The liver registration algorithm also corrects other anatomical structures within the 3D data sets. In all images shown, the native phase was subtracted from the arterial enhancement with 4A/4C for original and 4B/4D for registered data.
4A shows blooming of the renal cortex (arrowhead) without correction. Even under nearly perfect conditions, a slight mismatch can be observed in most liver scans. Rimming at the organ boarders is often a good indicator (arrows). The asterisk indicates artificial enhancement of the bone marrow for uncorrected subtracted phases (arterial minus native liver phase shown). **4C** and **4D** show magnified areas from the left liver lobe. In this patient with severe fibrosis and hepatocellular carcinoma, an overemphasis of the arterial enhancement is obvious (same window level for both images).

the subtracted two phases of a liver DCE. This can be recognized by the hyperintense rims of anatomical structures. However, areas with complete loss of signal can also be seen. "Blurring" of anatomical structures compared to the original, unsubtracted images can also be an indicator for an insufficient anatomical match.

After completion of a liver DCE, the quality and contrast-media timing of the individual phases as well as the results of the Inline calculation should be checked. While the liver registration algorithm does not compensate for noise bands, pulsations and breathing the artifacts may be present within the individual measurement of a liver DCE.

These artifacts may very often be easily separated from a potential malfunction of the non-rigid liver registration.
In conclusion, a clear improvement of the results of liver DCE scans can be achieved with *syngo* dynaVIBE without the need of further post-processing.

Contact
Matthias Lichy, M.D.
Siemens Healthcare
Magnetic Resonance
Karl-Schall-Str. 6
D-91052 Erlangen
Germany
matthias.lichy@siemens.com

→ Tips how to optimize the sequence parameters of 3D VIBE for liver DCE can be found in Eric Hatfield et al. **"Revisiting Liver Imaging with VIBE"** published in MAGNETOM Flash 2/2008 (page 11), which is available online at **www.siemens.com/magnetom-world.**

Market your MAGNETOM system

www.siemens.com/magnetom-world > Your MAGNETOM > MAGNETOM Marketing Tool Kit

This webpage provides you with Marketing Tools to promote your MAGNETOM system.

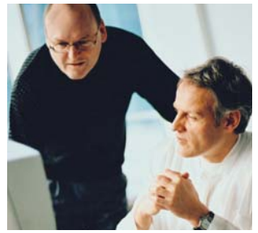

Multimedia

The future belongs to multimedia communications! In this section you will find specific powerpoint presentations and trailers helping to promote your system and its offerings to your customer.

> PowerPoint Presentation

> Trailers (Product Trailer, MRI Safety Video, Understanding MRI, MR Kids Cartoon)

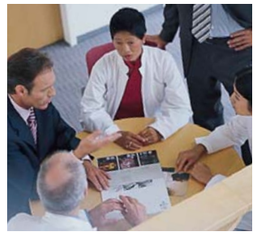

Print media

Effective print media continues to play a key role in successful communications. The contents in this section will help you to create professionally designed print pieces for promoting your new MR system.

> Advertisements

> Mailing

> Logbook

On-site material

Take a number of quite different marketing steps. This section contains valuable tips and checklists that will support you in all these individual activities.

> Appointment Calendar

> Posters

> Patient Information and Safety Guides

> Event Checklist

> Material for kids

Image gallery

A picture is worth a thousand words! Here are some sample images that say a great deal, and you can use them for many purposes.

> Product images

> Mood images

> Clinical images

PR basics

Revolutionary technology is news worthy! Your local news media can help you to publicize your MAGNETOM system. This press release makes it easy for you – and for them – to spread the exciting word.

> Press Release

Product News

VIBE for Liver Imaging with *syngo* MR B17

Agus Priatna, Ph.D.[1]; Stephan Kannengiesser, Ph.D.[2]

[1]MR R&D Collaborations, Siemens Medical Solutions, St Louis, MO, USA
[2]MR Applications Development, Siemens Healthcare, Erlangen, Germany

Volume Interpolated Breathhold Examination (VIBE) [1] is a well known technique for imaging of the liver. VIBE offers three-dimensional multi-phase acquisition before and following contrast administration under breathhold conditions. The dynamic behavior of the liver lesions and structures is typically analyzed by scanning pre-contrast, arterial, portal venous, early equilibrium and 5 minutes delayed equilibrium phases of enhancement. This allows more accurate characterization than static pre or post-contrast analysis.
In the *syngo* MR B17 software, new functionalities have been added to the VIBE sequence to better meet the clinical requirements. The following are the most critical requirements for VIBE: uniform fat suppression, excellent tissue contrast, image sharpness, few artifacts, and short scan time. The new functionalities include a new k-space reordering scheme, a new fat suppression scheme, and a new reconstruction functionality.

K-space reordering scheme

A new k-space reordering scheme was introduced to improve image quality: Linear reordering in the slice (3D / partition) direction produces clean image quality, as it is less susceptible to artifacts and motion due to its smooth magnetization trajectory. It also allows for shortening the scan time as it does not require 'dummy' pulses to drive the signal into the steady state condition. The linear reordering acquisition is still 'single-shot' to maintain the short scan time. Furthermore, the linear reordering scheme reduces artificial enhancement of the liver edges.

Fat suppression

Linear k-space reordering is used in conjunction with the Q-Fatsat option available in the Contrast UI tab card. Internally, the flip angle of the fat saturation pulse is adjusted for nulling the fat signal at the center of k-space. This scheme produces uniform fat suppression for the liver. If the condition of zero fat signal at the center of k-space cannot be met, the reordering reverts to centric reordering in the slice direction, which was the standard setting up to now. This condition is dependent on the resolution parameters in the slice direction, on TR, and on the imaging flip angle. It is recommended that opposed phase TE is used for dark fat suppression when using asymmetric echo. It is also possible to use a reversed echo asymmetry to shorten the scan time by manually reducing the TR while maintaining the TE constant. For this, the TE has to be long enough to allow a symmetric echo, and the echo optimization (on the Sequence – Part 1 UI tab card) must be None. Symmetric echo also produces uniform fat suppression with linear reordering scheme.

Reconstruction with Projection Onto Convex Sets (POCS)

A new option to enhance image reconstruction is also available in the *syngo* MR B17 software: Projection Onto Convex Sets or POCS can be selected on the Resolution – Filter UI tab card when using partial Fourier in the phase and/or read directions. POCS reconstruction will sharpen the image by reducing the blurring induced by partial Fourier acquisition.

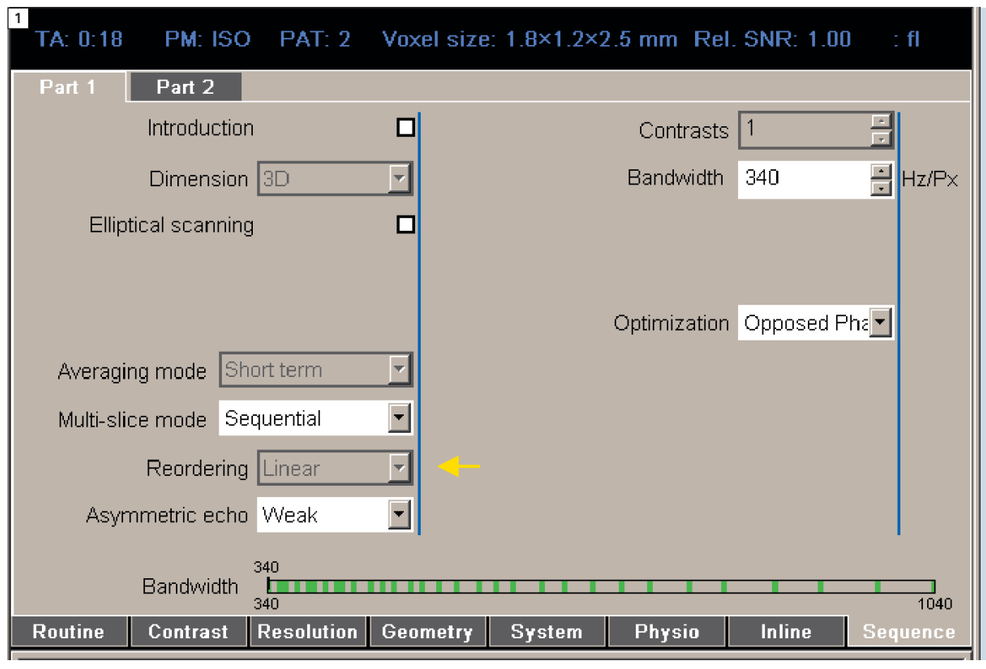

1 The linear reordering scheme as seen in the user interface (UI).

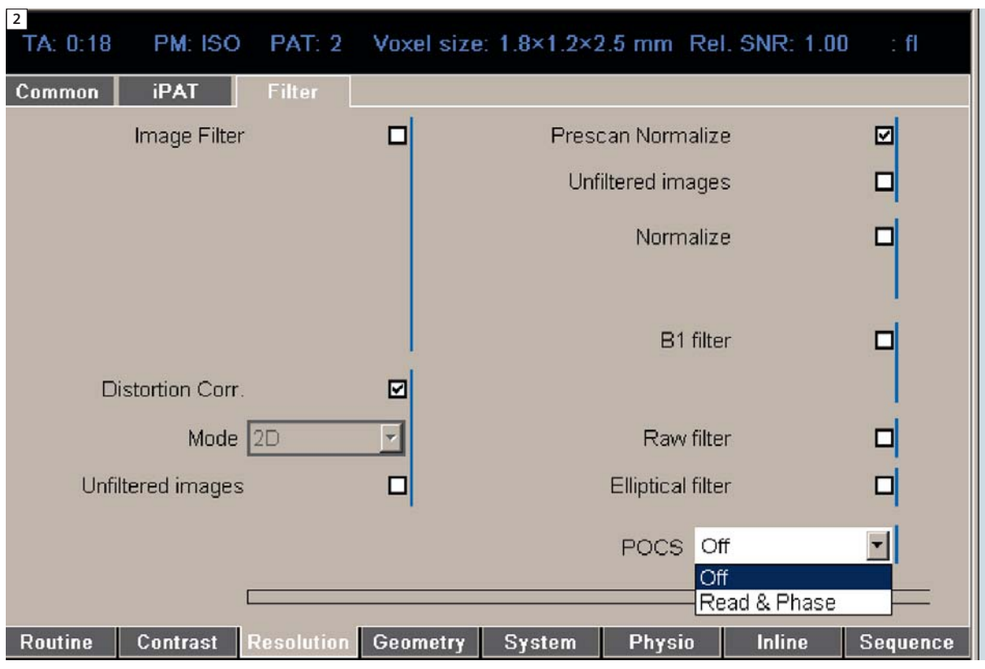

2 The POCS option as it appears on the resolution tab.

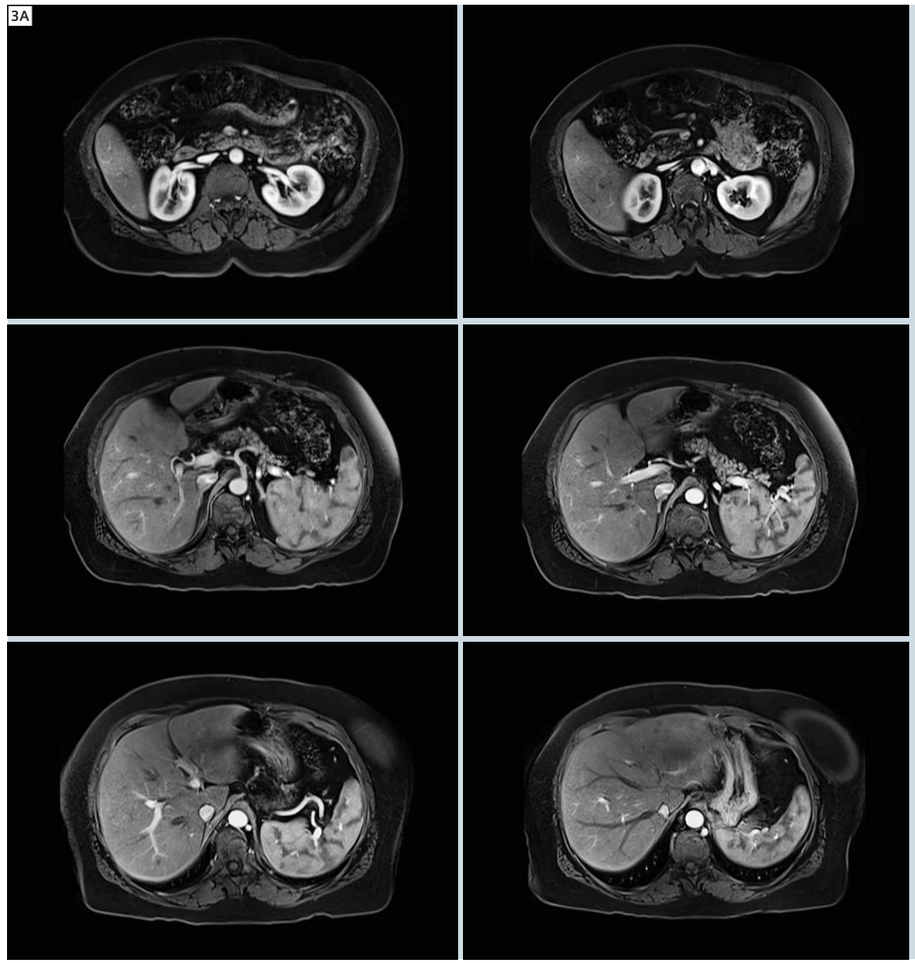

3 Typical VIBE images obtained at 3T MAGNETOM Trio, A Tim system
(A) Arterial phase.

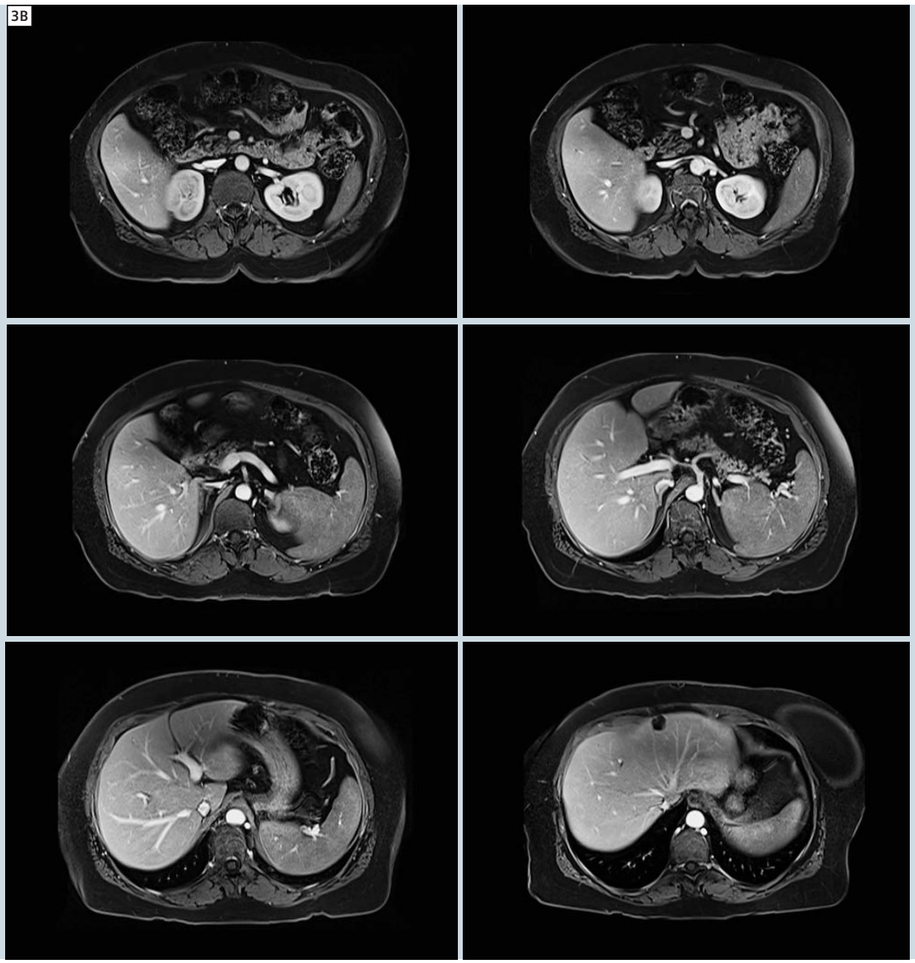

3 **(B)** Portal venous phase. *(Images courtesy of Washington University in St Louis.)*

Examples of protocols

The followings are recommendations to acquire good image quality of VIBE for liver imaging:

- Q-Fatsat with linear reordering.
- 320 base resolution to increase image sharpness.
- 10 degree excitation flip angle at 1.5T system and 9 degree at 3T system for uniform fat suppression.
- Symmetric echo for image sharpness.
- Opposed phase TE if using asymmetric echo for uniform fat suppression.
- Slice partial Fourier = 6/8.
- Phase partial Fourier = Off for image sharpness.
- If further scan time reduction is necessary, select 7/8 phase partial Fourier. Using POCS will reduce blurring.
- Prescan Normalize filter.

Figure 3 shows the typical image quality of the arterial phase (A) and the portal venous phase (B) acquired at 3T MAGNETOM Trio Tim with the following parameters: Q-Fatsat with linear reordering, BW 446 Hz/pixel, base resolution 320, slice thickness 3 mm, echo asymmetry Off, phase partial Fourier Off, TE 1.9 ms, TR 4.1 ms, 72 partitions, Prescan normalized, total acquisition time 19.72 seconds. These images show good fat suppression and good contrast enhancement.

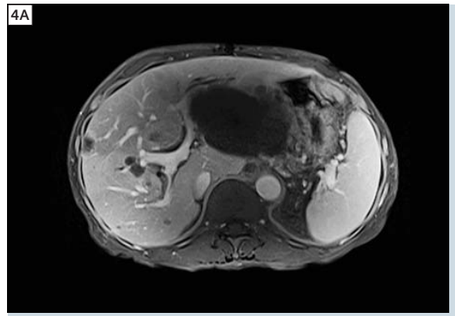

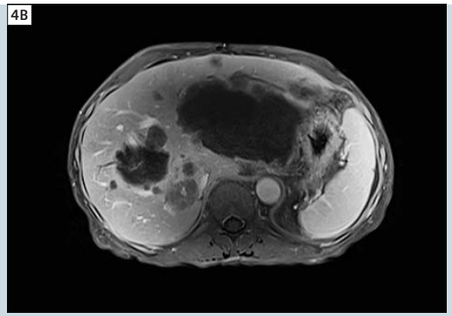

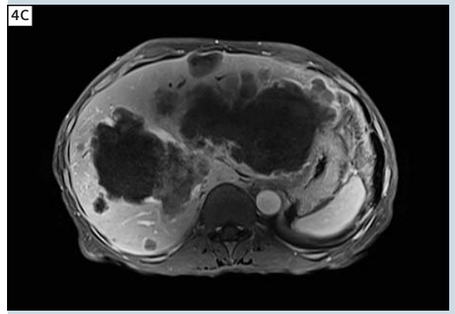

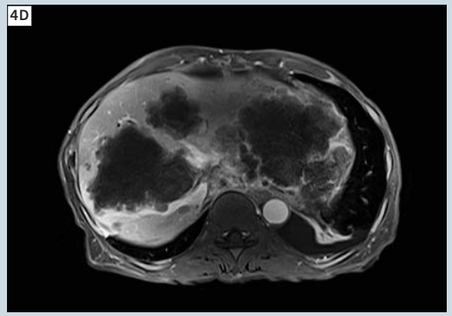

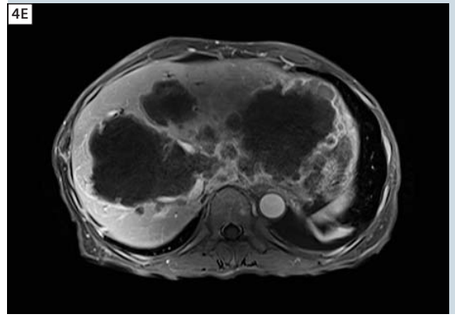

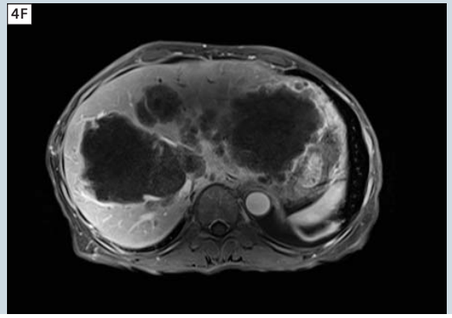

4 A portal venous phase as seen in a patient with colorectal cancer metastasis obtained at 3T MAGNETOM Trio with Tim system. *(Images courtesy of Washington University in St Louis.)*

Figure 4 shows another example of clinical cases obtained from 3T MAGNETOM Trio, A Tim system. Images shown are the portal venous phase of a patient with metastases from a colon cancer obtained with the same 3T protocol mentioned above. Image sharpness and contrast enhancement are seen in this example.

Figure 5 is an example of a multi-phase contrast-enhanced VIBE scan on a 1.5T open-bore MAGNETOM Espree system of a patient with metastases from colon cancer with the following protocol: Q-Fatsat with linear reordering, BW 390 Hz/pixel, Base resolution 320, slice thickness 3 mm, echo asymmetry Off, phase partial Fourier Off, TE 2.2 ms, TR 4.4 ms, 72 partitions, acquisition time 24 seconds. These images show sharpness, good contrast enhancement, uniform fat suppression and reduced artifacts on an open-bore system.

Conclusions

New functionality of the VIBE sequence in the *syngo* MR B17 software allows improvements in fat suppression, tissue contrast, image sharpness, residual artifact, and scan time. The improvements in image quality are shown on both 3T and 1.5T systems.

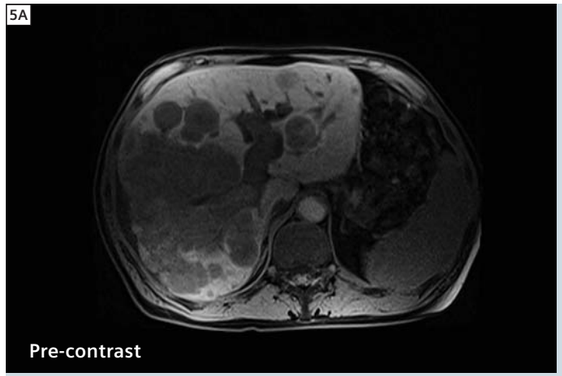

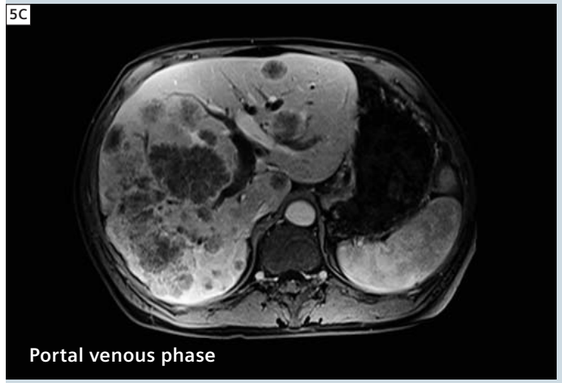

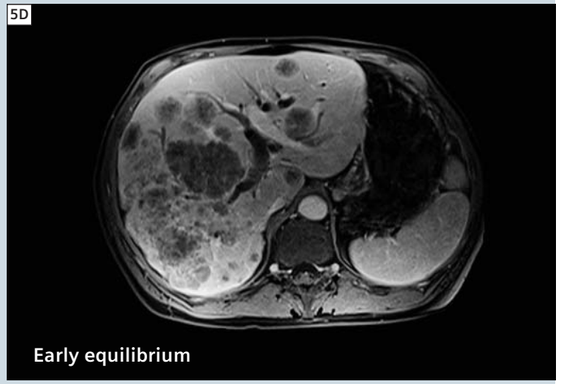

5 Dynamic contrast-enhanced images of a patient with metastases from a colon cancer obtained at 1.5T open-bore MAGNETOM Espree system. *(Images courtesy of Washington University in St Louis.)*

References

1 Rofsky NM, Lee VS, et al. Abdominal MR Imaging with a Volume Interpolated Breath-hold Examination. Radiology. 1999 Sept; 212(3):876-84.

Contact
Agus Priatna
Siemens Medical Solutions USA, Inc.
MR Research Collaborations
51 Valley Stream Parkway
Malvern, PA 19355-1406
USA
agus.priatna@siemens.com

Siemens Healthcare Publications

Our publications offer the latest information and background for every healthcare field. From the hospital director to the radiological assistant – here, you can quickly find information relevant to your needs.

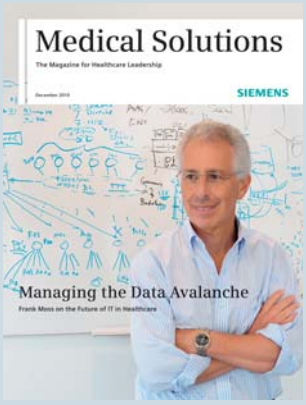

Medical Solutions
Innovations and trends in healthcare. The magazine is designed especially for members of hospital management, administration personnel, and heads of medical departments.

eNews
Register for the global Siemens Healthcare Newsletter at www.siemens.com/healthcare-eNews to receive monthly updates on topics that interest you.

AXIOM Innovations
Everything from the worlds of interventional radiology, cardiology, fluoroscopy, and radiography. This semiannual magazine is primarily designed for physicians, physicists, researchers, and medical technical personnel.

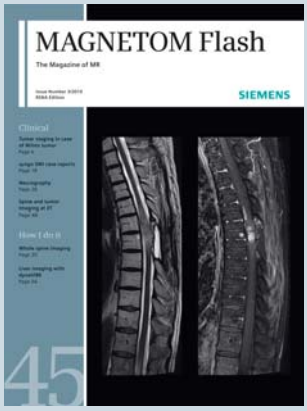

MAGNETOM Flash
Everything from the world of magnetic resonance imaging. The magazine presents case reports, technology, product news, and application tips. It is primarily designed for physicians, physicists, and medical technical personnel.

SOMATOM Sessions
Everything from the world of computed tomography. With its innovations, clinical applications, and visions, this semiannual magazine is primarily designed for physicians, physicists, researchers, and medical technical personnel.

For current and past issues and to order the magazines, please visit **www.siemens.com/healthcare-magazine.**

Among Europe's Best

Siemens Healthcare Publications received the Silver Award in the category "Best Crossmedia Solution" at the BCP Best of Corporate Publishing Congress in Hamburg, Germany. Under the topic "Healthcare Publications," Siemens Healthcare submitted its crossmedia publications portfolio, which consists of the business-to-business magazine *Medical Solutions*, the expert magazines *AXIOM Innovations* (angiography, radiography, and fluoroscopy), *SOMATOM Sessions* (computed tomography), *MAGNETOM Flash* (magnetic resonance imaging), and *Perspectives* (laboratory diagnostics), and the Healthcare Newsletter. The jury was comprised of more than 100 renowned experts from the areas of journalism, design, marketing, corporate/internal communication, print, and direct marketing. Obtaining the BCP Silver Award places Siemens Healthcare among the top corporate crossmedia publishers in Europe. The jury of the largest corporate publishing contest in Europe honored the best publications out of more than 600 entries in 29 permanent and four special categories. The BCP Award has enjoyed an excellent reputation since the first congress in 2003, and quantity and quality of entries is increasing. The 8th BCP congress 2010, under the patronage of the German Minister of Economics and Technology, Rainer Brüderle, took place with the slogan "Smart Content – All Media: Integration in Corporate Publishing." International experts discussed the future of print media and digital trends in the corporate publishing market before dedicating themselves to the award ceremony.

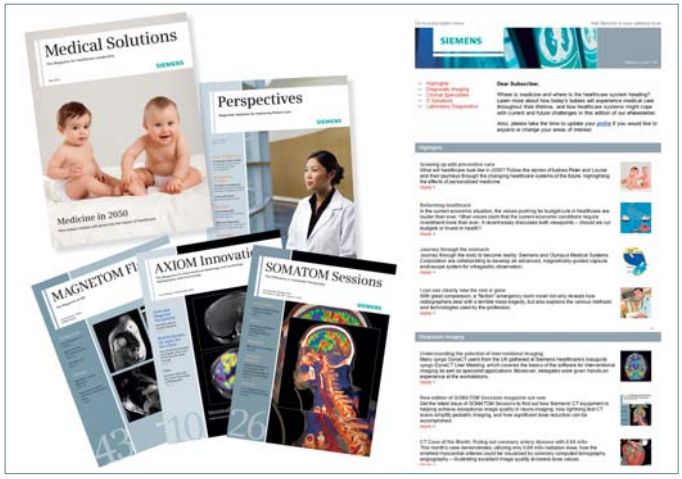

Already in 2008, Siemens Healthcare received two Silver Awards for its customer magazine *Medical Solutions*. This year, in the category "Best Crossmedia Solution," Siemens Healthcare Publications succeeded as the only crossmedia solution in the healthcare field nominated.

We hope you are just as satisfied with our media as the jury. Don't hesitate to tell us your opinion at antje.hellwich@siemens.com. If you would like to subscribe to any of our periodicals, please visit www.siemens.com/healthcare-magazine or www.siemens.com/healthcare-eNews.

MAGNETOM Flash – Imprint

Publisher:
Siemens AG
Medical Solutions
Business Unit Magnetic Resonance,
Karl-Schall-Straße 6, D-91052 Erlangen, Germany

Editor-in-Chief: Dr. Matthias Lichy, M.D. (matthias.lichy@siemens.com)

Associate Editor: Antje Hellwich (antje.hellwich@siemens.com)

Editorial Board: Ph.D.; Okan Ekinci, M.D.; Ignacio Vallines, Ph.D.; Wellesley Were; Milind Dhamankar, M.D.; Michelle Kessler; Gary McNeal; Sunil Kumar, M.D.

Production: Norbert Moser, Siemens AG, Medical Solutions

Layout: independent Medien-Design Widenmayerstrasse 16, D-80538 Munich

Printers: Farbendruck Hofmann, Gewerbestraße 5, D-90579 Langenzenn, Printed in Germany

MAGNETOM Flash is also available on the internet:
www.siemens.com/magnetom-world

MAGNETOM Flash with a total circulation of 20,000 copies is sent free of charge to Siemens MR customers, qualified physicians, technologists, physicists and radiology departments throughout the world. It includes reports in the English language on magnetic resonance: diagnostic and therapeutic methods and their application as well as results and experience gained with corresponding systems and solutions. It introduces from case to case new principles and procedures and discusses their clinical potential.

We welcome your questions and comments about the editorial content of MAGNETOM Flash. Please contact us at magnetomworld.med@siemens.com. Manuscripts as well as suggestions, proposals and information are always welcome; they are carefully examined and submitted to the editorial board for attention. MAGNETOM Flash is not responsible for loss, damage, or any other injury to unsolicited manuscripts or other materials. We reserve the right to edit for clarity, accuracy, and space. Include your name, address, and phone number and send to the editors, address above.

MAGNETOM Flash

The Magazine of MR

SIEMENS

Issue Number 3/2010
RSNA Edition

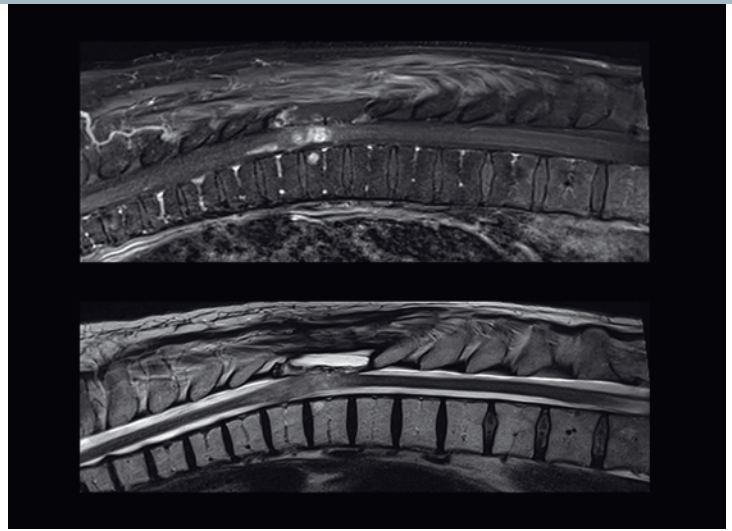

45

Please enter your business address

Institution

Department

Function

Title

Name

Street

Postal Code

City

State

Country

MR system used

Please include me in your mailing list for the following Siemens Healthcare customer magazine(s):

- ☐ Medical Solutions
- ☐ MAGNETOM Flash
- ☐ SOMATOM Sessions
- ☐ AXIOM Innovations

Stay up to date with the latest information Register for:

- ☐ the monthly e-Newsletter

E-mail

- ☐ Yes, I consent to the above information being used for future contact regarding product updates and other important news from Siemens.
- ☐ unsubscribe from info service

Please print clearly!

MAGNETOM Flash

Siemens AG
Medical Solutions
Magnetic Resonance
Antje Hellwich - Marketing
P.O. Box 32 60
D-91050 Erlangen
Germany

→ Visit www.siemens.com/magnetom-world for case reports, clinical methods, application tips, talks and much more clinical information.

SUBSCRIBE NOW!

– and get your free copy of future MAGNETOM Flash! Interesting information from the world of magnetic resonance – gratis to your desk. Send us this postcard, or subscribe online at www.siemens.com/MAGNETOM-World

Global Siemens Headquarters

Siemens AG
Wittelsbacherplatz 2
80333 Muenchen
Germany

Global Siemens Healthcare Headquarters

Siemens AG
Healthcare Sector
Henkestr. 127
91052 Erlangen
Germany
Phone: +49 9131 84-0
www.siemens.com/healthcare

www.siemens.com/healthcare-magazine

Order No. A91MR-1000-77C-7600 | Printed in Germany | CC MR 01000 ZS 111020. | © 11.10, Siemens AG

Global Business Unit

Siemens AG
Medical Solutions
Magnetic Resonance
Henkestr. 127
DE-91052 Erlangen
Germany
Phone: +49 9131 84-0
www.siemens.com/healthcare

Local Contact Information

In Asia
Siemens Pte Ltd
The Siemens Center
60 MacPherson Road
Singapore 348615
Phone: +65 6490-8096

In Canada
Siemens Canada Limited
Medical Solutions
2185 Derry Road West
Mississauga ON L5N 7A6
Canada
Phone: +1 905 819-5800

Europe/Africa/Middle East
Siemens AG
Medical Solutions
Henkestr. 127
91052 Erlangen
Germany
Phone: +49 9131 84-0

Latin America
Siemens S.A.
Medical Solutions
Avenida de Pte. Julio A. Roca No 516,
Piso 7
C1067ABN Buenos Aires
Argentina
Phone: +54 11 4340-8400

USA:
Siemens Medical Solutions U.S.A., Inc.
51 Valley Stream Parkway
Malvern, PA 19355-1406
USA
Phone: +1-888-826-9702